Electronic Thesis and Dissertation Repository

8-30-2019 10:00 AM

Long-Term Deflections of Reinforced Concrete Beams

Ziad Elaghoury, *The University of Western Ontario*

Supervisor: Bartlett, Michael F., *The University of Western Ontario*
A thesis submitted in partial fulfillment of the requirements for the Master of Engineering Science degree in Civil and Environmental Engineering
© Ziad Elaghoury 2019

ABSTRACT

The CSA A23.3 code provisions compute the long-term deflection of reinforced concrete flexural members by applying a multiplier to the short-term deflection, essentially ignoring the creep and shrinkage characteristics of concrete. The CAC Concrete Design Handbook presents more elaborate methods, but fails to account for the factors that influence the creep and shrinkage of concrete.

The four widely recognized models for computing creep and shrinkage strains yield predictions that differ by up to 30%. Studies by others to assess the accuracy of the models apply different of statistical analyses do different datasets and so yield contradicting outcomes, making it difficult to quantify the prediction error.

Mechanics-Based Methods for computing long-term deflections are proposed and used to derive Alternative Simplified Methods. The accuracy of existing and proposed methods is assessed by quantifying test/predicted ratios. The CAC Handbook Method yields mean test/predicted ratios ranging from 0.97 (conservative) to 1.34 (unconservative). The mean test/predicted ratio for the Mechanics-Based Method and the Alternative Simplified Method range from 0.92 to 0.94, and from 0.97 to 1.05, respectively. The A23.3 Multiplier Method overestimates the deflection of lightly-reinforced members.

Keywords: Reinforced concrete; Long-term deflection; Time-dependent analysis of concrete; Concrete creep; Concrete shrinkage Short-term deflection; Bischoff's Equation; Effective moment of inertia; Sustained loads

SUMMARY FOR LAY AUDIENCE

Serviceability, or functionality, is an important structural design criterion. Structures that exhibit excessive deflections may become unusable. Methods for checking deflections during the design of reinforced concrete structures must account for the instantaneous deflection and the additional long-term deflection due to concrete creep and shrinkage. The research reported in this thesis presents enhanced methods for computing creep and shrinkage deflections that may replace existing methods that have remained static since the mid 1970s.

ACKNOWLEDGMENTS

TABLE OF CONTENTS

LIST OF TABLES

LIST OF FIGURES

LIST OF APPENDICES

NOMENCLATURE

A	Regression coefficient quantifying the contribution of the creep coefficient to the long-term deflection
A_g	Gross area of the cross-section
A_s	Area of tension steel reinforcement
A_{sh}	Factor to account for the ratio of compression to tension reinforcement
A'_s	Area of compression steel reinforcement
B	Regression coefficient corresponding to the quantifying (ρ'/ρ) to the long-term deflection
B'	Modified regression coefficient corresponding to the quantifying (ρ'/ρ) to the long-term deflection, a function of ρ
b	Width of the cross-section
C	Regression coefficient
C'	Modified regression coefficient, a function of ρ
C_t	CAC Concrete Design Handbook Creep Coefficient
c	Correlation factor
D	Regression coefficient
d	Distance from extreme compression fiber to centroid of tension reinforcement
d'	Distance from extreme compression fiber to centroid of compression reinforcement
E	Regression coefficient
E_c	Young's Modulus of concrete
E_s	Young's Modulus of steel
$\overline{E_c}$	Age-adjusted Young's Modulus of concrete
$E_c I_e$	Effective flexural rigidity of the cracked member
$E_c I_g$	Flexural rigidity of the uncracked member

$\overline{E_c}\,\overline{I_{cr}}$	Time-dependent flexural rigidity cracked cross-section
F_{CEB}	Mean square error as computed by CEB method
F_j	Mean square error of the data points within a data set in an interval
$F_{c,t}$	Force at the level of the bottom reinforcement at time t
$F_{c,t}$	Force at the level of the top reinforcement
f_y	Specified yield strength of steel
f_r	Modulus of rupture of concrete
f_{ij}	Percent difference between test and predicted data points, i, in dataset j
f'_c	Specified compressive strength of concrete
h	Overall depth or height of member
I_{cr}	Moment of inertia of cracked section
I_e	Effective moment of inertia
I_g	Gross moment of inertia
$\overline{I_{cr}}$	Time-dependent cracked moment of inertia
K_{sh}	coefficient that accounts for the displacement boundary conditions in shrinkage deflection calculations
kd	Depth from the extreme compression fiber to the neutral axis
k_r	Creep strain reduction factor
k_{sh}	Gilbert and Kilpatrick's empirical shrinkage factor
$\overline{kd}$	time-dependent neutral axis depth
ℓ_n	Clear span length
M_a	Maximum applied service moment
M_{CEB}	Mean deviation as computed by CEB method
M_{cr}	Cracking moment
M_D	Dead load moment
M_f	Factored ultimate limit state design moment

M_j	Mean deviation of a single data set within interval j
M_L	Live load moment
M_s	Moment due to sustained load
N	Number of data sets considered
N_b	Number of histogram boxes
N_k	Number of time intervals
n	Modular ratio (E_s/E_c) or Number of creep or shrinkage data points
$\bar{n}$	Age-adjusted modular ratio
n_d	Number of decades on the logarithmic scale spanned by the measured data
n_w	Sum of the weights assigned to each data point in a data set
n_{ib}	Number of data points, i, in box b
n_{ij}	Number of data points, i, in data set j
n_{ik}	Number of data points in one decade.
p	Number of input parameters
RMS_k	Root mean square error within k^{th} time interval
$\overline{RMS}$	Root mean square error for all the time intervals
S_j	Standard error of the creep or shrinkage strain obtained from test j
S_t	Sustained load factor
s	Standard error of regression
T	Combined creep and shrinkage coefficient
t	Age of concrete, days
t_c	Curing period, days
t_o	Loading age, days
V_{BP}	Coefficient of variation as computed by BP method
V_{BL}	Coefficient of variation as computed by BL method
V_{CEB}	Coefficient of variation as computed by CEB method

V_G	Coefficient of variation as computed by CEB method
V_m	Modified coefficient of variation
V_j	Coefficient of variation of the test/predicted ratios for the jth data set
V_{BPj}	Coefficient of variation of test/predicted for the jth data set as computed by BP method
w_b	Weight assigned to the average of residuals for each box
w_{ib}	Statistical weight assigned to data points, i, in box b
w_{ij}	Weight assigned to the ith data point in the jth dataset
Y_j	Mean strain of "n" experimental creep or shrinkage strain data points
Y_k	Average experimental creep or shrinkage strain within the kth time interval
Y_{ij}	Observed i^{th} creep or shrinkage strain in j^{th} dataset
Y_{ik}	Observed creep or shrinkage strain for the ith data point in interval k
$\overline{Y}$	Average test creep or shrinkage strain for all time intervals
y_{ij}	Predicted i^{th} creep or shrinkage strain in j^{th} dataset
y_{ik}	Predicted creep or shrinkage strain for the ith data point in interval k
$\overline{y}$	weighted mean of the observed creep or shrinkage strain values
$\boldsymbol{\alpha}$	Gilbert and Kilpatrick's empirical creep factor
Δ_{cr}	Deflection due to creep
Δ_i	Initial or short-term deflection
Δ_{LT}	Total long-term deflection due to creep and shrinkage (i.e., $\Delta_{cr}+\Delta_{sht,t}$)
Δ_T	Total deflection, $(\Delta_i + \Delta_{LT})$
$\Delta_{sht,t}$	Deflection due to restrained shrinkage at time t
$\chi(t,t_o)$	Aging coefficient at age t and age at initial loading t_o
ε_{cr}	Creep strain at extreme compression fiber
ε_i	Instantaneous compression concrete strain at extreme fiber
$\varepsilon_{sh,t}$	Shrinkage strain at time t

$\varepsilon_{sh,u}$	Ultimate shrinkage strain at extreme compression fiber
$\varepsilon_{sh,t,B}$	Residual strain at the top fiber at time t
$\varepsilon_{sh,t,T}$	Residual strain at the bottom fiber at time t
$\overline{\varepsilon_{cr}(t,t_o)}$	Creep strain at time t for concrete loaded at time t_o
$\emptyset$	Ultimate creep coefficient
$\emptyset(t,t_o)$	Creep coefficient at age t and for concrete loaded at time t_o
ρ	Tension steel reinforcement ratio
ρ'	Compression steel reinforcement ratio
ρ_b	Balanced reinforcement ratio
ψ_{cr}	Curvature due to creep
ψ_i	Curvature due to applied load
$\psi_{sh,L}$	Shrinkage curvature computed at the left support
$\psi_{sh,M}$	Shrinkage curvature computed at the midspan
$\psi_{sh,R}$	Shrinkage curvature computed at the right support
$\psi_{sh,t}$	Net curvature due to restrained shrinkage at time t
$\overline{\psi_{cr}(t,t_o)}$	Average curvature due to creep at time t for concrete loaded at time t_o
$\sigma_{sh,t,B}$	Residual shrinkage stress at the bottom fiber at time t
$\sigma_{sh,t,T}$	residual shrinkage stress at the top fiber at time t
$\overline{\sigma(t,t_o)}$	Stress in the concrete at time, t, after creep has taken place

<div align="center">Chapter 1</div>

1 Background and Research Objectives

1.1 Deflection of Reinforced Concrete Flexural Members

Structural members must be designed to meet ultimate and serviceability limit states requirements. Ultimate limit states dictate the required strength of flexural members, which can be accurately quantified using the well-understood, mechanically sound equations of equilibrium. In fact, the flexural strength design of reinforced concrete members is further optimized using widely available high-strength steel (e.g., 650MPa yield strength), which implies that smaller cross-sections are needed to satisfy strength requirements. The major serviceability limit states in concrete structures are: excessive deflection; excessive cracking; and, excessive vibration (MacGregor and Bartlett, 2000). Building codes impose upper limits on the allowable deflection of concrete members to preserve the functionality of the structure (e.g., prevent damage to non-structural elements or aesthetic discomfort). Therefore, the design of reinforced concrete members is often governed by the deflection serviceability requirements. The total deflection is computed as the summation of the short-term deflection due to the applied load, and long-term deflections due to the sustained portion of the applied load and to warping due to restrained shrinkage.

Short-term deflections are computed using conventional structural analysis methods. The short-term deflection, Δ_i, of a cracked, simply supported concrete member carrying a uniformly distributed load is: $\Delta_i = 5M_a\ell_n^2/48E_cI_e$ where M_a is the magnitude of the applied service moment, ℓ_n is the clear span length, E_c is the Young's Modulus of concrete, and I_e is the effective moment of inertia of the cracked concrete cross-section. The method for computing I_e presented in the ACI 318-14 (ACI, 2014) and the CSA A23.3-14 (CSA, 2014) code provisions was initially proposed by Branson (1965). Bischoff (2007) showed that Branson's (1965) Equation is based on an incorrect mechanical model and proposed a new equation based on a correct mechanical model. The CSA A23.3-14 code provisions also require computing I_e based on half the modulus of rupture of concrete to account for the error in the equation and the effect of restrained shrinkage, which reduces the moment required to initiate cracking in a member. Scanlon and Bischoff (2008) recommend using

the Bischoff Equation based on two-thirds the modulus of rupture. Mancuso and Bartlett (2016) showed that using the Branson Equation based on half the modulus of rupture or the Bischoff Equation based on two-thirds the modulus of rupture yields very similar results.

The long-term deflection of steel-reinforced concrete members under sustained loads is due to the time-dependent effects of creep and shrinkage of concrete. Both creep and shrinkage are intrinsic material properties that are significantly influenced by the concrete mix design and ambient environmental conditions. However, unlike shrinkage, creep is load-dependent and is therefore influenced by factors pertaining to the loading conditions (e.g., age at loading and the magnitude of the applied compression stress). There are four widely recognized mathematical models for computing creep and shrinkage strains in plain concrete, that account for different factors and are at least partly empirical.

The long-term deflections are computed using ACI 318-14 or CSA A23.3-14 by simply applying a multiplier to the short-term deflection and are based on empirical methods proposed by Branson (1977). The A23.3 Multiplier Method implies that the magnitude of the long-term deflection is twice the short-term deflection for members with a sustained load duration greater than 60 months. Other design aids such as ACI 435-95 (ACI 435, 1995) and the Cement Association of Canada's Concrete Design Handbook (CAC, 2016) present a more detailed method for computing incremental deflections due to creep and shrinkage, also based on empirical methods proposed by Branson (1977). Using this method, creep deflections are computed as a direct function of the short-term deflection, and shrinkage deflections based on the thickness of the member and the tension and compression reinforcement ratios. These design aid and code provisions have not been modified since their introduction more than four decades ago (with the exception of the requirement that the effective moment of inertia be computed based on a reduced modulus of rupture introduced in 2009 (CSA, 2009)).

Computing long-term deflections using a single multiplier ignores the creep and shrinkage characteristics of concrete and is therefore fundamentally wrong (Gilbert, 2001). It does not explicitly account for: the change in the location of the neutral axis caused by creep; the residual strains at the top and bottom fibers due to restrained shrinkage (which can cause significant deflections even in unloaded members (Miller, 1958)); ambient

environmental conditions; and, age at loading. A note to Clause 9.8.2.5 in CSA A23.3-14 (CSA, 2014) notes that the Multiplier Method may yield unconservative deflections for members loaded at ages less than 28 days and recommends applying an additional multiplier to the total (immediate plus long-term) deflection. The additional multiplier is a function of the age at loading and ranges from 1.0 for members loaded at 28 days to 1.6 for members loaded at 7 days. However, the theoretical background and techniques used to derive this multiplier remain unclear.

Several studies including Large (1957), Yu & Winter (1960), Pauw and Meyers (1964), and Branson (1977) attempted to calculate the long-term deflection of cracked reinforced concrete members by analytically computing incremental deflections due to creep and shrinkage but failed to achieve satisfactory agreement with experimental data (Branson, 1977). This was primarily caused by difficulties in calculating the cracked moment of inertia and the associated elastic neutral axis location of doubly reinforced members. Further, these studies computed the effective moment of inertia of cracked sections based on empirical methods and did not account for the effect of restrained shrinkage on the short-term deflection. Other studies that were primarily focused on prestressed concrete, including Neville et al. (1983) and Dilger (1988), presented analytical methods for computing incremental deflections due to creep and shrinkage in uncracked sections (because prestressed concrete is typically uncracked at service loads). However reinforced concrete members are typically cracked at service loads and these methods must be refined to be applicable for use in the analysis and design of reinforced concrete members.

Thus, it is necessary to reevaluate the existing provisions for computing long-term deflections using the most recent methods for computing the short-term deflection since Branson's (1977) methods are strongly dependent on the short-term deflection. Further, analytical methods for computing long-term deflections can be derived based on procedures by others (e.g. Pauw and Meyers (1964) and Dilger (1988)) while accounting for the effects of restrained shrinkage on the effective moment of inertia and using mechanics-based methods for computing the neutral axis depth of singly and doubly reinforced members presented in Chapter 6 of the CAC Concrete Design Handbook (CAC, 2016).

1.2   Research Objectives

The primary objectives of this research are to:

1. Investigate factors that influence creep and shrinkage of concrete and evaluate existing mathematical models for computing creep and shrinkage strains using the most recent studies.

2. Critically evaluate existing empirical methods for computing incremental deflections due to creep and shrinkage (e.g., methods presented in the CAC Concrete Design Handbook (CAC, 2016)) and, if necessary, propose improved, Mechanics-Based Methods. The accuracy of the existing and proposed methods should be quantified using test/predicted ratios.

3. Critically evaluate the A23.3 Multiplier Method for computing the long-term deflections and, if necessary, present alternative simplified methods for computing long-term deflections based on short-term deflections.

1.3   Thesis Outline

Chapter 2 presents an overview of the factors that influence the creep and shrinkage of concrete as well as the widely recognized mathematical models for computing creep and shrinkage strains. It presents a review of the most recent studies that evaluate the accuracy of the prediction models and provides an overview comparison of the accuracy of the models based on the different studies.

Chapter 3 presents the existing methods for computing long-term deflections due to creep and shrinkage including a detailed description of their derivation. It also presents Mechanics-Based detailed methods for computing incremental deflections due to creep and shrinkage. The relevant experimental data on the long-term deflection of reinforced concrete beams were investigated and used to assess the accuracy of the existing and proposed methods for computing creep and shrinkage deflections. The proposed Mechanics-Based Methods are somewhat laborious but account for the necessary factors that influence creep and shrinkage deflections and are therefore the most accurate.

Chapter 4 presents a critique of the A23.3 Multiplier Method and identifies several shortcomings. It also presents an Alternative Simplified Method for computing the long-term deflections that is calibrated using the aforementioned Mechanic-Based Methods. A comparison between the A23.3 Multiplier Method and the Alternative Simplified Method is also presented.

Chapter 5 presents the summary, conclusions, and recommendations for future work.

Chapter 2

2   Comparison of Models for Computing Creep and Shrinkage Strains

As a first step towards assessing criteria for computing long-term deflections of reinforced concrete beams, it is appropriate to review the state of the knowledge concerning shrinkage and the creep of axially loaded specimens. in particular, the critiques by others of the four methods presented in ACI 209 (ACI 209, 2008) will be assessed. The details of these methods are clearly described in Appendix A of the ACI 209 *Guide of Modeling and Calculating Shrinkage and Creep in Hardened Concrete* (ACI 209, 2008). While some conclusions are drawn about the relative accuracy of these methods it will also be demonstrated that the various comparisons by others are inconsistent and yield uncertain conclusions.

2.1   Behavior of Plain Concrete in a Drying Environment

Deformation of concrete in a drying environment is attributed to two phenomena, creep and shrinkage. The former is a time-dependent deformation that occurs under sustained load, whereas the latter is independent of the applied stresses. Creep can be further categorized into basic creep, an intrinsic material property that is independent of factors relating to dissipation of water from the mix, and drying creep, which is defined as additional creep that occurs due to drying, but in excess of shrinkage (ACI 209, 2008). Similarly, shrinkage can be divided into drying and chemical (autogenous) shrinkage. Drying shrinkage occurs over a longer time span and is the most significant when considering long-term deformations of normal-strength concrete (Gilbert, 1988). High-strength concretes tend to undergo significant autogenous shrinkage (ACI 209, 2008; FIB, 2012) that therefore must be accounted for. However, it is unnecessary to differentiate between the various types of shrinkage when considering normal-strength concretes, and unless otherwise stated, the term shrinkage will hereafter refer to drying shrinkage.

Creep and shrinkage are affected to various degrees by (ACI 209, 2008): environmental factors including humidity and temperature; cement matrix properties including water/cement ratio and aggregate stiffness; and, factors pertaining to casting, curing, handling, and loading of the concrete. Models for calculating the creep and shrinkage

strains tend to account for different parameters, as will be discussed in the following subsections.

Table 2-1 indicates some factors considered to have the greatest impact on creep and shrinkage in concentrically loaded specimens, including their influence on the ultimate creep and shrinkage strains. Arrows pointing upwards indicate an increase of a particular parameter or the associated creep or shrinkage response phenomenon, and the opposite convention holds true. Apart from the aggregate stiffness, ACI 209 suggests that these are the most basic parameters that need to be included in any creep and shrinkage model (ACI 209, 2008). Creep is a load-dependent deformation and is often quantified using a compliance function. Compliance is defined as the sum of elastic and creep strains produced by a unit stress and so is usually reported in microstrains/MPa (ACI 209, 2008). The terms creep strain and compliance strains will be used interchangeably in the remainder of this chapter. Both basic and drying creep are greatly influenced by the age at loading, magnitude of the applied load, and compressive strength of the concrete. Additionally, drying creep is greatly affected by factors that contribute to the loss of moisture from the concrete, such as the water/cement ratio, size of the member, drying period before loading, and the ambient relative humidity. Shrinkage is also a drying property and is therefore influenced by the same factors.

Table 2-1: Effect of Different Parameters on Creep and Shrinkage Strains

Parameter		Shrinkage	Basic Creep	Drying Creep
Aggregate stiffness and content	↑	↓	↓	↓
Age at loading	↑	-	↓	↓
Relative humidity	↑	↓	-	↓
Volume/Surface area	↑	↓	-	↓
Water/Cement (or 1/f'$_c$)	↓	↓	↓	↓
Magnitude of applied load	↓	-	↓	↓
Drying period before loading	↑	↓	-	↓

Increased stiffness of both the fine and coarse aggregates has been shown to play an important role in reducing shrinkage and creep of concrete (Brooks, 2005; ACI 209, 2008). This is intuitive because creep and shrinkage originate in the cement paste, and aggregates are normally significantly stiffer than the cement paste. Therefore, stiffer aggregates are expected to provide a considerable restraint to creep and shrinkage. Brooks (2015) showed that creep of concrete is highly sensitive to values of elastic modulus of aggregate less than 70 GPa, but is relatively intensive to the aggregate stiffness for higher elastic moduli. Moreover, shrinkage is an intrinsic material property of cement paste and concrete mixtures with a high volume of aggregate will shrink less than those with high volumes of cement.

2.2   Experimental Data on Creep and Shrinkage

A database containing results from numerous experimental programs that studied the long-term behavior of plain concrete was created by Bazant and Panula (1978). It has since been further developed by other researchers and named the RILEM Databank (Mija, Roman, & Bazant, 2015). As of 2008, the RILEM Databank consisted of 426 shrinkage and 518 creep data sets. In 2015, a group of researchers led by Bazant presented a major expansion to the RILEM Databank and named it the NU (Northwestern University) Database (Mija, Roman, & Bazant, 2015). This expansion was primarily intended to include more data on modern high-performance concretes that are significantly influenced by chemical reactions other than hydration. The most recent test results in the database are from 2017.

Existing creep and shrinkage models have been validated against and/or fitted to data in the RILEM Databank. Therefore, unless subclassifications have been made, such as dividing shrinkage into chemical and drying shrinkage, most models are applicable to normal-weight concretes. A table showing the range of applicability of each model in ACI 209R-08 (2008) indicates that models that do not account for chemical shrinkage are applicable to concretes with compressive strengths up to 80 MPa.

2.3   Creep and Shrinkage Models

There are four widely recognized mathematical models for calculating ultimate strains due to creep and shrinkage: CEB-FIP MC90-99 (Comité Europeen du Béton, 1993), ACI 209 (ACI 209, 2008), GL2000 (Gardner & Lockman, 2001), and B3 (Bazant and Baweja, 1995, 2000). Some models, such as ACI 209 and GL2000, are entirely empirical. Others,

although based on mathematical derivations that attempt to evaluate physical phenomena, do not necessarily provide more accurate predictions, as will be demonstrated. Irrespective of the basis of the model, all were calibrated to fit experimental data and are therefore at least partly empirical. The CEB-FIP MC90-99, GL2000, and B3 models were all calibrated using data sets selected from the RILEM Databank.

2.3.1   Scope of Models

Each model was developed by a different group of researchers and accounts for different factors that are considered to influence creep and shrinkage. Table 2-2 summarizes the parameters explicitly accounted for in each model. All models account for the basic parameters that affect creep and shrinkage, as outlined in Section 2.1 and Table 2-1. However, they do not consistently account for other critical parameters such as: specimen shape; compressive strength at age of loading; Young's Modulus at age of loading; cement type; water/cement ratio; aggregate/cement ratio; and, curing type. Models B3 and ACI 209 require the largest number of parameters (15 and 14 parameters, respectively), and GL2000 requires the least (10 parameters). The most significant shortcoming of all methods is their failure to account directly for the influence of the stiffness of aggregate, which was shown to have a substantial impact on the creep and shrinkage of concrete (Brooks, 2005).

The accuracy of models is inherently limited by the difficulties in defining strength development of cementitious materials and assumptions used to relate concrete strength to modulus of elasticity (Gardner & Lockman, 2001). Therefore, it is unrealsitic for models to predict creep and shrinkage strains within plus or minus 20% of test data (ACI 209, 2008).

Table 2-2: Variables Explicitly Considered in Models

	Creep				Shrinkage			
	MC90-99	ACI 209	B3	GL2000	MC90-99	ACI 209	B3	GL2000
Relative Humidity	✓	✓	✓	-	✓	✓	✓	✓
Volume/Surface Area	✓	✓	-	✓	✓	✓	✓	✓
Specimen Shape	-	-	-	-	-	-	✓	-
28-day Compressive Strength	✓	✓	✓	✓	✓	-	✓	✓
28-day Young's Modulus	✓	✓	✓	✓	-	-	-	-
Compressive Strength at Age of Loading	-	✓	-	✓	-	-	-	-
Young's Modulus at Age of Loading	✓	✓		✓	-	-	-	-
Cement Type	✓	✓	✓	-	-	-	✓	✓
Water/Cement	-	-	✓	-	-	-	-	-
Aggregate/Cement	-	-	✓	-	-	-	-	-
Curing Types	-	✓	✓	-	-	✓	✓	-
Curing Period	-	-	-	-	✓	✓	✓	✓
Age at Loading	✓	✓	✓	✓	-	-	-	-

2.3.2 CEB-FIP MC90, MC90-99, & FIB MC2010

The first Commité European du Béton – Federation Internationale de la Précontrainte (CEB-FIP) model was published in 1970 and used multipliers obtained from both charts and equations to account for some of the parameters shown in Table 2-1 (Comité Euro-International du Béton, 1970). A 1978 revision divided creep into reversible and irreversible creep (Comité Euro-International du Béton, 1978). The CEB -FIP model code,

CEB-FIP MC90, abandoned the division of creep into components, replaced charts with mathematical equations, and was calibrated using the RILEM Databank (ACI 209, 2008). The MC90 version contains the current form of the model and, as it is still based on laboratory tests, is mostly empirical.

The CEB-FIP MC90 model for shrinkage does not differentiate between drying and autogenous shrinkage and is therefore only applicable to ordinary concretes with compressive strengths between 12 and 80 MPa(Comité Euro-International du Béton, 1993). The 1999 version of CEB-FIP model distinguishes between drying and autogenous shrinkage and so is suitable for normal and high-strength concretes with compressive strength ranging from 15 to 120 MPa (Comité Euro-International du Béton, 1999). This version was named the CEB-FIP MC90-99 model due to its close resemblance to its predecessor. Moreover, the slightly less complex CEB-FIP MC90 is still applicable to concretes with ordinary compressive strengths and it is the basis of some widely used analytical procedures such as those presented in the Canadian Highway Bridge Design Code (CHBDC) (CSA, 2014). As shown in Table 2-2, CEB models do not explicitly account for the curing period and conditions, which may impact the ultimate creep and shrinkage strains.

The CEB and FIP associations merged in 1998 to create a unified organization, Federation Internationale du Béton (FIB). FIB developed a model in 2012 that was based on CEB-FIP MC90-99, but with creep classified as basic and drying creep (International Federation for Structural Concrete (fib), 2012). The model also introduced a correction factor for the creep coefficient to account for sustained compressive concrete stress levels between 0.4 f'_c and 0.6f'_c. However, the relationships to calculate creep remain empirical and the shrinkage equation remained unchanged from that in CEB-FIP MC90-99. Figure 2-1 shows the minimal differences between compliance strain of normal-strength concrete calculated using MC90-99 (that is similar to MC90) and FIB MC2010. The FIB model has not been adopted by Canadian or American standards and few studies have explored its performance in comparison to other models using available test data. For this reason, and because it is very similar to MC90-99, it will not be considered further in the current study.
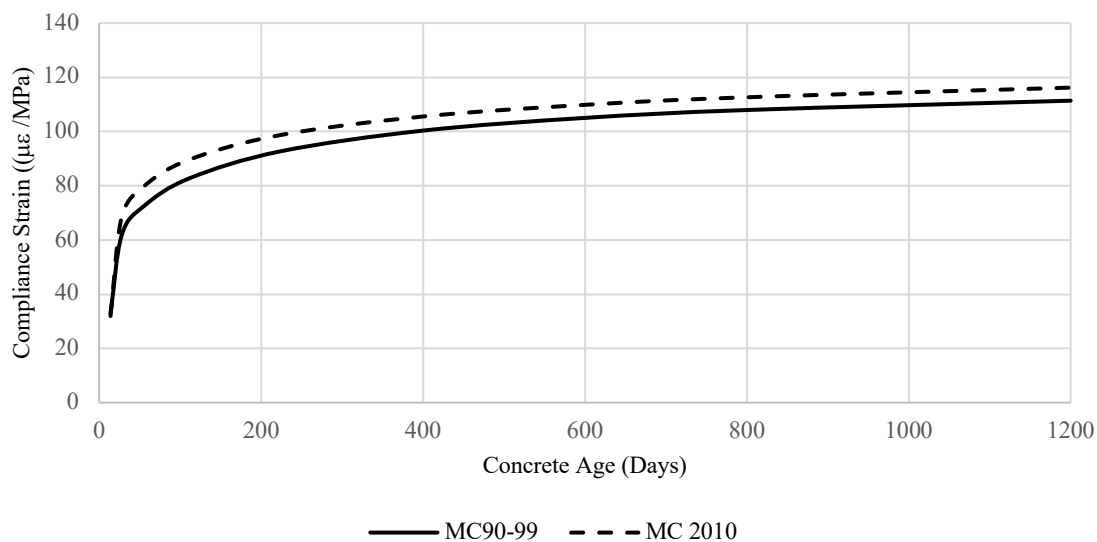
Figure 2-1: CEB-FIP MC90-99 & FIB MC2010 Compliance

2.3.3 ACI209R-92 Model

The ACI 209R-92 model is an empirical model originally created by Branson and Christianson in 1971, before the development of the RILEM Databank, and has undergone minor changes in 1978, 1982, and most recently 1992 (ACI 209, 1992). It was initially designed for the precast industry and was subsequently modified to be applicable to cast-in-place concretes, so its current form is applicable to both. Moreover, the model can be tuned based on any available data. At its most basic level, it only requires information on: age of concrete when drying starts; age at loading; curing method; relative humidity; element size; and, cement type. However, factors such as concrete slump, aggregate content, air content, and cement content can also be accounted for if such information is available. The impact of size and shape of the member on the time functions for creep and shrinkage can also be accounted for, which is necessary because larger members undergo drying at a slower rate. Unlike concrete composition correction factors, which are normally not excessively large and tend to offset each other (ACI 209, 2008), the effects of size and shape are believed to have an influence on the ultimate shrinkage strain and the early-age compliance strain (Gardner & Lockman, 2001). Figures 2-2 and 2-3 show that using the values recommended in ACI 209R-92 for the size and shape factor is a slightly more conservative approach than calculating the factor using equations provided in the same

standard. However, the discrepancy of the ultimate shrinkage strain, Figure 2-2, is minimal, and the compliance discrepancy, Figure 2-3, is negligible.
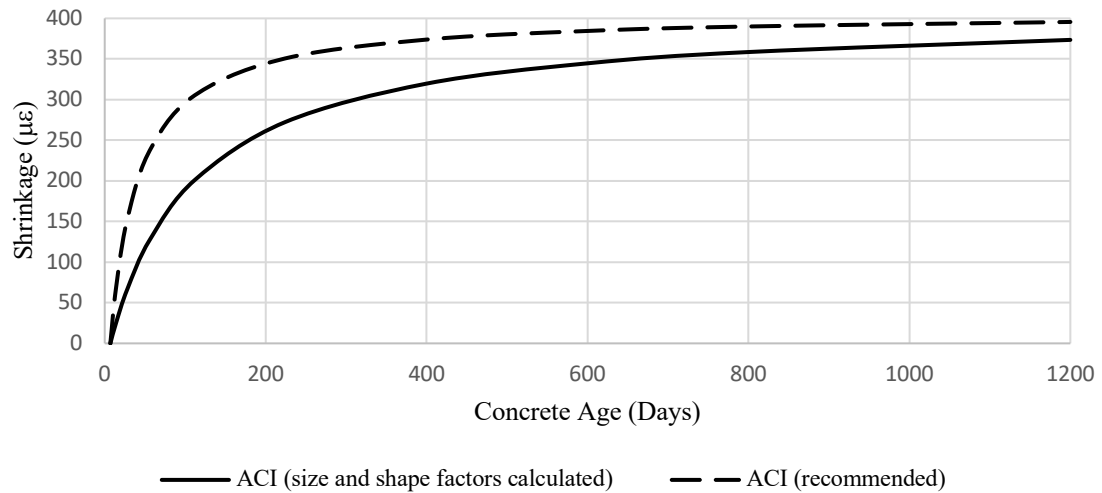
Figure 2-2: ACI 209 Shrinkage Strain
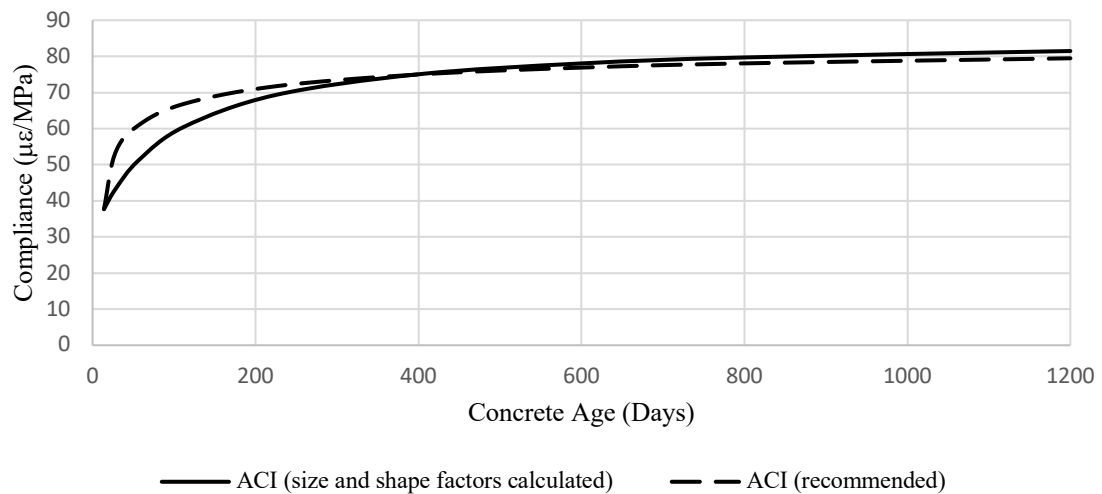
Figure 2-3: ACI 209 Creep Strain

There are many shortcomings associated with the ACI 209R-92 model. Its empirical nature makes it incapable of modelling the actual physical phenomena of creep and shrinkage. It fails to distinguish between drying and autogenous shrinkage, and between basic and drying creep. Instead, creep and shrinkage are predicted by calculating asymptotic ultimate

strain values and multiplying them by hyperbolic functions that approximate the temporal development of creep and shrinkage strains.

2.3.4   Bazant and Baweja Model B3

The Bazant-Baweja model, commonly referred to as B3, was initiated by Bazant (1978), and subsequently revised to account for additional factors that were believed to impact creep and shrinkage. The current (2000) model is based on the mathematical description of over ten physical phenomena including: effect of microcracking; linear and non-linear diffusion theory; solidification theory; desorption isotherm; activation energy theorem; and, spatial average of pore relative humidity over the cross section (Bazant and Kim, 1991; Bazant and Panula, 1978). More details on the physical phenomena considered in the B3 model are reported in Bazant and Panula (1978). The classification of creep as either basic or drying creep entails using two different compliance functions and taking their sum to obtain the overall creep coefficient. This allows the user to account for the physical phenomena responsible for basic and drying creep separately. The B3 Model is also the only model to account for water/cement ratio, aggregate/cement ratio, and specimen shape, as shown in Table 2-2. The compliance function for basic creep is composed of three empirical parameters to define aging: viscoelasticity; nonaging viscoelasticity; and, aging flow. These parameters are a function of the compressive strength and water/cement ratio of the mix. The compliance function defining drying creep is a function of the relative humidity, ultimate shrinkage, and compressive strength. Once compliance functions for basic and drying creep have been determined, they are added to an empirical function representing the instantaneous strain due to the applied stress to determine the average compliance.

The procedure in the B3 Model for calculating shrinkage strains accounts for size, shape, and relative humidity, and uses a time function that is based on the ratio of the 600-day Young's modulus to the Young's modulus at a given age. The initial form of this model (1995) did not account for autogenous shrinkage that mostly occurs before stripping the form and subsequently occurs only in the core (Bazant and Baweja, 2000). However, an extension to the model (Bazant and Baweja, 2000) allows calculation of autogenous shrinkage and so makes it applicable to a wider range of concretes.

2.3.5   GL2000 Model

The GL 2000 procedure was proposed by Garner and Lockman (2001, 2004) as a simplified design-office procedure for calculating creep and shrinkage strains. It requires basic information that is generally available at the time of design including: age of the concrete when drying starts; age at loading; relative humidity; size; and, cement type. Methods for calculating the mean compressive strength given only the specified design strength are provided. However, Gardner and Lockman suggest that higher accuracy could be achieved by using experimental values for mean compressive strengths. The aggregate stiffness, if available, can also be accounted for by using the average of the experimental cylinder strength and that back-calculated from the measured modulus of elasticity of the concrete in equations for creep and shrinkage.

2.4   Investigation of Model Accuracy by Others

2.4.1   Challenges in Investigating the Accuracy of Models

An analytical comparison between prediction models for a given set of parameters (i.e. not obtained from test data), such as that reported in Appendix C of ACI 209 (2008), indicates that their predicted creep and shrinkage strains differ by up to 30%. A comprehensive analysis would ideally compare strains obtained from these prediction models to those measured in actual structures. However, there is a lack of accurate long-term data to make such a comparison and the next best alternative is to use laboratory test data.

The RILEM Databank and the NU Database are valuable resources to facilitate a realistic comparison between models. However, there is a great deal of uncertainty associated with data they contain. First, the type of cement used in different datasets is not adequately described, which is problematic since cement properties can vary between countries. For example, Cement Types I-IV in America do not correspond to identically labelled cement types in Europe. While the manufacturing processes are similar, the standard test methods are different. For instance, ASTM C109 (American Society for Testing and Materials, 2016) specifies the use of 50mm cubes to measure the compressive strength of hydraulic mortars, whereas its European counterpart, EN 196 (British Standards Institute, 2016), utilizes 40x40x160mm prisms. Moreover, the RILEM Databank lacks: test results on the creep and shrinkage for large members that are representative of real structural elements;

creep data for drying before loading or loading before drying; and, long-term creep and shrinkage results (Brooks, 2015). Another source of uncertainty is ambiguity in interpreting the actual duration meant by authors when referring to "initial elastic" and instantaneous" strains that are subtracted from strain measurements to obtain creep strains (Bazant and Panula, 1978).

In addition to uncertainties in the data, researchers do not agree on which of the datasets are relevant for model development (ACI 209, 2008). Since all models are mostly empirical, using parameters that are strongly correlated to the data selected, discrepancy between models is inevitable.

2.4.2   Statistical Assessment of Models Presented in ACI 209R-08

A direct assessment of the accuracy of models can be carried out from test/predicted ratios using statistical indicators such as coefficient of variation, mean deviation, and mean square error, obtained using the method of least squares. The coefficient of variation, a dimensionless quantity equal to the sample standard deviation divided by the sample mean, is commonly used to quantify scatter, and so indicate the accuracy of the predicted strains compared to the measured values. An analytical method that yields a low coefficient of variation is desirable, whereas a high value implies greater variability of the test/predicted ratios.

Table 2-3 was extracted from ACI 209 (2008) and presents the results of statistical assessments of predictions models carried out by Gardner (2004) and Al-Manaseer and Lam (2005). It shows the coefficients of variation (COV) for test/predicted ratios as defined using test values obtained from the RILEM Databank and values predicted using each model. GL2000 and B3 yielded the lowest coefficients of variation according to both studies and are therefore deemed most accurate. The study by Gardner (2004) offers a comparison of the performance of the models when all the required data are available, as well as when only the average compressive strength (which is often the only information available at the time of design) is known. GL2000 yielded the most accurate results when only the compressive strength, f'_c, is known. Since studies by Al-Manaseer and Lam (2005) and Gardner (2004) were based on different data sets, the coefficients of variation shown can only be compared across a row but not along a column.

Table 2-3: Statistical Comparison of Models Using Coefficient of Variation as Reported in ACI 209 (2008)

	Study	COV Method	Overall Coefficient of Variation							
			MC90-99		ACI 209		B3		GL2000	
Available Data			All	f'c Only	All	f'c Only	All	f'c Only	All	f'c Only
Shrinkage	Al-Manaseer & Lam	CEB	37%	-	46%	-	41%	-	37%	-
		BP	48%	-	102%	-	55%	-	46%	-
	Gardner	Gardner	25%	32%	41%	34%	20%	31%	19%	25%
Creep	Al-Manaseer & Lam	CEB	38%	-	48%	-	36%	-	38%	-
		BP	80%	-	87%	-	61%	-	47%	-
	Gardner	Gardner	39%	37%	30%	-	27%	29%	22%	26%

2.4.2.1 Al-Manaseer and Lam (2005)

Al-Manaseer and Lam (2005) assessed the accuracy of models using five statistical indicators: the residual method; the coefficient of variation as computed by Bazant and Panula (BP) (1978), V_{BP}; the coefficient of variation as computed by CEB, V_{CEB}; mean square error as computed by CEB, F_{CEB}; and, the mean deviation as computed by CEB, M_{CEB}. Moreover, points beyond the range of applicability of an individual model were excluded from the study. Table 2-4 was extracted from ACI 209 (2008), as reported by Al-Manaseer and Lam (2005), and shows the ranges of applicability of the four models. Table 2-5 shows the number of data points used in the statistical analysis of test/predicted ratios for each model. The original publication by Al-Manaseer and Lam (2005) did not include a statistical analysis of the test/predicted ratios from the CEB-FIPMC90-99 model, even though it is included in the analysis by the same authors presented in ACI 209 (2008). Since the number of data points used to calibrate each model is presented in Al-Manaseer and Lam (2005) but not in ACI 209 (2008), the exact number of points used to analyze the test/predicted ratios for the CEB-FIP MC90-99 model is unknown.

Table 2-4: Range of Applicability of Prediction Models

	Model			
	ACI 209	B3	MC90-99	GL2000
f_c'(28 days), MPa	-	17-70	15-120	16 -82
Aggregate/Cement	-	2.5-13.5	-	-
Cement Content (kg/m^3)	279-446	160-720	-	-
Water/Cement	-	0.35-0.85	-	0.4-0.6
Relative Humidity (%)	40-100	40-100	40-100	20-100
Type of Cement	I, III	I, II, III	I, II, III	I, II, III
Curing Period, t_c (days)	≥ 1	≥ 1	< 14	≥ 1
Loading Age, t_o (days)	≤ 7	$t_o \geq t_c$	> 1	$t_o \geq t_c \geq 1$

Table 2-5: Number of Data Points used by Al-Manaseer and Lam (2005)

	Model			
	ACI 209	B3	MC90-99	GL2000
Shrinkage	2642	2388	Not Reported	1677
Creep	4795	5894	Not Reported	4166

Al-Manaseer and Lam (2005) computed the coefficient of variation using the different methods proposed by the CEB (1990), Bazant and Panula (1978), and Gardner (2004). All involve dividing the data into time intervals to account for the varying rates of change of creep and shrinkage strains. The CEB method (CEB-FIP, 1990) requires grouping the data considered in the study into 6 time intervals: 0-10, 11-100,101-365, 366-730, 731-1095,

and >1095 days and computing a mean coefficient of variation, V_{CEB}, for each interval separately. Since the RILEM Databank is comprised of data from studies by different researchers (referred to as data sets hereafter), V_{CEB} for a single time interval is computed by taking the root mean square of the individual coefficients of variation for each data set:

$$V_{CEB} = \sqrt{\frac{1}{N} \Sigma_{j=1}^{N} (V_j)^2} \tag{2-1}$$

where N is the number of data sets considered within each interval and V_j is the coefficient of variation of the test/predicted ratio for the jth data set, computed as

$$V_j = \frac{S_j}{Y_j} \tag{2-2}$$

where Y_j is the mean of "n" experimental creep or shrinkage strain data points, Y_{ij}, in data set j:

$$Y_j = \frac{1}{n} \Sigma_{i=1}^{n} (Y_{ij}) \tag{2-3}$$

S_j is the standard error of the creep or shrinkage strain obtained from test j, and is computed using the difference between the observed, Y_{ij} and predicted, y_{ij}, values:

$$S_j = \sqrt{\frac{1}{n-1} \Sigma_{i=1}^{n} (Y_{ij} - y_{ij})^2} \tag{2-4}$$

Al-Manaseer and Lam (2005) rank the various prediction models based on V_{CEB} values for the time interval t > 1095 days. V_{CEB} values for early-age intervals are not reported or considered in ranking models, presumably because only the ultimate creep or shrinkage strains are typically of practical importance in deflection calculations.

The V_{CEB} values reported in ACI 209 (2008) as shown in Table 2-3 are similar to those presented in Al-Manaseer and Lam (2005), but the two documents present different methods for computing V_{CEB}. Al-Manaseer and Lam (2005) compute unique V_{CEB} values for each time interval using V_j computed for individual data sets within that interval, which results in six unique V_{CEB} values. However, the method reported in Appendix B of ACI 209 (2008) requires computing V_j for all time intervals (as opposed to data sets), which would yield a single overall V_{CEB} value representing all six time intervals.

The Bazant and Panula (BP) method requires dividing the data in a particular data set into 4 time intervals or "decades" (0-10, 10-100 101-1000, and 1001-10000 days) and assigning each data point a weight based on the decade in which it falls and number of data points in that decade. Moreover, all data points in a decade are assigned equal weights. The COV for each data set is computed using Equation (2-3). However, Y_j, the mean of "n" creep or shrinkage strain data points, Y_{ij}, in data set j and is given as

$$Y_j = \frac{1}{n_w} \Sigma_{i=1}^{n} (w_{ij} Y_{ij})$$
(2-5)

where n_w is the sum of the weights assigned to each data point in a data set. Since all the data points in a data set are assigned equal weights, w_{ij}/n_w is equal to $1/n$. The weight assigned to each data point, w_{ij}, is based on the decade in which it falls and is given as

$$w_{ij} = \frac{n_{ij}}{n_d n_{ik}}$$
(2-6)

where n_{ij} is the number of data points in data set j, n_d is the number of decades on the logarithmic scale spanned by the measured data in data set j, and n_{ik} is the number of data points in one decade.

The COV of a single data set is computed as

$$V_{BPj} = \frac{1}{Y_j} \sqrt{\frac{1}{n_w-1} \Sigma_{j=1}^{n} (w_{ij}(Y_{ij} - y_{ij}))^2}$$
(2-7)

The overall coefficient of variation of a prediction model, V_{BP}, is computed as

$$V_{BP} = \sqrt{\frac{1}{N} \Sigma_{j=1}^{N} (V_{BPj})^2}$$
(2-8)

where N is the number of data sets considered in the study and V_{BPj} is the COV of each data set.

Weighing the data points in a data set based on the decade in which they fall allows computing a single COV for each data set that is inclusive of all the time ranges and the overall COV computed using the individual coefficients of variation is representative of all the time intervals and data sets. Therefore, this approach will yield a single coefficient of variation that is representative of data in all four time intervals.

Other statistical indicators used by Al-Manaseer and Lam (2005) to rank models are the mean square error and the mean deviation. The mean deviation is a measure of variability that quantifies the average deviation of the predicted values from test values. Like the mean coefficient of variation, the data are divided into six time intervals and the mean deviation of a single data set within an interval, M_j, is computed using the mean predicted/test ratio (note, not test/predicted) as

$$M_j = \frac{1}{n} \sum_{j=1}^{n} \frac{y_{ij}}{Y_{ij}} \qquad (2\text{-}9)$$

The mean deviation of multiple data sets within a single interval, M_{CEB}, is computed as

$$M_{CEB} = \frac{1}{N} \sum_{j=1}^{n} M_j \qquad (2\text{-}10)$$

where N is the number of data sets within that interval.

The mean square error provides an indication of the accuracy of various models in predicting test values. It involves dividing data into six time intervals and computing the percent difference between test and predicted data points, f_{ij}, as

$$f_{ij} = \frac{y_{ij} - Y_{ij}}{Y_{ij}} * 100 \qquad (2\text{-}11)$$

The mean square error of the data points within a data set in an interval is computed as

$$F_j = \sqrt{\frac{1}{n-1} \sum_{i=1}^{n} (f_{ij})^2} \qquad (2\text{-}12)$$

The mean square error of data sets within a single time interval is computed as

$$F_{CEB} = \sqrt{\frac{1}{N} \sum_{j=1}^{N} (F_j)^2} \qquad (2\text{-}13)$$

The mean deviation and mean square error values reported in ACI 209 (2008) are extracted from Al-Manaseer and Lam (2005) and represent the mean deviation of the last time interval (t > 1095 days).

Table 2-6 shows the mean deviation and mean square error for each model as presented in ACI 209 (2008), based on Al-Manaseer and Lam (2005). If the predicted values are, on average, greater than the test values the model is overestimating the test results, with a mean deviation greater than 1. Similarly, an underestimating model has a mean deviation

less than 1. The mean square error is an indication of the scatter of the predicted-to-test ratios: lower values indicate less scatter and so a better fit. Table 2-6 shows that all models are nearly equally accurate in predicting creep strains, and the CEB-FIP M90-99 Model provides the most accurate predictions of shrinkage strains. It also shows that based on the mean square error, the ACI 209 Model is generally as accurate as the B3 and GL2000 Models in predicting shrinkage strains. However, it appears to be inferior to the B3 Model based on the mean deviation. These conclusions are clearly different than the ones made based on the coefficients of variation shown in Table 2-3.

Table 2-6: Mean Deviation and Mean Square Error in ACI 209 (2008) based on Al-Manaseer and Lam (2005)

	Mean Deviation				**Mean Square Error**			
	MC90-99	ACI 209	B3	GL2000	MC90-99	ACI 209	B3	GL2000
Creep	0.89	0.86	0.93	0.92	32%	32%	35%	34%
Rank	3	4	1	2	1	1	3	2
Shrinkage	0.99	1.22	1.07	1.26	65%	83%	84%	84%
Rank	1	3	2	4	1	2	3	3

2.4.2.2   Gardner (2004)

Gardner (2004) assessed the accuracy of the models based only on the coefficients of variation. His method for computing the coefficient of variation involves dividing data into seven sets of half-logarithmic intervals (3-9.9, 10-31.5, 31.6-99, 100-315, 316-999, and 1000-3159 days) and computing the average experimental creep or shrinkage strain within the kth time interval, Y_k, as

$$Y_k = \frac{1}{n}\sum_{i=1}^{n} Y_{ik} \tag{2-14}$$

where Y_{ik} is the observed creep or shrinkage strain for the ith data point in interval k. The root mean square error within each interval as

$$\text{RMS}_k = \sqrt{\frac{1}{n-1} \Sigma_{i=1}^{n} (y_{ik} - Y_{ik})^2} \qquad (2\text{-}15)$$

where y_{ik} is the predicted creep or shrinkage strain for the ith data point in interval k. The average test creep or shrinkage strain of all time intervals (without accounting for the number of data sets in each times interval) is computed as

$$\overline{Y} = \frac{1}{N_k} \sum_{k=1}^{N} Y_k \qquad (2\text{-}16)$$

where N_k is the number of time intervals.

The root mean square error for all the time intervals is computed as

$$\overline{\text{RMS}} = \frac{1}{N_k} \Sigma_{k=1}^{N_k} (\text{RMS}_k) \qquad (2\text{-}17)$$

Finally, the overall coefficient of variation is computed as

$$V_G = \frac{\overline{\text{RMS}}}{\overline{Y}} \qquad (2\text{-}18)$$

The methods proposed by Bazant and Panula (1978) and CEB are slightly different yet share the same fundamental mathematical principles. However, Gardner does not use the conventional definition of coefficient of variation (ACI 209, 2008). The average root mean square error, $\overline{\text{RMS}}$, is computed as a linear average and not the average of the squared individual root mean square errors, (i.e., RMS_k instead of RMS_k^2). This approach will always yield COV values smaller than those calculated using the CEB and BP methods, as shown in Table 2-3.

2.4.3 Statistical Assessment by Bazant and Li (2008)

Bazant and Li (2008) suggest that although the mean coefficient of variation is a rational method for investigating problems concerning structural safety, it is irrelevant when dealing with the central range of a distribution of errors. Existing methods for conducting statistical assessment of prediction models require dividing the overall dataset into time intervals or data sub-sets, computing the COV within each subset, and finally computing a

mean or overall COV. Therefore, data subsets are treated as separate, unrelated groups of data. However, these subsets are not independent because each value in a dataset is correlated to the next value, obtained at a later time, in the same data subset. They argue that ignoring this correlation could result in a misleading comparison of models. Additionally, factors other than age, such as size and relative humidity have a substantial effect on creep and shrinkage, and so must be considered in a comprehensive analysis. Therefore, the Bazant and Li divide the creep data into groups with similar loading ages and relative humidities, and shrinkage data into groups with similar drying periods and specimen sizes. These groups can be represented on a 3-dimensional histogram with loading age or drying age on one axis and size or relative humidity on another axis and frequency on the third axis: these groups are referred to as boxes (i.e. histogram boxes) and denoted by the subscript b hereafter. Although these are not the only factors affecting creep and shrinkage, the authors argue that introducing more variables could result in boxes containing fewer data points than needed to provide a meaningful statistical assessment.

Bazant and Li suggest that a comprehensive statistical analysis must be carried out with respect to the common trends, and not simply the data mean. Predictions from each model are plotted on a logarithmic scale and the least square regression line is fitted to the data. The residual errors (also called the band width) are computed as the vertical distance from the regression line to each test data point. The scatter of the test data is then analyzed based on two distinct dimensionless indicators of scatter that can be derived from the regression analysis. The first is the coefficient of variation of the residual errors, which characterizes the ratio of the scatter band width to the mean values, and therefore should be minimized. It is obtained by first computing the standard error, s, representing the standard error of regression as

$$s = \sqrt{\frac{n}{n-p} \sum_{b=1}^{N_b} w_b * \sum_{i=1}^{n} (y_{ib} - Y_{ib})^2} \qquad (2\text{-}19)$$

where p is the number of input parameters and N_b is the number of boxes. The statistical weight, w_{ib}, assigned to data points in each box (all the points in a single box are assigned the same weight i.e., $w_{ib} = w_b$), is computed as

$$w_{ib} = \frac{1}{n_{ib}\overline{w}} \tag{2-20}$$

where n_{ib} is the number of data points in box b and

$$\overline{w}_i = \sum_{b=1}^{N_b} \frac{1}{n_{ib}} \tag{2-21}$$

Next, the weighted mean of the observed value, $\overline{y}$, is computed as

$$\overline{y} = \frac{\overline{w}}{n} \sum_{b=1}^{N_b} w_{ib} \sum_{i=1}^{n_{ib}} Y_{ib} \tag{2-21}$$

The coefficient of variation of regression errors is computed as

$$V_{BL} = \frac{s}{\overline{y}} \tag{2-22}$$

The second step is to compute the correlation factor, which characterizes the ratio of the scatter band width to the overall standard deviation and should be maximized. It is computed as

$$c = \sqrt{1 - \frac{s^2}{\overline{s}^2}} \tag{2-23}$$

where s the standard error of regression as defined by Equation (2-19) and $\overline{s}^2$ is computed as

$$\overline{s}^2 = \sum_{b=1}^{N_b} w_b \sum_{i=1}^{n_{ib}} (Y_{ib} - \overline{y})^2 \tag{2-24}$$

Table 2-7 shows the results of a statistical comparison of the different models by Bazant and Li (2008). The models were compared using the two dimensionless indicators of scatter previously mentioned, the coefficient of variation of residual errors and the correlation coefficient. Moreover, a single set of data was used to compare all models. B3 and GL2000 were found to be the most accurate because they yielded the lowest coefficients of variation of residual errors and the highest correlation coefficients. These results, however, are not included in ACI 209 (2008).

Table 2-7: Statistical Comparison of Models by Bazant and Li (2008)

	COV of Regression of Errors				Correlation Coefficient			
	MC90-99	ACI 209	B3	GL2000	MC90-99	ACI 209	B3	GL2000
Creep	31.0%	42.6%	27.3%	30.2%	0.78	0.51	0.84	0.79
Rank	3	4	1	2	3	4	1	2
Shrinkage	47.4%	42.3%	28.5%	31.0%	0.70	0.77	0.90	0.89
Rank	4	3	1	2	4	3	1	2

2.4.4   Statistical Assessment by Al-Manaseer and Prado (2015)

Al-Manaseer and Prado (2015) conducted a statistical analysis to evaluate the accuracy of various prediction models based on the extended RILEM and NU databases. Five different statistical indicators were used to rank prediction models: the residual method; the coefficient of variation as computed using CEB method, V_{CEB}; mean square error as computed using CEB method, F_{CEB}; the mean deviation as computed using CEB method, M_{CEB}; and V_m, a coefficient of variation method based on the one proposed by Bazant and Li (2008).

Al-Manaseer and Prado (2015) suggest that the method proposed by Bazant and Li (2008) may provide misleading results because weights are applied to individual points rather than groups of data or boxes. They use a modified equation for computing the standard error, s, using the average of residuals for each box and a weight, w_b, assigned to each average value. Equation 2-19 for computing the standard error is rewritten as

$$s_m = \sqrt{\sum_{b=1}^{N_b} w_b * \frac{1}{n_b} \sum_{i=1}^{n} (y_{ib} - Y_{ib})^2} \qquad (2\text{-}25)$$

and compute the weighted mean of the measured value as

$$\overline{y_m} = \sum_{b=1}^{N_b} w_{ib} * \frac{1}{n_b} \sum_{i=1}^{n_i} Y_{ib} \qquad (2\text{-}26)$$

The modified coefficient of variation, V_m, is computed as

$$V_m = \frac{S_m}{y_m} \tag{2-27}$$

the quantities V_{CEB}, F_{CEB}, and M_{CEB} values are computed using Equations 2-1, 2-10, and 2-14, respectively. However, V_k, F_k, and M_k are computed for all the data within a time interval rather than for a single data set. V_k for time interval k is computed as

$$V_k = \frac{1}{Y_k} \sqrt{\frac{1}{n-1} \Sigma_{i=1}^{n} (y_{ik} - Y_{ik})^2} \tag{2-28}$$

where Y_k is the mean shrinkage or creep strain in data set k computed as

$$Y_k = \frac{1}{n} \Sigma_{i=1}^{n} (Y_{ik}) \tag{2-29}$$

F_k for a time interval is computed as

$$F_k = \sqrt{\frac{1}{n-1} \Sigma_{i=1}^{n} (f_{ik})^2} \tag{2-30}$$

where f_{ik} is the percent difference between test and predicted values computed using Equation 2-11.

Similarly, M_k for a time interval is computed as

$$M_k = \frac{1}{n} \Sigma_{i=1}^{n} \frac{y_{ki}}{Y_{ki}} \tag{2-31}$$

Therefore, only a single value of V_{CEB}, F_{CEB}, and M_{CEB} is computed, unlike Al-Manaseer and Lam (2005) where six values, one for each time interval, were computed for each set of test/predicted creep or shrinkage values.

The analysis of residual error is a basic statistical analysis tool that indicate bias and dispersion. Residual errors are computed by subtracting experimentally measured creep or shrinkage strains from those predicted using the various models: a positive value indicates an overestimating model and a negative value indicates an underestimating model.

Al-Manaseer and Prado (2015) assessed the sensitivity of prediction models to the data chosen from the RILEM and NU Databanks using a three-phase screening process and ranked the performance of the models at each stage using the aforementioned statistical indicators. The first screening stage applied general elimination criteria followed by specific elimination criteria. Data points were eliminated if they reported zero creep or

shrinkage strain or swelling instead of shrinkage (i.e. positive shrinkage strain), or if 28-day concrete compressive strength values were not reported. The remaining data points were further filtered to exclude points beyond the application of individual models as reported in Table 2-3. The second screening stage excluded data with square of percent difference between test and predicted values (i.e. (predicted-test)/test) greater than 50. The third screening stage excluded points that appeared to be consistent outliers in all prediction models.

Table 2-8 shows the number of creep and shrinkage data points from the RILEM and NU Databanks analyzed by Al-Manaseer and Prado (2015) to evaluate the models at different phases. These numbers are significantly larger than those considered in the previous study (Al-Manaseer and Lam, 2005), shown in Table 2-5. The accuracy of models as concluded from V_{CEB}, F_{CEB}, and M_{CEB} was generally improved by eliminating data points using the three-phase screening process. The impact was more pronounced in the larger NU Databank than in the RILEM Databank. This is expected since Phases 2 and 3 involve excluding outliers and data points with excessively large normalized differences. However, excluding these points also means that models are assessed for their ability to predict only data points that are within their range of application and with no extreme or unforeseen values. This results in mild discrepancies between statistical indicators for the various models, which make the model ranking rather futile. For example, CEB-FIP MC90-99, ACI 209, and GL2000 ranked as the second, third and fourth most accurate despite their very similar V_{CEB} values of 44%, 45%, and 46%, respectively. Moreover, V_{CEB} for shrinkage strains after Phase 3 ranged from 39% to 46%. Similarly, V_{CEB} values for creep strains ranged from 37 to 44% at Phase 3 and the models were assigned different ranks despite the negligible discrepancy of V_{CEB} values. Ranking models based on such relatively small discrepancies is deceiving, especially considering the wide spectrum of uncertainties associated with the nature of the creep and shrinkage phenomena. Therefore, it may be more reasonable to rank models based on Phase 1. Details of the ranking of the models after each phase are shown in Appendix A.

The modified coefficient of variation method, V_m, provided consistent results for all the screening phases. This is likely due to the consistency produced by assigning the data points to boxes and assigning the same weight to all the data points within each box. This

method also yielded significantly larger coefficients of variation for creep than for shrinkage. This is expected because experimental creep strains are calculated by subtracting two experimentally measured values, initial strain due to applied load and final strain, and are therefore expected to have larger uncertainty.

Al-Manaseer and Prado (2015) ranked the models based on Phase 3 of the screening process and concluded that the ACI 209 model provided the most accurate shrinkage strain predictions, followed by the B3, CEB-FIP MC90-99, and GL2000 models respectively. ACI 209 also provided the most accurate predictions for creep strains, followed by B3, GL2000, and CEB-FIP MC90-99 models respectively. This contradicts the findings of Al-Manaseer and Lam (2005), Gardner (2004), and Bazant and Li (2008), where the either the B3 or GL2000 models were the most accurate models and ACI 209 consistently ranked as the least accurate model.

Table 2-9 shows the percentages of overestimating or underestimating residuals, which can be used to assess the tendency of models to overestimate or underestimate predictions. The majority of overestimating residual percentages are between 45 and 55%, indicating that no model should be deemed to be overestimating or underestimating. However, the distribution of residuals was also shown to be heavily dependent on the databank used. For instance, the B3 and GL2000 Models were found to be overestimating models in predicting creep using the RILEM Databank, but underestimating models based on the NU Databank. Furthermore, the B3 Model is underestimating for shrinkage, and the CEB-FIP MC90-99 Model is underestimating for creep irrespective of the dataset considered.

Table 2-8: Number of Data Points used by Al-Manaseer and Prado (2015)

	RILEM						NU					
	Shrinkage			Creep			Shrinkage			Creep		
Phase	1	2	3	1	2	3	1	2	3	1	2	3
ACI 209	4360	4348	4250	9184	9184	9090	4531	4518	4344	5485	5485	5390
B3	4134	4067	3926	9944	9944	9870	4327	4260	4000	6178	6178	6140
GL2000	4394	4338	4197	11306	11306	11212	4593	4537	4271	7149	7147	7053
MC90-99	4307	4167	4026	11640	11640	11546	4506	4358	4093	8354	7982	7637
Total Points Available	7153			13769			8326			11825		

Table 2-9: Summary of Residuals

	Phase	RILEM						NU					
		Shrinkage			Creep			Shrinkage			Creep		
		1	2	3	1	2	3	1	2	3	1	2	3
ACI 209	Overestimating %	54	54	55	45	45	46	53	53	55	33	33	33
	Underestimating %	46	46	45	55	55	54	47	47	45	67	67	67
B3	Overestimating %	36	35	36	57	57	57	34	33	35	40	40	40
	Underestimating %	64	65	64	43	43	43	66	67	65	60	60	60
GL2000	Overestimating %	44	43	45	59	59	60	42	42	44	46	46	47
	Underestimating %	56	57	55	41	41	40	58	58	56	54	54	53
MC90-99	Overestimating %	53	52	53	37	37	37	52	50	53	33	29	30
	Underestimating %	47	48	47	63	63	63	48	50	47	67	71	70

2.4.5   Overall Comparison of Models

Tables 2-10 and 2-11 summarize the ranking of the accuracy of the models, using various statistical indicators, according to each of the aforementioned studies. It can be concluded that the ranking of the models is strongly dependent on 1) the data set subjectively chosen by the analyst and 2) the statistical indicator used to assess the performance of the models. The choice of data sets in each study is drastically different yet seemingly justifiable. For example, Bazant and Li (2008) choose to evaluate all the models based on the same set of data, which may be a more objective approach. However, Al-Manaseer and Prado (2015) and Al-Manaseer and Lam (2005) discard data beyond the application of individual models because it would be unfair to evaluate models based on data points that are outside their limitations. Both studies present a strong argument in favor of their choice of data and neither can be considered superior or more credible.

Most statistical indicators (with the exception of Gardner's COV method, Equation 2-17) are mathematically sound and so present a meaningful comparison of the models. However, the same statistical indicator can be applied in different ways to potentially yield different results. For instance, Al-Manaseer and Lam (2005) computed V_{CEB} based on time intervals whereas Al-Manaseer and Prado (2015) compute the same statistical indicators based on data sets. Although both studies use the same mathematical formulation for computing V_{CEB}, the former will yield a V_{CEB} value for each time interval, whereas the latter will yield one value for all time intervals. Arguments can be made to support either method. Computing V_{CEB} for each time interval allows for assessing the models based on the long-term time intervals (e.g. $t > 1095$ days when computing V_{CEB}), which are of most importance to designers. On the other hand, computing a single V_{CEB} value that is inclusive of all time intervals may provide a better understanding of the overall accuracy of the models.

Each statistical analysis technique can have its advantages and must be considered when comparing models. Tables 2-10 and 2-11 show the weighted mean ranking of each model based on the ranking it received in each of the four studies considered in this chapter. All four studies were considered equally credible and assigned an equal weight of 0.25 (i.e., the sum of the weights of all four studies is 1). Al-Manaseer and Lam (2015) included

separate analyses for the RILEM and NU Databanks and so each was assigned a weight of 0.125. Moreover, all statistical indicators within a study were considered of equal importance and assigned equal weights. The mean ranking is the ranking of the model out of 4 and the closer the mean ranking is to 1, the better the relative accuracy of the model. The CEB-FIP MC90-99 Model received a mean ranking of 2.84 for shrinkage and 3.15 for creep and is therefore the worst-performing model. B3 was the best performing model for predicting shrinkage with a weighted mean rating of 1.75 and the second best for predicting creep with a mean rating of 1.78. GL2000 was the best preforming model for creep with a mean ranking of 1.69 and the second best for shrinkage with a mean ranking of 2.25. ACI 209 was the third-best performing model for both creep and shrinkage.

The B3 Model is the most theoretically-justified model and Table 2-10 shows that it is superior to the other models in predicting shrinkage strains. However, Table 2-11 shows that the strictly empirical GL2000 Model is more effective in predicting creep strains. Creep of concrete is a complex mechanism that is not yet fully understood (Gilbert and Ranzi, 2011). Therefore, an empirical model may be more effective than a theoretical model.

Table 2-10: Summary of Ranking of Shrinkage Prediction Models

Study	Criterion	Ranking			
		ACI 209	B3	GL2000	MC90-99
Al-Manaseer and Lam (2005)	V_{CEB}	3	2	1	1
	V_{BP}	4	3	1	2
	M_{CEB}	3	2	4	1
	F_{CEB}	1	3	3	4
Gardner (2004)	V_G	3	1	2	2
Bazant and Li (2008)	V_{BL}	3	1	2	4
	c	3	1	2	4
Al-Manaseer and Prado (2015) – RILEM	V_{CEB}	2	1	3	3
	V_m	1	3	4	2
	M_{CEB}	1	3	2	4
	F_{CEB}	1	3	2	4
Al-Manaseer and Prado (2015) – NU	V_{CEB}	2	1	3	4
	V_m	1	3	4	2
	M_{CEB}	1	3	2	4
	F_{CEB}	1	3	2	4
Mean Ranking		2.50	1.75	2.25	2.84
Standard Deviation		1.03	0.91	0.96	1.15

Table 2-11: Summary of Ranking of Creep Prediction Models

Study	Criterion	Rankings			
		ACI 209	B3	GL2000	MC90-99
Al-Manaseer and Lam (2005)	V_{CEB}	3	1	2	2
	V_{BP}	3	2	1	3
	M_{CEB}	4	1	2	3
	F_{CEB}	1	3	2	1
Gardner (2004)	V_G	3	2	1	4
Bazant and Li (2008)	V_{BL}	4	1	2	3
	c	4	1	2	3
Al-Manaseer and Prado (2015) – RILEM	V_{CEB}	3	1	2	4
	V_m	2	4	3	1
	M_{CEB}	1	4	2	3
	F_{CEB}	1	3	2	4
Al-Manaseer and Prado (2015) – NU	V_{CEB}	3	1	2	4
	V_m	3	1	2	3
	M_{CEB}	3	2	1	4
	F_{CEB}	1	3	2	4
Mean Ranking		2.97	1.78	1.69	3.15
Standard Deviation		1.08	1.10	0.50	1.00

2.5 Conclusions

This chapter presented an overview of the phenomena and the factors affecting creep and shrinkage of concentrically loaded plain concrete. It also described the available models for predicting creep and shrinkage strains, namely the ACI 209, B3, GL2000, and CEB-FIP MC90-99 models and evaluated the relative accuracy of prediction models using analyses presented by others. The conclusions of this chapter are:

1. Increased aggregate stiffness is effective in reducing shrinkage and creep of concrete because creep and shrinkage originate in the cement paste. Shrinkage is an intrinsic material property of cement paste so concrete mixtures with a high volume of aggregate will shrink less than those with high volumes of cement. Moreover, stiffer aggregates are expected to provide a considerable restraint to both shrinkage and creep. The most significant shortcoming of creep and shrinkage prediction models is their failure to account for the effect of aggregate stiffness.

2. All creep and shrinkage prediction models have been calibrated using experimental data forom the RILEM or NU Databanks and are therefore at least partly empirical.

3. Creep and shrinkage predictions obtained using the various models for a given set of parameters can differ by up to 30%.

4. A comparison of the effectiveness of the various models in predicting experimental creep and shrinkage strains is facilitated using the RILEM and the NU Databanks. However, these databanks lack: test results on the creep and shrinkage for large members that are representative of real structural elements; creep data for drying before loading or loading before drying; and, long-term creep and shrinkage results. Moreover, there is a great deal of uncertainty regarding the interpretation the actual duration meant by authors when referring to "initial elastic" and instantaneous" strains associated with data presented in these databanks. Furthermore, the type of cement used in different datasets is not adequately described. All of these uncertainties cast doubt on the validity of the outcomes of any comparison.

5. Researchers do not agree on which data subsets to use from the RILEM and NU Databanks when evaluating and comparing models. Al-Manaseer and Lam (2005) and Al-Manaseer and Prado (2015) argue that models should only be evaluated based on data points that lie within their range of application. Bazant and Panula (2000) and Bazant and Li (2008) counter that a fair comparison entails using the same set of data to compare all models.

6. Another questionable aspect of model comparison is the appropriate use of statistical indicators. Al-Manaseer and Lam (2005) compute statistical indicators such as V_{CEB}, M_{CEB}, and F_{CEB} for time intervals, while Al-Manaseer and Prado (2015) compute the same indicators for data sets. The former method will evaluate the performance of the models during each time interval separately, which is useful for designers who are generally interested in the long-term deflections of concrete. The latter, on the other hand, will provide an assessment of the overall performance of the models, which could provide a better assessment of the overall accuracy of the models. Bazant and Li (2008) evaluate models based on a regression analysis (instead of the population analysis used by Al-Manaseer and Lam and Al-Manaseer and Prado) to capture the common trend between the data points used in the analysis.

7. A number of studies, such as Gardner (2004), Al-Manaseer and Lam (2005), Bazant and Li (2008), and Al-Manaseer and Prado (2015), have compared the models using various methods of statistical analysis. However, despite the mathematical soundness of these studies, they yield contradicting outcomes. This makes it difficult to quantify the prediction error.

8. A mean ranking of the models where each of the four statistical analyses presented in this chapter was considered of equal importance showed that B3 is the most effective model in predicting shrinkage strains. The strictly empirical GL2000 is the more effective than the mostly theoretical B3 Model in predicting creep strains.

9. The CEB-FIP MC90-99 Model received a mean ranking of 2.84 for shrinkage and 3.15 for creep and is therefore the worst-performing model. This model forms the

basis of the method presented in the Canadian Highway Bridge Design Code (CHBDC, 2016).

10. The percentage of overestimating residual errors typically falls between 45 and 55%, which means that no model should be explicitly labelled as an overestimating or underestimating model. However, these percentages were also shown to be dependent on the databank used. The B3 Model mostly underestimated shrinkage, and the CEB-FIP MC90-99 Model mostly underestimates creep, irrespective of the database considered.

Chapter 3

3   Long-Term Deflections of Reinforced Concrete Beams

The long-term deflection of reinforced concrete flexural members subjected to a sustained load is primarily attributed to creep and shrinkage. Chapter 2 outlined the various factors that contribute to the development of creep and shrinkage strains, as well as the uncertainties associated with computing these values. Methods for computing short-term deflections described in the 4th Edition of the Cement Association of Canada Concrete Design Handbook (CAC, 2016) account for the effect of restrained shrinkage on the effective moment of inertia, but are based on simplifying assumptions. However, methods for computing long-term deflections due to creep and shrinkage presented in the same source are empirically based and utilize simplified equations for computing creep coefficients and shrinkage strains that could result in the underestimation of long-term deflections. Gilbert and Kilpatrick (2017) present another method for computing incremental deflections due to creep and shrinkage, based on a method proposed by Gilbert (2001). This method provides improvements to the provisions of AS3600-2009 (AS, 2009).

The aforementioned methods are all empirical. However, analytical methods for computing incremental deflections due to creep and shrinkage based on the principles of mechanics are not excessively complex by comparison. Therefore, the objectives of this chapter are to:

1. Critically evaluate existing methods for computing long-term deflection increments due to creep and shrinkage.
2. Present mechanics-based methods for calculating long-term deflection increments due to creep and shrinkage.
3. Assess the accuracies of existing and proposed methods by investigating test/predicted ratios for the total (i.e. immediate plus long-term) deflections.
4. Outline any shortcomings with existing methods and propose improvements.

3.1   Restrained Shrinkage and Tension Stiffening

The ultimate shrinkage strain is inversely proportional to the length of the moist-curing period, meaning that members exposed to prolonged drying exhibit significant shrinkage strains. Unlike plain concrete members that are free to shrink without restraint, reinforced

concrete members subject to shrinkage strains develop tensile stresses in the concrete due to restraint of shrinkage by the reinforcing steel. As concrete shrinks, it imposes a compressive force on the reinforcing steel, which in turn imposes an equal tensile force on, and associated tensile stresses in, the concrete. These tensile stresses, which occur in addition to tensile stresses due to the applied load, have the following effects on short-term and long-term deflection of reinforced concrete members:

1. They reduce the applied moment, M_{cr}, necessary to initiate flexural cracking (e.g. Bischoff, 2007). Since cracked members experience larger curvature (and hence deflection) than uncracked members, the reduction of M_{cr} causes an increased short-term deflection due to the applied load.

2. They may result in a non-uniform distribution of residual strains, particularly for the common case where the compression reinforcement area is much less than the tensile reinforcement area, and therefore causes additional time-dependent deflection due to warping.

The deformation of a concrete flexural member is affected by the rigidity, $E_c I$, where E_c is Young's Modulus of the concrete and I is the moment of inertia. The moment of inertia at the location of a crack, I_{cr}, is significantly smaller than the gross moment of inertia, I_g, away from the crack. Additionally, the concrete is assumed to carry no tension at the location of the crack, but has a capacity assumed equal to the modulus of rupture away from the crack. The contribution of the tension carried by the uncracked concrete, between adjacent cracks, to the stiffness and corresponding deformation of a concrete member is known as tension stiffening (Bischoff, 2007). The Canadian design standard, CSA A23.3 (CAC 2016), and American concrete design code, ACI318 (ACI, 2014), use an effective moment of inertia, I_e, to account for the impact of tension stiffening on the flexural stiffness, where I_e is typically larger than I_{cr} but smaller than I_g.

3.2   Review of Short-Term Deflection by Others

Mechanics-based methods for computing the short-term deflection are well-established. The procedure involves calculating the depth of the neutral axis, kd, using conventional mechanically derived equations (e.g., CAC, 2016) and subsequently calculating the

effective moment of inertia, I_e. The deflection of a simply supported concrete member carrying a uniformly distributed load is

$$\Delta_i = \frac{5 M_a \ell_n^2}{48 E_c I_e}$$

(3-1)

where ℓ_n is the clear span length and M_a is the maximum applied moment at midspan. Two equations for calculating I_e are described in the Concrete Design Handbook (CAC, 2016). The empirical equation proposed by Branson is based on an incorrect mechanical model that overestimates the effect of tension-stiffening in lightly reinforced members and therefore underestimates deflection (Bischoff, 2007). It is given as

$$I_e = I_{cr} + \left(I_g - I_{cr}\right) \left(\frac{M_{cr}}{M_a}\right)^3 \leq I_g$$

(3-2)

Scanlon and Bischoff (2008) showed that the effect of restrained shrinkage is most pronounced in members with reinforcement ratio less than 1%, and less pronounced in members with higher reinforcement ratios. The equation proposed by Bischoff (2007) is based on a correct mechanical model and is given as

$$I_e = \frac{I_{cr}}{1 - \left(\frac{M_{cr}}{M_a}\right)^2 \left[1 - \frac{I_{cr}}{I_g}\right]} \leq I_g$$

(3-3)

Moreover, the flexural rigidity of the cracked member, $E_c I_e$, must not exceed the flexural rigidity of the uncracked member, $E_c I_g$ (hence $I_e \leq I_g$).

Scanlon and Bischoff (2008) recommended that the cracking moment, M_{cr}, be calculated based on two-thirds the modulus of rupture, f_r, when using the Bischoff Equation to account for the effect of restrained shrinkage. Using the Branson Equation with M_{cr} based on $0.5 f_r$ yields similar results to using the Bischoff Equation with $0.67 f_r$ (CAC, 2016). Additionally, Mancuso and Bartlett (2016) showed that the short-term deflection computed using the Branson Equation with M_{cr} based on $1.0 f_r$ yields test/predicted ratios greater than 1 (unconservative) with a high coefficient of variation. They also showed that using either the Branson Equation with M_{cr} based on $0.5 f_r$ or the Bischoff Equation with M_{cr} based on

$0.67f_r$ provides conservative results with a mean test/predicted ratio between 0.82 to 0.84 and a significantly lower coefficient of variation. Gilbert (2012) recommended that I_e be calculated based on $0.7M_{cr}$ for computing the short-term deflection of members where shrinkage has occurred before loading, and $1.0M_{cr}$ if shrinkage has not occurred prior to loading.

3.3   Long-Term Deflection due to Creep

3.3.1   Mechanics-Based Approach

Creep of concrete at time t is quantified in terms of a creep coefficient, $\emptyset(t,t_o)$, where t_o is the age at initial loading. The creep coefficient can be obtained experimentally as the ratio of creep strain to initial strain or computed using the various prediction models described in Chapter 2. It increases as the concrete ages and as the age at loading decreases. The effect of creep on a flexural member is treated as a delayed elastic strain and is analogous to a gradual reduction of Young's Modulus of concrete, $E_c(t)$ (Gilbert and Ranzi 2011, ACI 209, 1992). The time-dependent Young's Modulus, $\overline{E_c}$, at time $t > t_o$ is quantified using the Age-Adjusted Effective Modulus Method (ACI 209, 1992) as

$$\overline{E_c} = \frac{E_c(t)}{[1+\chi(t,t_o)\emptyset(t,t_o)]} \tag{3-4}$$

where $\chi(t,t_o)$ is an aging coefficient that generally ranges between 0.4 and 1.0 and is commonly taken as 0.8 for practical cases (e.g., Scanlon and Bischoff (2008); Gilbert (1988); Dilger (1982)). This is consistent with the recommendations of ACI 209 (1992), where a value of approximately 0.8 is assumed for concretes loaded at ages less than 10 days and with a creep coefficient of 3. Equations derived theoretically for computing $\chi(t,t_o)$ are reported by Gilbert and Ranzi (2011) and Bazant (1972).

The change in Young's modulus of the concrete will result in a change in the modular ratio, $n = E_s/E_c$, where E_s is the Young's Modulus of the reinforcing steel. The age-adjusted modular ratio, $\bar{n}$, is therefore

$$\bar{n}=E_s/ \overline{E_c} = n[1+ \chi(t,t_o)\emptyset(t,t_o)] \tag{3-5}$$

The time-dependent neutral axis depth after creep, $\overline{kd}$, can be computed using the age-adjusted modular ratio, $\bar{n}$, in place of n in conventional mechanics-based equations for calculating kd reported in the CAC Concrete Design Handbook. The change of the depth of the neural axis requires computing the associated I_{cr}, denoted as $\overline{I_{cr}}$.

Section 3.2 showed that short-term deflection computations are based on an effective moment of inertia, I_e, to account for the contribution of the uncracked regions the overall flexural rigidity of a member (i.e., tension stiffening). However, the effect of creep is more significant in tension than in compression (Brooks and Neville, 1977; Orta, 2009). Further, Equation 3-4 shows that creep significantly reduces Young's Modulus of the Concrete. This will cause the long-term effect of tension stiffening to dissipate and so the long-term effective moment of inertia essentially equals $\overline{I_{cr}}$. Therefore, the effective maximum compressive stress in the concrete due to a sustained load, M_s, after creep has taken place can be calculated as

$$\overline{\sigma(t,t_o)}= \frac{M_s\overline{kd}}{\overline{I_{cr}}} \tag{3-6}$$

Since the creep coefficient is defined as $\emptyset(t,t_o)= \varepsilon_{cr}/\varepsilon_i$, the creep strain at time t is given as

$$\overline{\varepsilon_{cr}(t,t_o)}= \emptyset(t,t_o)\frac{\overline{\sigma(t_o)}}{E_c(t_o)} \tag{3-7}$$

where $E_c(t_o)$ is Young's Modulus at the age of loading t_o. The average curvature due to creep at time t after loading is therefore

$$\overline{\psi_{cr}(t,t_o)}= \frac{\overline{\varepsilon_{cr}(t,t_o)}}{\overline{kd}} \tag{3-8}$$

The incremental deflection due to creep for a simply supported beam subjected to a uniformly distributed load can be calculated from standard deflection equations as

$$\Delta_{cr}=\frac{5M_s\ell_n{}^2}{48\,\overline{E_c}\,\overline{I_{cr}}}=\frac{5\overline{\psi_{cr}(t,t_o)}\ell_n{}^2}{48} \tag{3-9}$$

where M is the maximum midspan moment and $\overline{E_c}$ is age-adjusted Young's Modulus for concrete.

3.3.2   Branson/CAC Concrete Design Handbook

The current empirically based methods for computing long-term deflections due to creep and shrinkage, referenced in ACI318 (ACI 2014) and presented in the Concrete Design Handbook (CAC 2016), were originally proposed by Branson (1977). The creep deflection is proportional to the short-term deflection, and therefore inversely proportional to I_e. On the other hand, shrinkage deflection depends only on the ultimate shrinkage strain, the compression and tension reinforcement areas, and the overall depth of the member. Several researchers including Branson have developed analytical tools to calculate deflection due to shrinkage. However, these methods have been criticized due to uncertainties in quantifying the impact of creep on Young's Modulus of concrete and uncertainties in computing I_e (Branson 1977).

The equation for computing creep deflection is founded on the fundamental assumption that the increase in curvature due to creep is smaller than the increase in external fiber compressive strain due to creep. This assumption is appropriate because the depth of the neutral axis and hence the compression region increases when creep occurs. It is formulated as

$$\frac{\psi_{cr}}{\psi_i} = k_r \frac{\varepsilon_{cr}}{\varepsilon_i} \qquad (3\text{-}10)$$

where k_r is a dimensionless factor less than 1, ε_{cr} is the creep strain, ε_i is the instantaneous strain, ψ_{cr} is the curvature due to creep, and ψ_i is the instantaneous curvature. An equation for calculating k_r for partially prestressed beams was derived theoretically by Shaikh and Branson (1970) and was later modified to fit test data for non-prestressed beams (Branson 1977). This modified empirical equation for k_r is

$$k_r = \frac{0.85}{1 + 50\rho'} \qquad (3\text{-}11)$$

where ρ' is the compression steel reinforcement ratio. Moreover, the creep coefficient, C_t, is defined as the ratio of the creep strain ε_{cr} to the initial strain ε_i (ACI 2008). The ratio of incremental creep deflection to initial deflection, Δ_{cr}/Δ_i, is given by

$$\frac{\Delta_{cr}}{\Delta_i}=k_r\frac{\varepsilon_{cr}}{\varepsilon_i} \tag{3-12}$$

Thus, combining Equations (3-19) and (3-20) and accounting for C_t yields:

$$\Delta_{cr}=\left[\frac{0.85C_t}{1+50\rho'}\right]\Delta_i \tag{3-13}$$

The Concrete Design Handbook (CAC, 2016) proposes $C_t=0.8S_t$, where S_t, the long-term deflection factor under sustained loads specified in A23.3 (CSA 2014), has a maximum value of 2.0. The associated maximum value of C_t is therefore 1.6.

3.3.3   Gilbert and Kilpatrick (2017)

Gilbert and Kilpatrick (2017) proposed an empirical method form computing incremental deflections due to creep and shrinkage. The incremental deflection due to creep, Δ_{cr}, is computed as

$$\Delta_{cr}=\left[\frac{\varnothing(t,t_o)}{\alpha}\right]\Delta_i \tag{3-14}$$

where α for a cracked section is

$$\alpha=[0.48\rho^{-0.5}]\left[\frac{I_{cr}}{I_e}\right]^{0.33}\left[1+(125\rho+0.1)\left(\frac{A_s'}{A_s}\right)^{1.2}\right] \tag{3-15}$$

and for an uncracked section is

$$\alpha=[1-15\rho]\left[1+(140\rho-0.1)\left(\frac{A_s'}{A_s}\right)^{1.2}\right] \tag{3-16}$$

Figure 3-1 shows the variation of α with ρ for $A_s'/A_s = 0.5$ and $I_{cr}/I_e = 1$. Since Equation 3-14 implies that the deflection due to creep increases with a decrease in α, Figure 3-1

suggests that the creep deflection increases with ρ, ultimately reaching a constant value at $\rho \geq 0.015$.
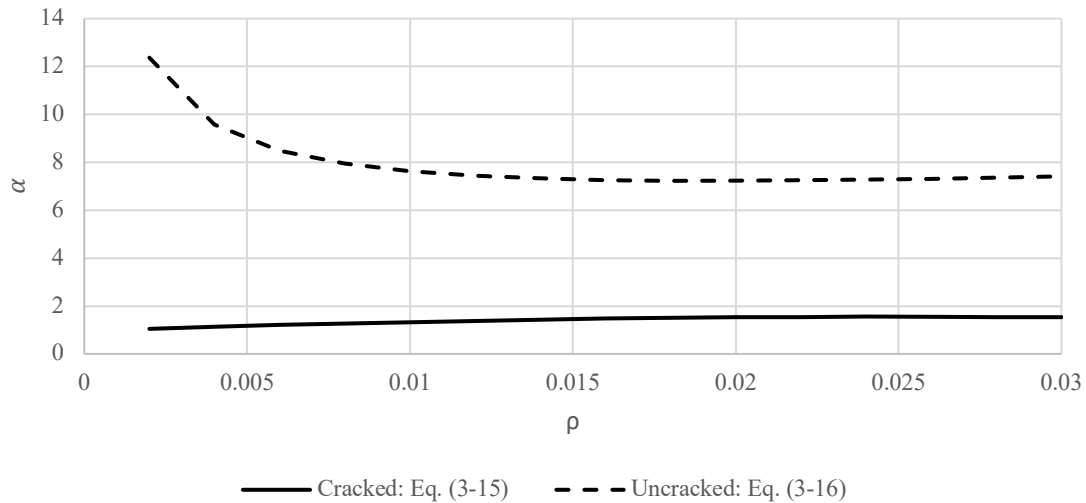
Figure 3-1: Variation of α with ρ

3.4 Long-Term Deflection Due to Shrinkage

3.4.1 Mechanics-Based Approach

Shrinkage-induced curvature in reinforced concrete beams is primarily due to the restraint of shrinkage by the reinforcing steel. Figure 3-2 (b) shows an unreinforced concrete section that, due to the absence of reinforcing steel, experiences a uniform shrinkage strain distribution, over the depth of the section. This does not result in curvature, warping, or vertical deflection. Figures 3-2 (c) and (d) show the impact of various reinforcing steel layouts on the shrinkage strain distribution and hence curvature due to shrinkage. Singly reinforced sections, as shown in Figure 3-2 (c), experience significant restrained shrinkage and therefore a considerable tensile force in the concrete at the level of the reinforcement. This force produces tensile strains at the bottom fiber and compressive strains at the top fiber, and this non-uniform strain distribution causes curvature and vertical deflection.

Adding a second layer of reinforcement near the top fiber produces an additional tensile force in the concrete at the level of the top reinforcement. Figure 3-2 (d) shows a doubly reinforced section where the area of the top steel is less than the area of bottom steel and

so the associated tensile force is smaller. The top and bottom extreme fibers experience unequal tensile strains, resulting in a non-uniform strain distribution that is less pronounced than that of a singly reinforced section. As a result, providing double reinforcement near both the top and bottom beam faces are equal, and equally spaced from the section mid-height, markedly reduces the curvature and associated deflection due to restrained shrinkage.

If the areas of the top and bottom reinforcement are equal and the distance from the reinforcement centroids to the adjacent extreme fibers are equal, the extreme fiber strains are also equal. A more uniform strain distribution is produced, as shown in Figure 3-2 (e). In this case, the extreme fiber strains due to restrained shrinkage result in a uniform strain distribution over the depth of the member, which does not induce curvature or vertical deflection. Moreover, the net concrete strain due to restrained shrinkage is markedly smaller than the free shrinkage strain so the axial shortening is reduced.

(a) Beam Elevation

(b) Strain in Plain Concrete due to Unrestrained Shrinkage

(c) Strain due to Restrained Shrinkage ($A'_s = 0$)

(d) Strain due to Restrained Shrinkage ($A'_s < A_s$)

(e) Strain due to Restrained Shrinkage ($A'_s = A_s$)
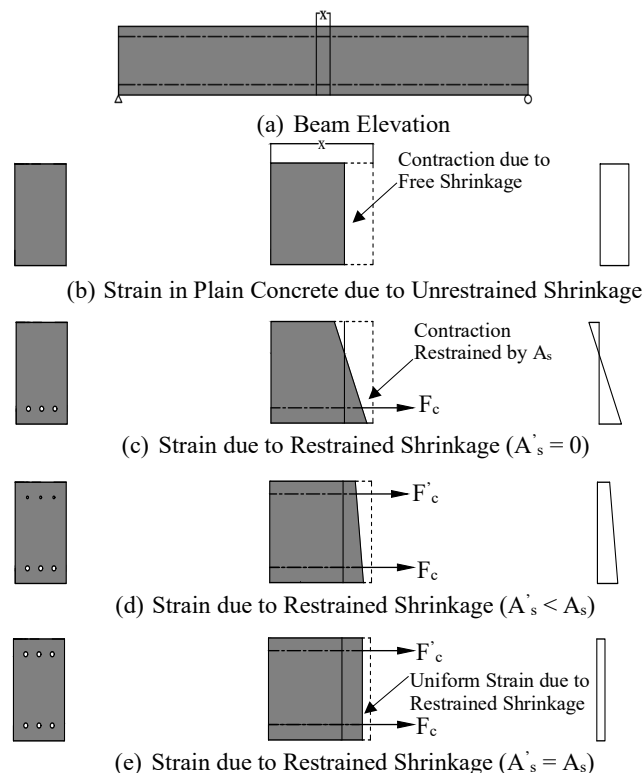
Figure 3-2: Strains due to Restrained Shrinkage in Concrete Beams

The tensile force in the concrete at the level of the steel due shrinkage strains in an uncracked section can be calculated using fundamental principles of mechanics as described in Scanlon and Bischoff (2008). For a rectangular section, the force at the level of the bottom reinforcement at time t, $F_{c,t}$, is

$$F_{c,t} = \frac{-E_s A_s \varepsilon_{sh,t}}{1 + \bar{n}\rho \left(\frac{d}{h}\right)\left(1 + 12\left(\frac{d}{h} - 0.5\right)^2\right)} \tag{3-17}$$

where $\varepsilon_{sh,t}$ is the shrinkage strain at time t, A_s is the area of the bottom steel, ρ is the reinforcement ratio, d is the effective depth, h is the overall depth of the member and $\bar{n}$, the age-adjusted modular ratio, is as defined in Equation 3-5. The sign convention adopted is compression positive.

Similarly, the force at the level of the top reinforcement, $F'_{c,t}$, is

$$F'_{c,t} = \frac{-E_s A'_s \varepsilon_{sh,t}}{1 + \bar{n}\rho' \left(\frac{d}{h}\right)\left(1 + 12\left(0.5 - \frac{d'}{h}\right)^2\right)} \tag{3-18}$$

where A'_s is the area of the top steel, and d' is the depth of the top reinforcement from the top fiber and ρ' is the reinforcement ratio of the top steel. Equations 3-17 and 3-18 are based on the effective modular ratio, $\bar{n}$, instead of n because shrinkage is a time-dependent deformation and the effect of the change in the Young's Modulus of concrete must be accounted for.

The residual stresses at the top and bottom fibers, $\sigma_{sh,t,T}$, and $\sigma_{sh,t,B}$, respectively, can be calculated as

$$\sigma_{sh,t,T} = \frac{F_{c,t}}{A_g} - \frac{F_{c,t}(d-0.5h)(0.5h)}{I_g} + \frac{F'_{c,t}}{A_g} - \frac{F'_{c,t}(0.5h-d')(0.5h)}{I_g} \tag{3-19}$$

and

$$\sigma_{sh,t,B} = \frac{F_{c,t}}{A_g} + \frac{F_{c,t}(d-0.5h)(0.5h)}{I_g} + \frac{F'_{c,t}}{A_g} + \frac{F'_{c,t}(0.5h-d')(0.5h)}{I_g} \quad (3-20)$$

where A_g is the gross area of the cross-section. The strain at the top fiber and bottom fibers at time t, $\varepsilon_{sh,t,T}$ and $\varepsilon_{sh,t,B}$, respectively, are therefore

$$\varepsilon_{sh,t,T} = \frac{\sigma_{sh,t,T}}{\overline{E_c}} \quad (3-21)$$

and

$$\varepsilon_{sh,t,B} = \frac{\sigma_{sh,t,B}}{\overline{E_c}} \quad (3-22)$$

and the net curvature (i.e., the curvature that causes warping) is

$$\psi_{sh,t} = \frac{\varepsilon_{sh,t,B} - \varepsilon_{sh,t,T}}{h} \quad (3-23)$$

The curvature due to restrained shrinkage, $\psi_{sh,t}$, is constant along the length of the beam and therefore the beam deforms as an arc of a circle with radius of curvature, R, of $1/\psi_{sh,t}$. From the geometry of the circle:

$$\Delta_{sh,t} = R - \sqrt{R^2 - \left(\frac{\ell_n}{2}\right)^2} \quad (3-24)$$

where $\Delta_{sh,t}$ is the maximum deflection due to restrained shrinkage at time t at the center of the span.

Most available methods, including Branson's (1977) and Gilbert's (1999) empirical methods, compute shrinkage curvature assuming the section to be uncracked. This is justifiable because the curvature caused by shrinkage restraint depends on the size of the uncracked section (Gilbert and Ranzi 2011) since shrinkage shortening occurs only in the uncracked regions (Branson 1977). Therefore, the effect of restrained shrinkage may not be significantly influenced by the presence of cracks. Moreover, Branson (1977) suggests

that the majority of shrinkage occurs in the first few weeks after casting, before the application of the design live loads and before cracking. However, this may be questionable because construction loading can often exceed twice the self-weight of the member (Zhou and Kokai, 2010).

3.4.2　Branson/CAC Concrete Design Handbook

Branson (1977) recommends computing shrinkage deflection from the curvature due to shrinkage, which is assumed to be directly proportional to the free shrinkage strain and an inversely proportional to the overall member depth. Branson's Method uses the equation

$$\Delta_{sh,t} = K_{sh} \psi_{sh,t} \ell_n^2 \tag{3-25}$$

where, K_{sh} is a coefficient that accounts for the displacement boundary conditions of the member, and $\psi_{sh,t}$ is defined as

$$\psi_{sh,t} = A_{sh} \frac{\varepsilon_{sh,t}}{h} \tag{3-26}$$

where A_{sh} is a factor to account for the ratio of top to bottom reinforcement and is obtained from tables created by Branson (1977) that are reproduced in the CAC Concrete Design Handbook (CAC, 2016).

Branson recommended that the ultimate free shrinkage strain be taken as $\varepsilon_{sh,u} = 400\mu\varepsilon$ in the absence of information on free shrinkage under local conditions. The Concrete Design Handbook recommends that $\varepsilon_{sh,u}$ be computed as

$$\varepsilon_{sh,u} = \frac{S_t}{2.0} 400\mu\varepsilon \tag{3-27}$$

Since $S_t \leq 2.0$, $\varepsilon_{sh,u}$ computed using Equation 3-27 cannot exceed $400\mu\varepsilon$.

3.4.3　Gilbert & Kilpatrick (2017)

Gilbert and Kilpatrick's (2017) method for computing long-term shrinkage deflections involves computing the shrinkage curvature using empirical methods, and subsequently computing the shrinkage deflection using mechanics-based methods. The curvature due to restrained shrinkage is given as

$$\Psi_{sh,t} = \frac{k_{sh}\varepsilon_{sh,t}}{h} \tag{3-28}$$

where k_{sh} for a cracked section is

$$k_{sh} = 1.2 \left(\frac{I_{cr}}{I_e}\right)^{0.67} \left(1 - 0.5\frac{A_s'}{A_s}\right)\left(\frac{h}{d}\right) \tag{3-29}$$

and for an uncracked section with reinforcement ratio, ρ, greater then 1% is

$$k_{sh} = (100\rho - 2500\rho^2)\left(\frac{d}{0.5h} - 1\right)\left(1 - \frac{A_s'}{A_s}\right)^{1.3} \tag{3-30}$$

or k_{sh} for an uncracked section with ρ, less than 1% is

$$k_{sh} = (40\rho + 0.35)\left(\frac{d}{0.5h} - 1\right)\left(1 - \frac{A_s'}{A_s}\right)^{1.3} \tag{3-31}$$

Figure 3-3 shows the variation of k_{sh} with reinforcement ratio, ρ, and was derived based on effective depth to total depth ratio, $d/h = 0.9$, and tension to compression reinforcement ratio, $A_s'/A_s = 0.5$ and $I_e/I_{cr} = 1$. Since k_{sh} for a cracked section is independent of ρ, the curvature due shrinkage, as computed using Equation (3-28), is also independent of ρ. On the other hand, k_{sh} for an uncracked section increases linearly with ρ for $\rho < 1\%$ and increases at a decreasing rate for $0.01 < \rho < 0.02$. However, k_{sh} begins to decrease for an uncracked section with $\rho > 0.02$. This is contrary to findings presented in Section 3.4.1 where it was shown that the curvature of an uncracked section increases with ρ, regardless of its magnitude.
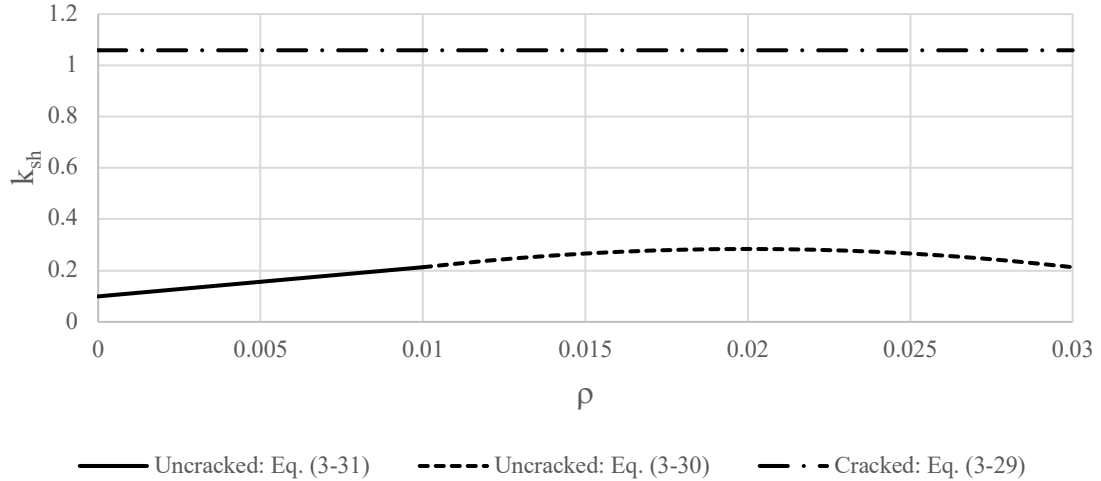
Figure 3-3: Variation of k_{sh} with ρ

The deflection due to restrained shrinkage for a simply-supported member is computed as

$$\Delta_{sh} = \frac{\ell_n^2}{96}(\psi_{sh,L}+10\psi_{sh,M}+\psi_{sh,R}) \tag{3-32}$$

where $\psi_{sh,M}$ is the shrinkage curvature computed at the midspan, and $\psi_{sh,L}$ and $\psi_{sh,R}$ are the shrinkage curvatures at the left and right supports respectively. Equation (3-32) was derived using double integration for a parabolic curvature diagram (Gilbert, 2008). Since simply-supported members are likely uncracked near the supports and cracked at midspan, $\psi_{sh,L}$ and $\psi_{sh,R}$ are computed based on an uncracked k_{sh}, while the $\psi_{sh,M}$ is computed based on a cracked k_{sh}.

3.5   Comparison Between Prediction Models and Experimental Data

There is a lack of long-term tests on beams and slabs under sustained loading, and few studies report all data needed to carry out a comprehensive analysis (Kilpatrick and Gilbert 2017). Two sources of experimental data on the long-term behavior of simply supported concrete members is available, namely Washa and Fluck (1952) and Gilbert and Nejadi (2004).

3.5.1   Washa and Fluck (1952)

The empirically-derived Branson (1977) Equation was partly based on an experimental study by Washa and Fluck (1952), among others. Washa and Fluck (1952) explored the behavior of singly and doubly reinforced simply supported beams with span-to-depth ratios ranging from 20 to 70 and tension reinforcement ratios of approximately 1.5%. The specimens were moist cured for 5 days (t_c = 5 days) and a load, sustained for 915/ days (nearly 5 years), was applied at 14 days after casting (t_o = 14 days). The midspan moment due to the sustained load was 40-50% of the ultimate capacity of the beam.

Washa and Fluck's (1952) test specimens were classified into five groups: A; B; C; D; and, E, based on their dimensions. Each group included a total of six specimens; Specimens 3 and 6 were singly reinforced, Specimens 2 and 5 were doubly reinforced with the area of the top steel equal to half the area of the bottom steel, and Specimens 1 and 4 were doubly reinforced with equal areas of top and bottom steel. As a result, Specimens 3/6, 2/5, and 1/4 were reported to have the same deflection (for example, the deflection of B3 is equal to the deflection of B6, and the deflection of C2 is equal to the deflection of C5, etc.). Washa and Fluck reported an error in the initial reading of Group A specimens. Moreover, Group D specimens had an identical cross-section to those belonging to Group C and included specimens made of low-density and air-entrained concretes.

Concrete properties such as the compressive strength at age of loading, $f'_c(t_o)$, and Young's Modulus at age of loading, $E_c(t_o)$, were obtained from cylinder test. Although Specimens 3/6, 2/5, and 1/4 were reported to have the same deflection, they each had a unique $f'_c(t_o)$ (details of test specimens are shown in Appendix B). Since the deflection is dependent on f'_c it will be computed for each specimen separately based on the reported $f'_c(t_o)$ and $E_c(t_o)$. Washa and Fluck (1952) also reported test results for companion loaded and unloaded cylinders that are used to determine experimental values for creep coefficients and shrinkage strains. The test specimens were found to have a creep coefficient of 4.5 and shrinkage strain of 720$\mu\varepsilon$.

3.5.2   Gilbert and Nejadi (2004)

The most recent experimental study on the behavior of concrete members under sustained loading was conducted by Gilbert and Nejadi (2004), where twelve singly-reinforced,

simply supported concrete members with spans of 3.5 meters and reinforcement ratios less than 1% were subjected to sustained loads for periods of 400 days. Of the twelve specimens, six had a width to effective depth ratio of 1.2 to represent beams (indicated by the prefix B). The other six specimens were representative of slab elements (indicated by the prefix S) and had a width to effective depth ratio of 0.3. Specimens within each series were designed using a different combination of parameters (indicated by the number beside the uppercase letter) such as the thickness of the cover and the spacing between reinforcing steel bars. Two load ratios were applied to each set of specimens and indicated by the lower-case letters "a" and "b". Type "a" specimens were subjected to a sustained load at midspan equal to 50% of the ultimate moment capacity of the beam, and "b" specimens were loaded to 30% of their capacity. For example, B1a and B1b had identical dimensions and parameters, but subjected to two different loads, while B1a and B3a were subjected to similar loads but had different reinforcement ratios. Gilbert and Nejadi (2004) also reported an experimental creep coefficient of 1.7 and shrinkage strain of 825$\mu\varepsilon$.

3.5.3   Quantification of Test/Predicted Ratios

Table 3-1 shows the overall mean values and coefficients of variation for ratios of experimental and predicted long-term deflections as computed using the Mechanics-Based Method, the Branson/CAC Design Handbook Method, and Gilbert and Kilpatrick (2017) Method, respectively. The Mechanics-Based Method was found to yield conservative results (i.e., test/predicted ratios less than 1) for both sets of test results. Short-term deflections were computed using the Branson Equation with M_{cr} based on $0.5f_r$ to maintain consistency with the requirements of CSA A23.3-14 the and recommendations in the Concrete Design Handbook (CAC 2016). Analytical predictions were carried out using the reported experimental creep coefficients and shrinkage strains, while predictions based on the Concrete Design Handbook were conducted using values recommended therein.

The Branson Method, as presented in the CAC Concrete Design Handbook, yields unconservative test/predicted ratios for Washa and Fluck's (1952) test specimens, with a mean test/predicted ratio of 1.32, and a slightly conservative ratios for Gilbert and Nejadi's (2004) test specimens with a mean test/predicted ratio of 0.96. The Gilbert and Kilpatrick (2017) Method was also found to follow the same trend, yielding a mean-test/predicted ratio of 1.05 for Washa and Fluck's specimens and a conservative ratio of 0.89 for Gilbert

and Nejadi's specimens. The Mechanics-Based Method was found to be conservative for both sets of experimental data, yielding a mean test/predicted ratio of 0.94 for Washa and Fluck's specimens and 0.92 for Gilbert and Nejadi's Specimens.

Table 3-1: Statistical Parameters of Test/Predicted Ratios

Method	Mechanics-Based		CAC Handbook		Gilbert & Kilpatrick	
	Washa & Fluck	Gilbert & Nejadi	Washa & Fluck	Gilbert & Nejadi	Washa & Fluck	Gilbert & Nejadi
Mean	0.94	0.92	1.34	0.96	1.06	0.89
COV (%)	10.30	4.98	9.78	5.14	10.01	8.13

Table 3-2 further breaks down these data by showing unique mean test/predicted ratios for singly reinforced members ($A'_s = 0$) and doubly reinforced members with $A'_s = 0.5A_s$ and with $A'_s = A_s$. The Mechanics-Based method yields accurate and conservative results for singly reinforced members, with a mean test/predicted ratio of 0.92-0.93. The Branson Method and the method presented by Gilbert and Kilpatrick (2017) yielded conservative results for Gilbert and Nejadi's test data (mean test/predicted ratio of 0.96 and 0.89, respectively), and unconservative results for Washa and Fluck's data (mean test/predicted ratio of 1.40 and 1.08, respectively).

The Mechanics-Based Method also yields a conservative mean test/predicted ratio of 0.92 for the doubly reinforced members with $A'_s = 0.5A_s$. The other two methods yield unconservative results with mean test/predicted ratios of 1.27 and 1.01 for the Branson and Gilbert and Kilpatrick (2017) Methods respectively.

A total of eight symmetrically-reinforced members ($A'_s = A_s$) with equal areas of top and bottom reinforcement, reported by Washa and Fluck (1952), are considered in the present study. Specimens E1 and E4 yielded test/predicted ratios that are inconsistent with the range of ratios obtained, using all three methods investigated herein, for the other six specimens and therefore appear to be outliers. Beams E1 and E4 were impractically slender with span-to-depth ratios of 70. The mechanics-based method provided test/predicted ratios of 1.12 and 1.09 for E1 and E4 respectively, while the other two methods provided

unconservative test/predicted ratios between 1.28 and 1.62. Table 3-2 shows unique analyses of the test/predicted ratios for the eight specimens with Specimens E1 and E4 either included or excluded. Naturally, the ratios for all three methods have a relatively high coefficient of variation (COV) when the suspected outliers are included in the analysis, and a significantly lower COV when they are excluded. For example, the COV for the Mechanics-Based Method decreases from 15.1% to 3.5% after the suspected outliers are removed. The associated mean test/predicted ratios reduced from 0.94 to 0.86 when the suspected outliers were excluded. The Branson Method yielded unconservative mean test/predicted ratios of 1.35 and 1.27 when the suspected outliers were included or excluded, respectively. The method presented by Gilbert and Kilpatrick (2017) yielded more accurate ratios of 1.10 and 1.06 when the suspected outliers were included or excluded, respectively, which are slightly unconservative.

Table 3-2: Mean Test/Predicted Ratios for Various A'_s/A_s Fractions

Method		$A'_s = 0$		$A'_s = 0.5A_s$	$A'_s = A_s$	
		Washa & Fluck	Gilbert & Nejadi	Washa & Fluck	Washa & Fluck	Washa & Fluck Excluding Outliers
Mechanics-Based	Mean	0.93	0.92	0.95	0.94	0.86
	COV (%)	7.8	5.0	5.9	15.1	3.5
CSA Handbook	Mean	1.40	0.96	1.27	1.35	1.21
	COV (%)	6.1	5.1	4.1	14.3	4.0
Gilbert & Kilpatrick (2017)	Mean	1.08	0.89	1.01	1.10	1.06
	COV (%)	6.5	8.1	4.6	14.5	4.2

3.6   Discussion of Proposed and Existing Methods

3.6.1   Branson/CAC Design Handbook

The method presented in the Concrete Design Handbook yields a high mean test/predicted ratio of 1.4 for the results reported by Washa and Fluck (1952), but a significantly more accurate and slightly conservative ratio of 0.96 for the results reported by Gilbert and Nejadi (2004). The discrepancy can be attributed, in varying degrees, to:

1. Degree of conservatism of I_e computed based on a reduced modulus of rupture.
2. Oversimplification of Branson's creep coefficient, C_t.
3. Underestimation of ultimate shrinkage strains, $\varepsilon_{sh,u}$.

Short-term deflections predicted using I_e based on a reduced modulus of rupture overestimate Gilbert and Nejadi's (2004) observed deflections, with a mean test-predicted ratio of 0.67. On the other hand, the same method provided significantly more accurate, yet slightly unconservative ratios for the results of Washa and Fluck (1952), where the mean test/predicted ratio is 1.09. This inconsistency may be due to Gilbert and Nejadi's specimens not being exposed to drying, and consequently not shrinking significantly before loading ($t_o=t_c$). In this case, using one-half the modulus of rupture to account for reduction of the cracking moment due to restrained shrinkage is overly conservative. Conversely, Washa and Fluck's (1952) test specimens were left to dry in the laboratory environment for nine days prior to loading and therefore were likely to have experienced significant shrinkage. Using a reduced modulus of rupture is clearly appropriate in this case. The overestimation of short-term deflections for Gilbert and Nejadi's specimens compensated for shortcomings in methods for predicting creep and shrinkage deflections to provide accurate predictions of total deflections. On the other hand, the predicted short-term deflections for Washa and Fluck's specimens were reasonably accurate, which emphasized the deficiencies in methods for computing incremental deflections.

Moreover, the creep coefficient is oversimplified. The experimental creep coefficient ($\emptyset(t,t_o) = 1.71$) reported by Gilbert and Nejadi (2004) is relatively close to the creep coefficient computed using equations provided in the CAC Handbook ($\emptyset(t,t_o) = 1.15$). This, combined with the overestimated short-term deflection, yielded accurate creep deflections. On the other hand, the experimental creep coefficient of approximately 4.4

reported by Washa and Fluck (1952) was significantly larger than the creep coefficient of 1.4 computed using the CAC Handbook (CAC, 2016) equations, which mean that the creep deflection was significantly underestimated. Additionally, the experimental shrinkage strains reported by Gilbert and Nejadi (2004) and Washa and Fluck (1952) were approximately twice as large as those computed using equations provided in the CAC Handbook, which led to the underestimation of shrinkage deflections.

In summary, the CAC Concrete Design Handbook Method underestimated shrinkage deflection for both Gilbert and Nejadi's (2004) and Washa and Fluck's (1952) test specimens. It overestimated the short-term deflection for Gilbert and Nejadi's specimens, thereby yielding relatively accurate creep and total deflections. However, since it accurately predicted the short-term deflection for Washa and Fluck's specimens, the creep deflection and total deflection were markedly underestimated.

Table 3-3 shows values recommended by Branson (1977) for computing creep and shrinkage deflections. For a typical concrete member in the interior of a building where the age at loading is between 3 and 14 days and relative humidity is approximately 50% (ACI 209, 2008), C_t has a minimum value of 2.00. Similarly, $\varepsilon_{sh,u}$ varies between 506 and 795$\mu\varepsilon$. However, the Concrete Design Handbook recommends simplified methods for computing C_t and ε_{sh} that yield maximum values of 1.6 and 400$\mu\varepsilon$, respectively. C_t and ε_{sh} were computed, using this technique, to be 1.4 and 349 $\mu\varepsilon$ for Washa and Fluck's test specimens and 1.15 and 287 $\mu\varepsilon$ for Gilbert and Nejadi's specimens respectively. These values are all smaller than those shown in Table 3-3, and so the associated creep and shrinkage deflections are therefore likely to be underestimated. Unfortunately, neither Gilbert and Nejadi (2004) nor Washa and Fluck (1952) reported the relative humidities in their test data, and therefore deflections cannot be computed using the Branson (1977) Method with the appropriate C_t and ε_{sh} values.

Table 3-3: Creep Coefficients and Ultimate Shrinkage Strains Proposed by Branson (1977)

Age at Loading (days)	Average Relative Humidity, Ultimate Creep Coefficient or Shrinkage Strain											
	≥90%		80%		70%		60%		50%		≤ 40%	
	C_t	$\varepsilon_{sh,u}$ ($\mu\varepsilon$)	C_t	$\varepsilon_{sh,u}$ ($\mu\varepsilon$)	C_t	$\varepsilon_{sh,u}$ ($\mu\varepsilon$)	C_t	$\varepsilon_{sh,u}$ ($\mu\varepsilon$)	C_t	$\varepsilon_{sh,u}$ ($\mu\varepsilon$)	C_t	$\varepsilon_{sh,u}$ ($\mu\varepsilon$)
1	-	281	-	562	-	655	-	749	-	842	-	936
7	1.57	234	1.72	468	1.88	546	2.04	624	2.21	702	2.35	780
10	1.50	182	1.63	364	1.79	425	1.94	485	2.10	546	2.23	607
20	1.37	149	1.49	298	1.64	347	1.78	397	1.92	447	2.05	496
28	1.32	130	1.44	260	1.58	303	1.72	347	1.86	390	1.97	433
60	1.21	86	1.32	172	1.45	201	1.57	230	1.70	259	1.81	287
90	1.17	66	1.27	131	1.39	153	1.51	175	1.63	197	1.74	218

3.6.2   Consideration of Mechanics-Based Method by Others

The proposed mechanics-Based Method for computing long-term deflections due to creep is inspired by the "increased 'n'" approach described in numerous references, including Pauw and Meyers (1964), Yu and Winter (1960) and Branson (1977), where creep deflections are obtained by computing a neutral axis depth based on an age-adjusted modular ratio. Branson pursued the "increased 'n'" approach with great interest but was unsuccessful in obtaining satisfactory agreement with experimental data, including that reported by Washa and Fluck (1952), likely due to difficulties in computing kd and I_e. Methods then available for computing kd for doubly reinforced beams were iterative and fairly complex, which created room for uncertainties (e.g., Pauw and Meyers (1964)). Additionally, Branson computed I_e using an empirical equation based on an incorrect mechanical model (Equation 3-2) and did not account for the effect of restrained shrinkage on the magnitude of M_{cr} used to compute I_e. The "increased 'n'" approach when

implemented in the current study using appropriate, mechanics-based methods to compute kd and I_e yields satisfactory test/predicted ratios, and the effect of compression reinforcement, creep coefficients, and shrinkage strains on the total deflection can be accurately represented.

Final creep deflections were computed based on the concrete stress at time t, after creep has taken place. Since creep causes a lowering of the neutral axis (i.e., $\overline{kd} > kd$), the maximum compressive concrete stress at time t is smaller in magnitude than the short-term maximum compressive stress at time t_o. More conservative creep deflections could be obtained by computing creep deflections based on the short-term concrete stress. This might be a practical consideration if creep deflections at time young and intermediate are of interest but appears to be overly conservative when only the final deflection is of interest.

Deflections due to shrinkage were computed for an uncracked section as justified in Section 3.3.2. The net curvature was computed based on residual strains at the top and bottom fibers caused by shrinkage restraint by the top and bottom steel areas. This reflects the efficiency of compression reinforcement in markedly reducing the deflection due to shrinkage warping.

The effect of restrained shrinkage is most pronounced in singly reinforced members and achieving a satisfactory prediction is necessary to assure the serviceability of structures. The Mechanics-Based Method provided a mean test/predicted ratio of 0.92 (COV = 7.2%) for Gilbert and Nejadi's (2004) and 0.93 (COV = 5.0%) Washa and Fluck's (1952) singly-reinforced specimens. The similarity of these two values may be an indication of the accuracy and consistency of this method in predicting long-term deflections, despite differences in reinforcement ratio, concrete strength, Young's Modulus and other factors unique to each experimental study.

3.7   Conclusions

This chapter has critically evaluated two existing methods for computing the incremental deflections due to creep and shrinkage. The first is the method described in the CAC Concrete Design Handbook (CAC, 2016), which is based on an empirical method proposed by Branson (1977). The second is an empirical method proposed by Gilbert and Kilpatrick

(2017), which presents an improvement to the method in the AS3600-2009 code provisions. It also presented a Mechanics-Based Method for computing the incremental deflections due to creep and shrinkage, and outlined discrepancies between the three methods. Moreover, the accuracy of these methods in predicting long-term deflections was quantified using test/predicted ratios.

The conclusions of this chapter are as follows:

1. Short-term deflections computed using I_e based on a reduced modulus of rupture were overestimated for Gilbert and Nejadi's (2004) test specimens because they were not exposed to drying before loading and so any effects of restrained shrinkage were likely slight. On the other hand, short-term deflections were more accurately predicted for Washa and Fluck's (1952) test specimens that were exposed to drying prior to loading and so experienced restrained shrinkage.

2. Methods for computing incremental deflections due to creep and shrinkage described in the CAC Concrete Design Handbook are based on empirical methods proposed by Branson (1977). However, the Concrete Design Handbook provisions for computing ultimate shrinkage strains and creep coefficients are simplifications of the values tabulated by Branson (1977). The CAC Concrete Design Handbook Method yielded an unconservative mean test/predicted ratio of 1.34 for the total deflection of Washa and Fluck's (1952) test specimens. More accurate and slightly conservative test/predicted ratios were obtained for the total deflection of Gilbert and Nejadi's (2004) test specimens, with a mean test/predicted ratio of 0.97. This is due to the overestimation of the short-term deflection for Gilbert and Nejadi's test specimens, which compensated for the underestimation of incremental deflections due to creep and shrinkage.

3. Incremental deflections due to creep and shrinkage can be more accurately predicted using the method described in the Concrete Design Handbook using creep coefficients and ultimate shrinkage strains recommended by Branson (1977).

4. The Mechanics-Based Method for computing creep deflection based on an age-adjusted modular ratio and a lowered neutral axis, and shrinkage deflection based on strains due to forces imposed by the top and bottom reinforcing steel on the concrete, was found to yield accurate and slightly conservative predictions. The

mean test/predicted ratio computed using this approach is 0.94 for Washa and Fluck's (1952) specimens and 0.92 for Gilbert and Nejadi's (2004) specimens. The coefficients of variation of test/predicted ratios are 5.0% for Gilbert and Nejadi's (2004) specimens and 10.3% for Washa and Fluck's (1952) specimens.

5. Gilbert and Kilpatrick's (2017) method provided a slightly unconservative mean test/predicted ratio of 1.06 for Washa and Fluck's (1952) test specimens, but a slightly conservative ratio of 0.89 for Gilbert and Nejadi's (2004) specimens

Chapter 4

4 Simplified Methods for Computing Long-Term Deflections

The Mechanics-Based Method for computing incremental deflections due to creep and shrinkage described in Chapter 3 provides consistent and slightly conservative predictions of long-term deflections. It is also straightforward, using familiar equations readily available in the CAC Concrete Design Handbook (CAC, 2016). However, its somewhat laborious nature makes it time-consuming for designers, who often estimate the initial depth of a member based on deflection criteria. The CSA A23.3 design standard (CSA, 2014) presents a simplified method for computing long-term deflections based on the short-term deflection using a single multiplier that accounts for the effects of creep and shrinkage. The unified multiplier is independent of the magnitude of the applied load. However, the long-term deflection, particularly due to creep, was shown in previous chapters to be heavily dependent on the maximum concrete compressive strains and so on the magnitude of the applied load. The unified multiplier is also independent of the creep coefficient and shrinkage strains. Chapter 2 showed that accurate predictions of creep coefficients and shrinkage strains difficult and including them as independent variables is desirable. Therefore, this chapter will:

1. Critically evaluate the sustained load deflection multiplier in A23.3.

2. Assess the accuracy of the A23.3 Multiplier in comparison to the Mechanics-based Method described in Chapter 3.

3. Present an Alternative Simplified Method for computing long-term deflections based on short-term deflections.

4. Compare the results obtained using the A23.3 Multiplier with the Mechanics-Based and Alternative Simplified Methods

4.1   A23.3 Multiplier for Computing Long-Term Deflections

4.1.1   Background of Sustained Load Multiplier in A23.3

The CSA A23.3 design standard (CSA, 2014) presents a simplified method for computing long-term deflections, Δ_{LT}, using a multiplier applied to the short-term deflection, Δ_i, intended to account for the combined effect of creep and shrinkage. The total deflection, Δ_T, can then be computed as $\Delta_T = \Delta_{LT} + \Delta_i$. The long-term deflection is computed as

$$\Delta_{LT} = \left[\frac{S_t}{1+50\rho'}\right]\Delta_i \tag{4-1}$$

where ρ' is the compression reinforcement ratio, A'_s/bd, and S_t, a factor that accounts for the duration of the sustained load, has a maximum value of 2.0 for load durations greater than 60 months.

This approach is based on an empirical method proposed by Branson (1977) and has an identical form to Branson's Equation for computing creep deflection discussed in Section 3.3.2 (Equation 3-13). Branson's Empirical Method computes the combined creep and shrinkage deflection as

$$\Delta_{LT} = \left[\frac{T}{1+50\rho'}\right]\Delta_i \tag{4-2}$$

where T, the combined creep and shrinkage coefficient, is recommended by Branson (1977) to be taken as 2.5. This value is similar to the creep coefficient of 2.5, commonly assumed by designers and researchers when parameters such as relative humidity and age at loading are not known (e.g. Scanlon and Bischoff, 2008; Gilbert, 1999; Dilger, 1982).

Figure 4-1 was extracted from a revision proposed by ACI Committee 435 to ACI 318-71 building code committee (ACI 435, 1978), based on figures presented in Branson (1977). The vertical axis is the ratio of the sustained load deflection factor (i.e., the ratio of long-term to short-term deflection) for a member with tension and compression reinforcement to the sustained load deflection factor for a member with the same area of tension reinforcement. The variation of this ratio with the compression reinforcement ratio for three

experimental programs (Washa & Fluck, 1952; Yu & Winter, 1960; and Hollington, 1970) is shown. The figure was used to demonstrate the adequacy of Equation (4-2).
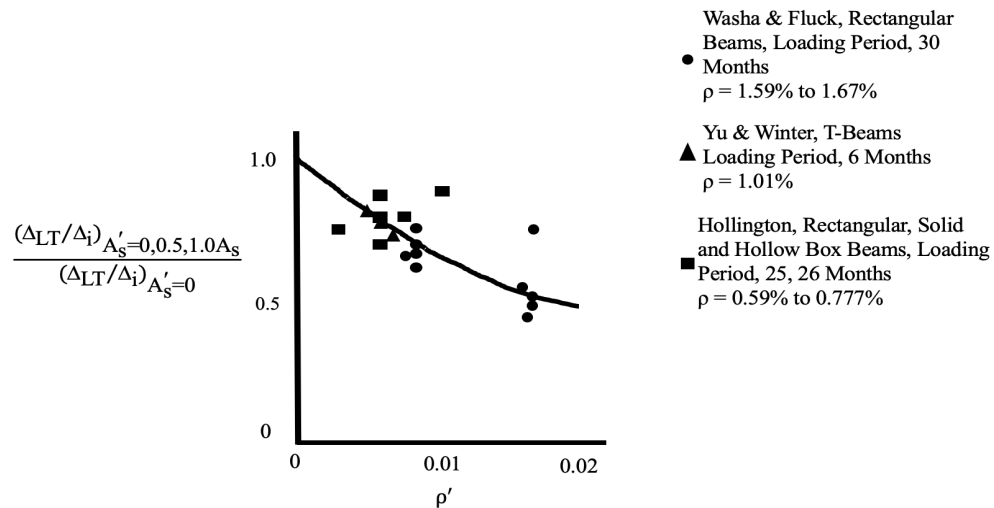
Figure 4-1: Fit of Branson's Empirical Method to Test Data (ACI 435, 1978)

Inspection of Figure 4-1 shows that Branson's Empirical Method is unconservative for a number of experimental data points. Yu & Winter (1960) applied a sustained load for six months, whereas Washa & Fluck (1952) and Hollington (1970), according to ACI Committee 435 (ACI 435, 1978), applied a sustained load for 26-30 months. However, figures in Branson (1977) and the CAC Concrete Design Handbook (2016) imply that the long-term deflection at six months is approximately 70% of the long-term deflection at 30 months, and so deriving an empirical equation based on the ratio of long-term to short-term deflection may be inappropriate. Furthermore, the Branson Empirical Method was developed based on the combined results of experimental programs by Yu & Winter (1960), who tested T-beams exclusively, and Washa & Fluck (1952), who only conducted tests on rectangular beams. This may be problematic since the long-term deflection is attributable to creep and shrinkage, which are intrinsic material properties, while the short-term deflection is dependent on the geometry of the cross-section as reflected by the moment of inertia and so is independent of the creep and shrinkage properties of concrete. It is also common for T-beams to have a neutral axis depth less than the thickness of the flange and, in some cases, less than the depth of the cover (MacGregor and Bartlett, 2000), which would imply that any compression reinforcement may not be particularly effective in reducing the long-term deflections. Moreover, parameters pertaining to ambient

environmental conditions and testing practice such as creep coefficients, shrinkage strains and age at loading were likely to have varied between the different experimental programs but were not considered in deriving Branson's Empirical Equation. Previous chapters have demonstrated the substantial impact of these factors on the long-term deflections and neglecting them in deriving an empirical method for computing long-term deflections may yield an unsatisfactory result. However, experimental creep coefficients and shrinkage strains were not reported in the studies by Yu & Winter (1960) and Hollington (1970) and therefore a direct comparison cannot be made.

4.1.2   Variation of Deflection with Reinforcement Ratio

The A23.3 Multiplier (Equation 4-1) is independent of the magnitude of the applied service load relative to the reinforcement ratio, ρ. In practice, the magnitude of the applied load increases with ρ. For a typical concrete flexural member where the ultimate limit state design load is $M_f = 1.25M_D + 1.5M_L$, and the ratio of live load to dead load, $k = M_D/M_L$, is between 0.5 and 1.5, the magnitude of M_D can be calculated for any given ρ. The magnitude of the service load, M_s, can subsequently be computed to quantify the expected maximum concrete strain.

Figure 4-2, derived on this basis, shows the essentially linear increase of M_s/M_{cr} with ρ for $k = 1.5$. Members with $\rho = 0.002$ were found to have M_s/M_{cr} less than 1.0, even for M_{cr} computed using a reduced modulus of rupture, and therefore remain uncracked.
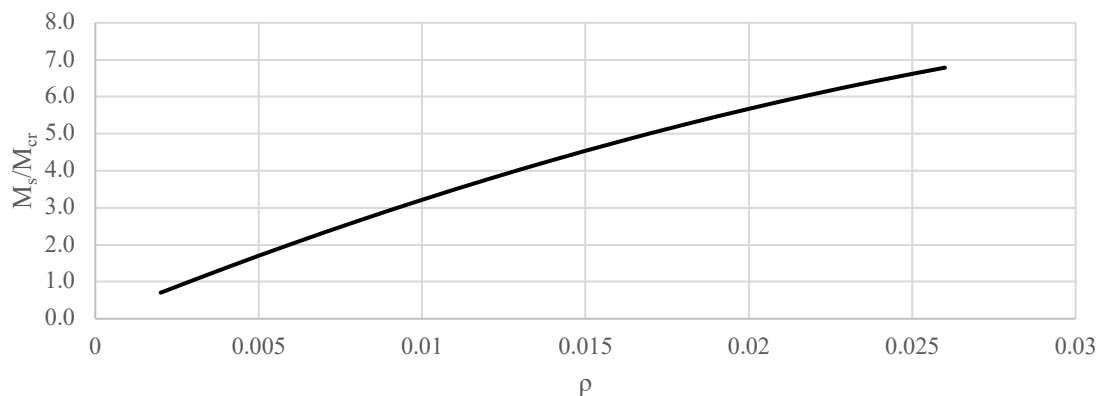
Figure 4-2: Variation of Applied Load with Reinforcement Ratio

Figure 4-3 shows the variation of the short-term deflection, Δ_i, with ρ and M_s/M_{cr} for various ρ'/ρ ratios. It is derived based on a concrete compressive strength, $f'_c = 30MPa$; reinforcement steel yield strength, $f_y = 400MPa$; span-to-depth ratio, $\ell/h = 14$; aspect ratio, $b/h = 0.67$; effective depth to overall depth, $d/h = 0.9$; and, $k = 1.5$. The short-term deflection is proportional to M_s/E_cI_e, where I_e, the effective moment of inertia essentially increases linearly with ρ (CAC 2016). Moreover, M_s, was shown in Figure 4-2 to be approximately proportional to ρ. As a result, the short-term deflection does not change significantly with M_s and ρ for $\rho > 0.01$. Members with $\rho < 0.004$ are uncracked and the short-term deflection computations are based on the gross moment of inertia, I_g, which yields identical short-term deflections for all members regardless of the compression reinforcement ratio. Figure 4-3 also shows that the short-term deflection does not vary greatly with the ratio of ρ'/ρ. This is intuitive since compression reinforcement does not have a significant contribution to the moment capacity of a flexural member (MacGregor & Bartlett, 2000). The relatively slight decrease in short-term deflection is due to the increase in I_{cr} caused by adding compression reinforcement (CAC, 2016).
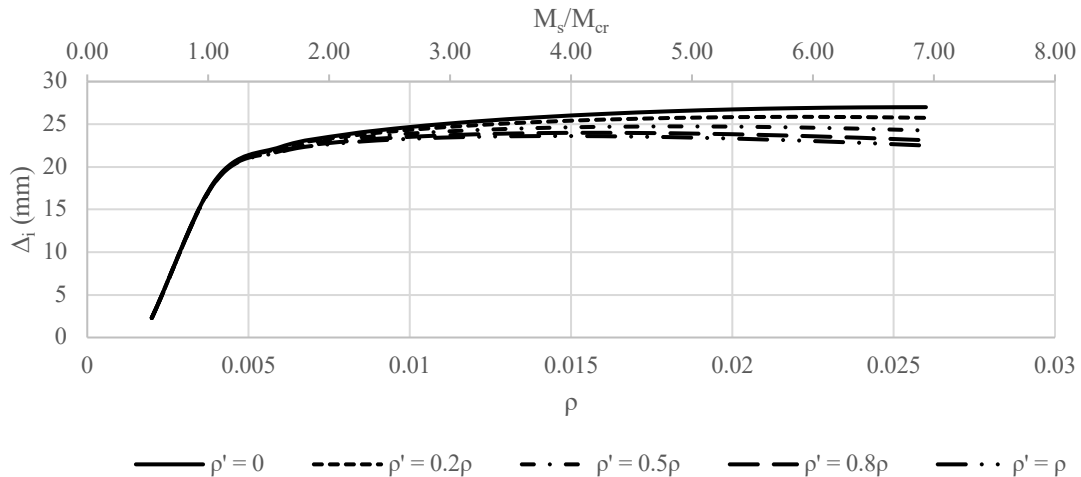
Figure 4-3: Variation of Short-Term Deflection with Reinforcement Ratio

4.1.3   Practical Compression/Tension Reinforcement Ratios

There are four main reasons for using compression reinforcement in concrete beams: reducing sustained load deflection; increasing ductility; changing the mode of failure from

compression-initiated to tension-initiated; and, fabrication ease (MacGregor & Bartlett, 2000). The amount of steel is primarily governed by the requirements for changing the mode of failure and fabrication ease (e.g., to support stirrups). Designers often add compression steel so that $(\rho-\rho') \leq 0.5\rho_b$, where ρ_b is the balanced reinforcement ratio, to ensure ductile failure (MacGregor & Bartlett, 2000). For example, a flexural member made of 30 MPa concrete with ρ = 2% would require a ρ'/ρ ratio less than 0.35. Similarly, members with lower reinforcement ratios would have a smaller ρ'/ρ upper limit. Designers also frequently use 2-15M reinforcing bars to support stirrups (i.e. $A'_s = 400$ mm^2).

Table 4-1 shows ρ'/ρ ratios for single-span and continuous beam examples presented in the CSA Concrete Design Handbook (CAC, 2004) and MacGregor & Bartlett (2000). Beams were found to trypically have a ρ'/ρ ratio of 0.2-0.35. On the other hand, one-way slabs have a ρ'/ρ ratio of zero in positive moment regions but may have ρ'/ρ ratios as high as 1 in negative moment regions due to detailing requirements for the bottom steel reinforcement.

Table 4-1: Typical ρ'/ρ Ratios for Practical Applications

Source		A_s (mm^2)	A'_s (mm^2)	ρ'/ρ
CSA Concrete Design Handbook (2016)	Example 2.1	1200	400	0.33
	Example 2.2	2500	400	0.16
	Example 2.3	4000	1400	0.35
	Example 2.4	7000	1400	0.2
MacGregor and Bartlett (2000)	Example 4-3	1500	400	0.27
	Example 5-5	2000	600	0.3
	Example 10-2	1300 to 2600	400	0.16
	Example 10-1 (One-way Slab)	10M @ 275mm	10M @ 275mm (Exterior Support)	1.0
		10M @ 275mm	0 (Interior Support)	0

4.1.4 Long-Term Deflections Computed According to A23.3

Figure 4-4 shows the variation of long-term deflection, Δ_{LT}, computed using the A23.3 Multiplier, normalized by the short-term deflection, with ρ and M_s/M_{cr}. The ratio of Δ_{LT}/Δ_i decreases with ρ and M_s for members with compression reinforcement and remains constant for members with only tension reinforcement. This trend is unrealistic since the warping due to restrained shrinkage in singly reinforced members is expected to increase with ρ. Further, the long-term deflection of beams with compression reinforcement is mostly attributable to the load-dependent creep deflection (Chapter 3 demonstrated that deflections due to restrained shrinkage are significantly reduced by adding compression reinforcement). The ratio of Δ_{LT}/Δ_i is therefore expected to follow the same trend as the short-term deflection (i.e., remain nearly constant) for higher ρ'/ρ ratios.
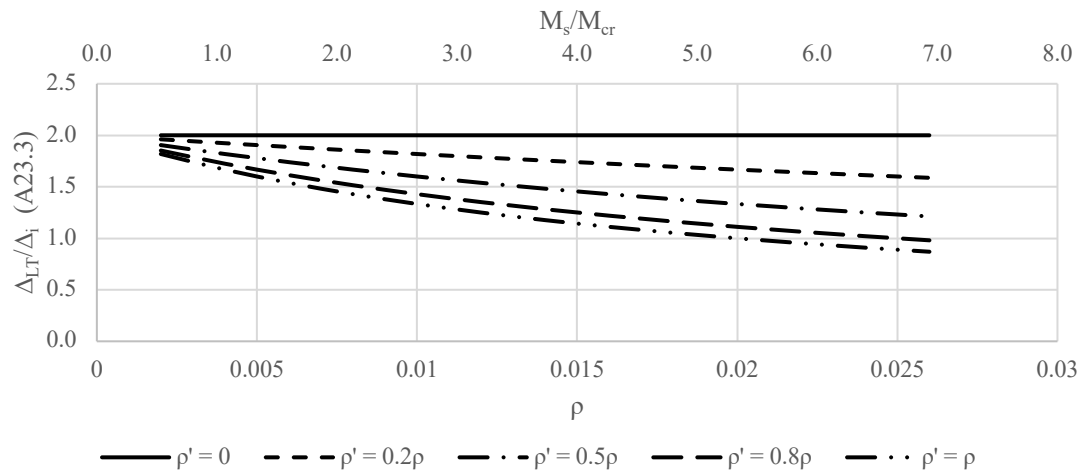
Figure 4-4: Variation of Δ_{LT}/Δ_i Computed Using A23.3 Multiplier with Reinforcement Ratio

Figure 4-5 shows the variation of the long-term deflection computed using the A23.3 Multiplier with ρ and M_s/M_{cr} based on the same material and geometric properties used to derive Figure 4-3. The long-term deflection of doubly reinforced members decreases with an increase in ρ and M_s/M_{cr}. The long-term deflection of singly reinforced members is similar to the short-term deflection curve because the A23.3 Multiplier is constant when $\rho'/\rho = 0$, as shown in Figure 4-4, and so the long-term deflection of singly reinforced

members is proportional to the short-term deflection. Therefore, conclusions similar to those discussed previously can be drawn: the A23.3 Multiplier results in an illogical trend where the long-term deflection decreases as the applied load increases and so does not accurately represent the impact of the reinforcement ratio on the shrinkage deflection of doubly reinforced members.
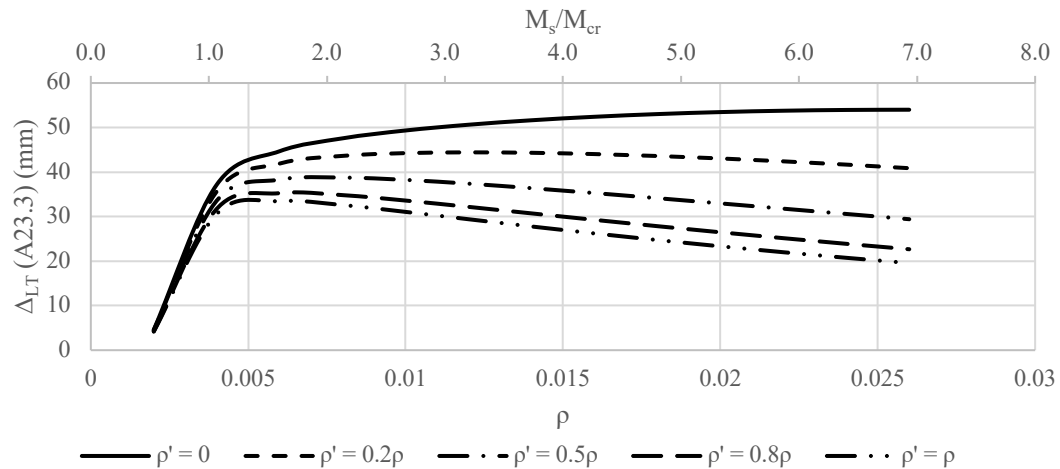
Figure 4-5: Variation of Long-Term Deflection Computed Using A23.3 Multiplier

These discrepancies can be traced back to the form of Equation (4-1), particularly the assumption that Δ_{LT} is directly proportional to Δ_i, (i.e., the long-term deflection is computed by multiplying the short-term deflection by a scalar) and the utilization of ρ' in the denominator. The short-term deflection was shown in Figure 4-3 to be essentially insensitive to variations of ρ and M_s/M_{cr}. However, when ρ' increases with ρ for a given ratio of ρ'/ρ, the long-term deflection computed using Equation (4-1) decreases.

4.2 Comparison Between Mechanics-Based and Simplified (A23.3) Long-Term Deflection Calculations

4.2.1 Description of Mechanics-Based Method

The mechanics-based Mechanics-Based Method for computing long-term deflection due to creep and shrinkage described in Chapter 3 depends on the creep coefficient, shrinkage strain, and the areas of top and bottom reinforcement. It was shown to yield satisfactory and slightly conservative test/predicted ratios compared to experimental data, including

those by Washa and Fluck (1952) used to derive the A23.3 Unified Multiplier (Equation 4-1). Therefore, the Mechanics-Based Method is the most accurate method for computing long-term deflections.

Using the Mechanics-Based Method, the load-dependent creep deflection is computed based on the magnitude of the time-dependent applied stress relative to the depth of the time-dependent neutral axis, which are both strongly correlated to the creep coefficient. The proven effectiveness of compression reinforcement in reducing the long-term creep deflection (Washa & Fluck (1952), Branson (1977), MacGregor & Bartlett (2000), Gilbert & Ranzi (2011)) is captured by the change in the neutral axis depth computed for single and double reinforced members. The creep deflection is not, however, a direct function of the short-term deflection. The shrinkage deflection is independent of the applied load and is strongly dependent on the ratio of top to bottom reinforcement. Singly reinforced members experience the largest deflection due to shrinkage, whereas symmetrically reinforced members do not exhibit shrinkage deflection.

4.2.2   Implications of mechanics-Based Method

Figure 4-6 shows the variation of the long-term deflection computed using the Mechanics-Based Method, normalized by the short-term deflection, with ρ and M_s/M_{cr}. The ratio of long-term to short-term deflection of a cracked section (i.e., $M_s/M_{cr} > 1$) was found to continuously increase with ρ and M_s/M_{cr} for single reinforced members $\rho'/\rho = 0$. This is intuitive because singly reinforced members experience the largest deformation due to restrained shrinkage, which is proportional to the area of tension reinforcement. Additionally, the magnitude of creep deflection relative to the short-term deflection is more pronounced due to the absence of compression reinforcement. Similarly, the Δ_{LT}/Δ_i gradient continues to decrease as ρ'/ρ increases since warping due to restrained shrinkage and creep deflection both decrease as the amount of compression steel increases. The long-term deflection ultimately reaches a limiting value of $\Delta_{LT} = \Delta_i$ for symmetrically reinforced members with $\rho'/\rho = 1$.

Figure 4-6 also shows that Δ_{LT}/Δ_i is significantly larger for uncracked members than than for cracked members. For example, when $\rho' = 0$, $\Delta_{LT}/\Delta_i = 3.5$ for $\rho = 0.002$ and $\Delta_{LT}/\Delta_i = 1.8$ for $\rho = 0.026$. This is because the short-term deflection of uncracked sections is

relatively small, while creep and shrinkage, both intrinsic material properties, cause at least some time-dependent deflections.
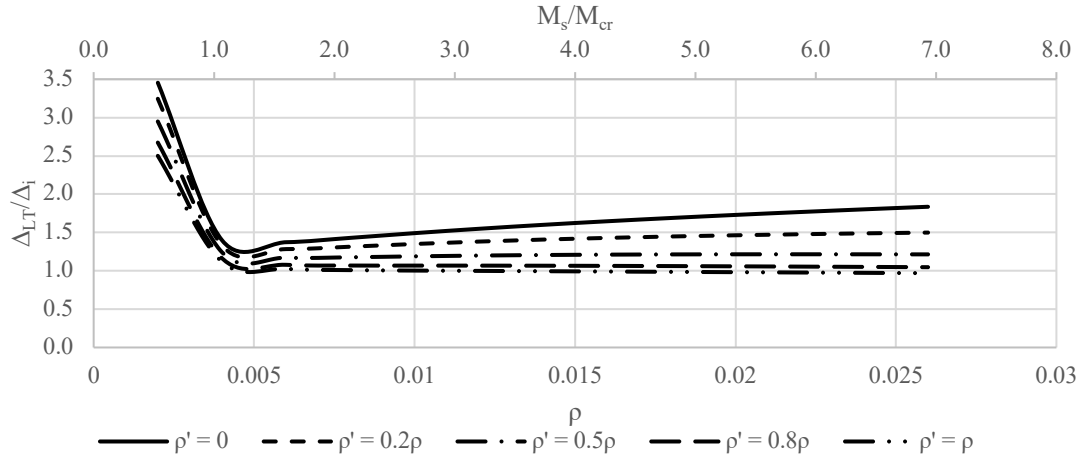
Figure 4-6: Variation of Δ_{LT}/Δ_i with Reinforcement Ratio

Figure 4-7 shows the variation of the long-term deflection computed using the Mechanics-Based Method with ρ and M_s/M_{cr} for the same geometric and material parameters used to derive Figure 4-3. It depicts a similar trend to that of Figure 4-6, where the long-term deflection increases with ρ and M_s for members with $\rho'/\rho < 0.5$ and is approximately constant for members with $\rho'/\rho \geq 0.5$. The decrease in the gradient of the long-term deflection computed using the mechanics-Based Method as ρ'/ρ increases reflects the effectiveness of compression reinforcement in reducing long-term deflections due to both creep and shrinkage.
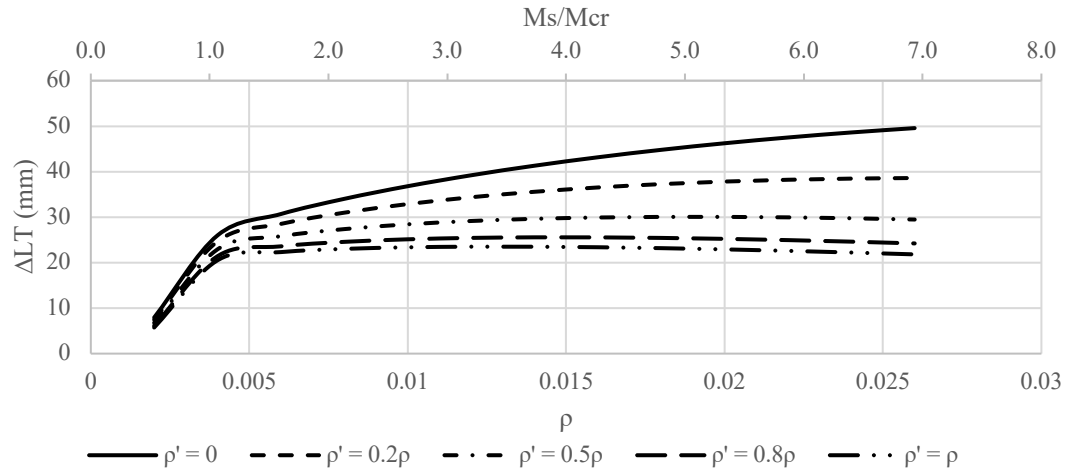
Figure 4-7: Variation of Long-Term Deflection with Reinforcement Ratio

Figures 4-8 and 4-9 show the contribution of creep and shrinkage to the total long-term deflection, respectively. Creep deflection contributes 75-100%, i.e., the majority, of the long-term deflection. Similarly, shrinkage deflection contributes 0-25% of the long-term deflection, assuming equal top and bottom concrete cover. These calculations were based on a shrinkage strain of $800\mu\varepsilon$, and a creep coefficient of 2.5, commonly used by designers and researchers and also consistent with Branson's (1977) recommendations for members existing in an environment with 50% average relative humidity and loaded at an age of seven days (Table 3-3).
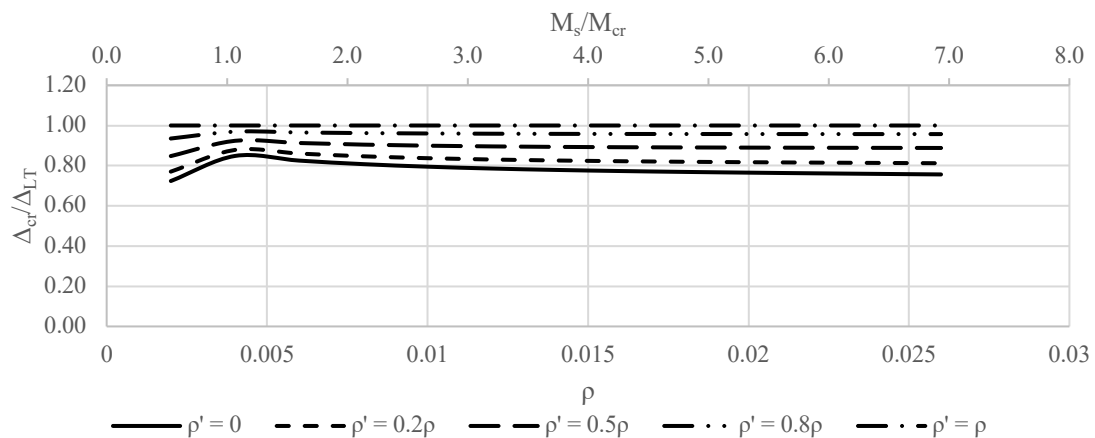
Figure 4-8: Contribution of Creep to Long-Term Deflection
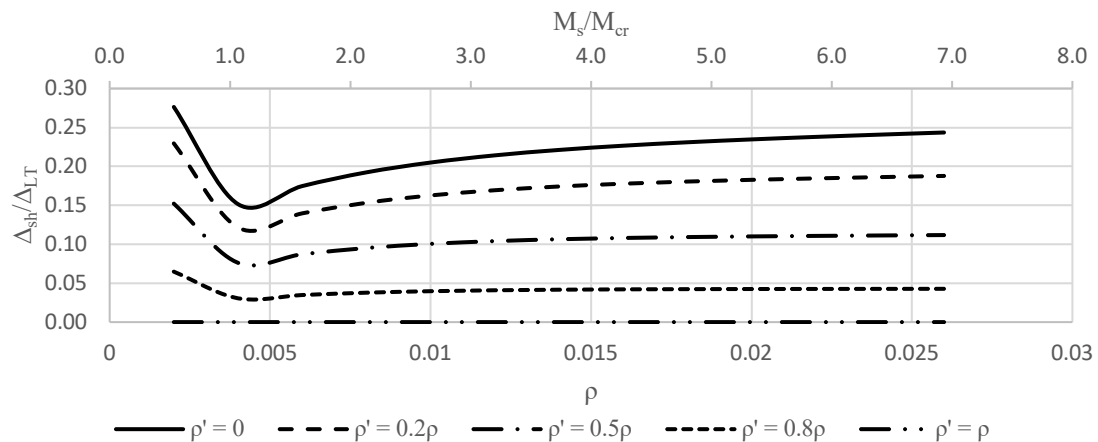
Figure 4-9: Contribution of Shrinkage to Long-Term Deflection

4.2.3   Comparison between A23.3 Multiplier and Mechanics-Based Method

Figures 4-10 (a) through (e) show a direct comparison between long-term deflections computed using the mechanics-Based Method and the A23.3 Multiplier. They are derived based on concrete compressive strength, $f'_c = 30MPa$; reinforcement steel yield strength, $f_y = 400MPa$; span-to-depth ratio, $\ell/h = 14$; aspect ratio, $b/h = 0.67$; effective depth to overall depth, $d/h = 0.9$; and, 100% sustained live load. The immediate deflection is also shown for reference. The A23.3 Multiplier consistently overestimates the long-term deflection of members with $\rho < 0.02$ and becomes increasingly conservative as ρ decreases. This trend is due to the long-term deflection being strongly dependent on the magnitude of the maximum concrete compressive strain and so on the applied load, which is not directly considered in the A23.3 Multiplier. The magnitude of the applied load (and therefore the long-term deflection) was shown in Figure 4-2 to decrease with ρ, which would result in reduced long-term deflections.

The overestimation of long-term deflection for lightly reinforced members suggests that the A23.3 Multiplier underestimates the effectiveness of compression reinforcement in reducing long-term deflections. This observation is expected because Branson's Empirical Method, which seems the basis of the derivation of the A23.3 Multiplier, was dominated by Washa and Fluck's (1952) specimens, where ρ was between 0.016 and 0.017 (Figure 4-1).

(a) ρ' = 0

(b) ρ' = 0.2ρ

(c) ρ' = 0.5ρ

(d) ρ' = 0.8ρ

(e) ρ' = ρ
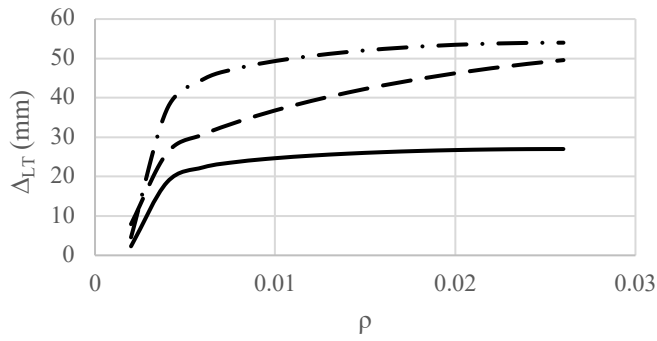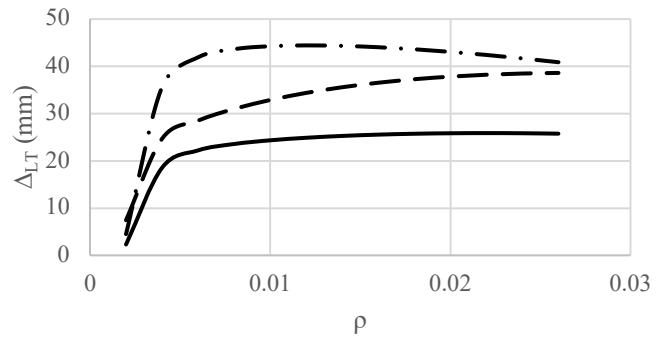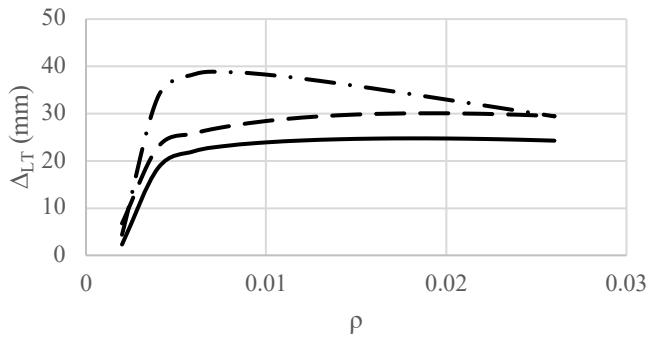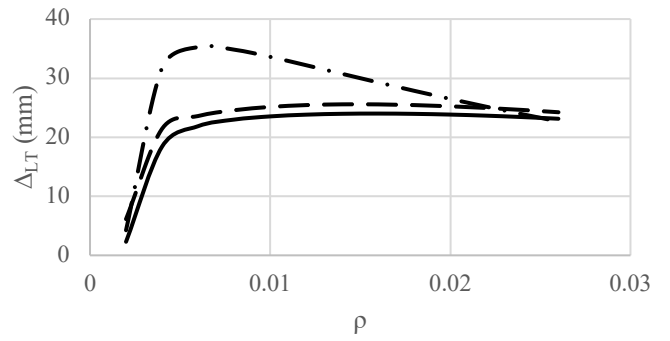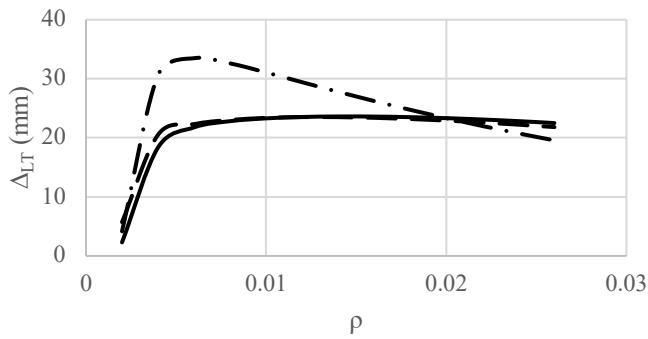
Figure 4-10: Comparison between Mechanics-Based and A23.3 Methods for Computing Long-Term Deflections

The use of compression reinforcement to support stirrups means that the areas of compression and tension reinforcement are often uncorrelated. Although Table 4-1 shows that the use of 2-15M bars in compression (A'_s = 400 mm^2) typically entails a ρ'/ρ ratio between 0.2 and 0.3, other ratios are possible. Figure 4-10 showed that the A23.3 Multiplier is most conservative for low reinforcement ratios and small ρ'/ρ ratios. Therefore, if ρ' is fixed at a certain value, say that corresponding to A'_s = 400 mm^2, the A23.3 Multiplier is expected to be most conservative for low reinforcement ratios and least conservative for high reinforcement ratios.

4.3   Alternative Simplified Method for Computing Long-Term Deflections

Sections 4.1 and 4.2 showed that the A23.3 Multiplier Method is conservative for many practical applications, which may be uneconomical. This section will present a simplified equation for computing long-term deflections based on the short-term deflection, which accounts for the factors that have the largest influence on the long-term deflection.

4.3.1   Selection of Variables for Simplified Deflection Equations

The sensitivity of the long-term to short-term deflection, Δ_{LT}/Δ_i, was evaluated using a parametric study considering: creep coefficient; ultimate shrinkage strain; dead to live load ratio; effective depth to overall depth ratio; and, concrete compressive strength. The Δ_{LT}/Δ_i ratio was found to be mostly influenced by the creep coefficient and ultimate shrinkage strain. It will be further assumed that 100% of the live load is sustained to maintain consistency with the existing A23.3 Multiplier Method.

Figure 4-11 shows the variation of Δ_{LT}/Δ_i with ρ'/ρ for various creep coefficients, $\emptyset$, and a given reinforcement ratio of 0.014. The Δ_{LT}/Δ_i ratio increases with the creep coefficient by approximately 40% for all ρ'/ρ ratios. The creep coefficient was shown in Figure 4-7 to have the most significant impact on the long-term deflection and is therefore integral to the derivation of accurate simplified methods for computing long-term deflections.
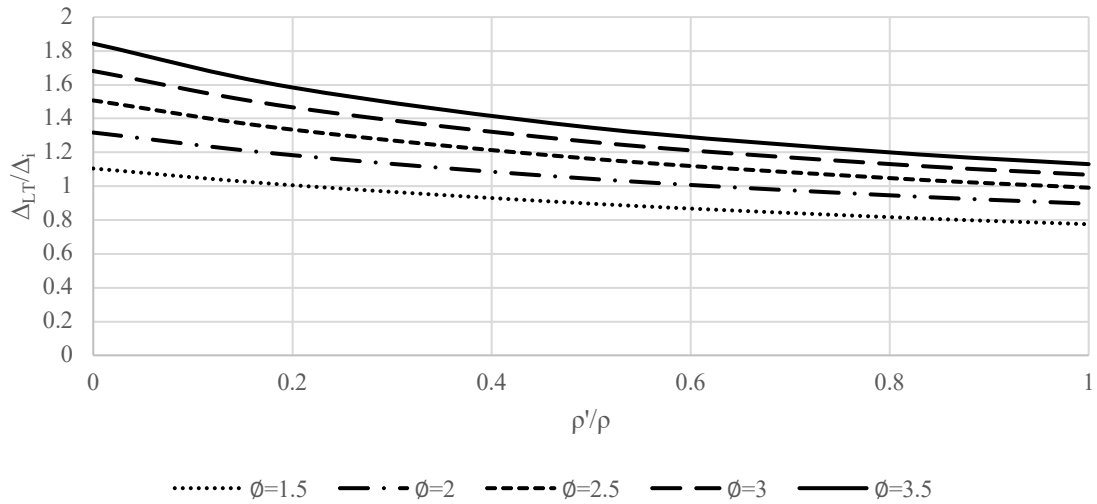
Figure 4-11: Impact of Creep Coefficient on Long-Term Deflection

Figure 4-12 shows the variation of Δ_{LT}/Δ_i with ρ'/ρ for various shrinkage strains, $\varepsilon_{sh,u}$ and a given reinforcement ratio of 0.014 (hence constant M_s and Δ_i values) and creep coefficient of 2.5. The sensitivity of Δ_{LT}/Δ_i to $\varepsilon_{sh,u}$ is most pronounced in singly reinforced members, where Δ_{LT}/Δ_i ratio was found to increase with $\varepsilon_{sh,u}$ by approximately 15%, and becomes less significant as ρ'/ρ increases. Symmetrically reinforced members (i.e., $\rho'/\rho = 1$) do not undergo deflection due to restrained shrinkage and the long-term deflection, exclusively due to creep, is identical to that shown in Figure 4-11 for $\emptyset = 2.5$.
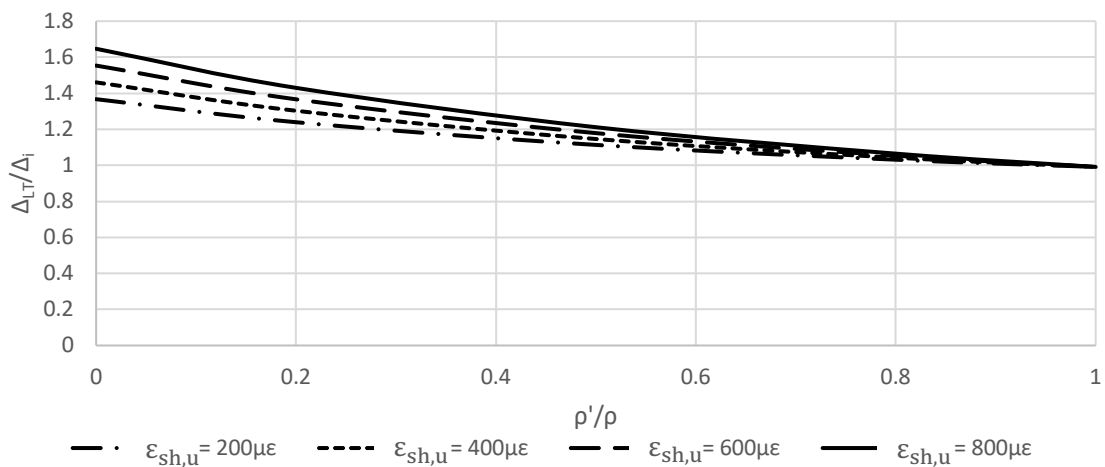
Figure 4-12: Impact of Ultimate Shrinkage Strain on Long-Term Deflection

Members located in the interior of a building typically experience an average relative humidity of approximately 50% (ACI 209, 1992), while exterior members often experience a spectrum of high and low relative humidities, depending on the geographic location. Figure A3.1.3 in the Canadian Highway Bridge Design Code (CSA, 2014) shows annual mean relative humidities based on geographic location. Mean relative humidities were found to range from 50% in the driest Canadian cities, such as Calgary and Edmonton, to 90% in the most humid cities, such as St. John's. Cities in south-western Ontario typically experience a a mean annual relative humidity of 60-70%. The contribution of the shrinkage strain to the long-term deflection decreases with $\varepsilon_{sh,u}$, which is inversely related to the relative humidity (as shown in Chapter 2). Figure 4-8 showed that the shrinkage strain contributes to no more than 25% of the long-term deflection based on $\varepsilon_{sh,u}$ of 800με, and would therefore have a smaller contribution in environments with higher relative humidities. For instance, the contribution of shrinkage deflection to the total deflection based on a shrinkage 400με, which corresponds to a relative humidity of 70% (Branson, 1977), was found to not exceed 10%. Furthermore, ambient conditions were shown in Chapter 2 to have similar influences on both creep and shrinkage. Therefore, a low creep coefficient is likely to be associated with low ultimate shrinkage strain and vice versa.

The introduction of shrinkage strains as a variable in a simplified equation for computing long-term deflections based on short-term deflection adds unnecessary complexity in the derivation and introduces a source of uncertainty for designers. In return, it will not result in a significant improvement in the overall accuracy of the equation. This is also suggested by the A23.3 Multiplier Method (Equation 4-1) since it is based on Branson's (1977) Method for computing creep deflection (Equation 3-13), but not shrinkage deflection. Therefore, the proposed simplified method for computing long-term deflections will be based on $\varepsilon_{sh,u} = 800$με, an upper-bound value that corresponds to a relative humidity of 50%.

4.3.2   Alternative Multiplier for Deflection of Doubly Reinforced Members

The previous sections, as well as the experimental program by Washa & Fluck (1952) demonstrated the effectiveness of compression reinforcement in reducing the long-term

deflection. Furthermore, singly reinforced members were shown to experience the largest deformations due to creep and shrinkage. Therefore, two unique equations for long-term deflection multipliers will be investigated: one for beams with tension and compression reinforcement and the other for beams with only tension reinforcement.

Simplified methods for computing long-term deflections of doubly reinforced members based on short-term deflections must account for the creep coefficient and ρ'/ρ. Figure 4-13 shows the variation of Δ_{LT}/Δ_i with ρ'/ρ and $\emptyset$ for a given reinforcement ratio (e.g. $\rho = 0.014$), which can be used to obtain a relationship between Δ_{LT}/Δ_i, ρ'/ρ, and $\emptyset$ using a multiple regression analysis.
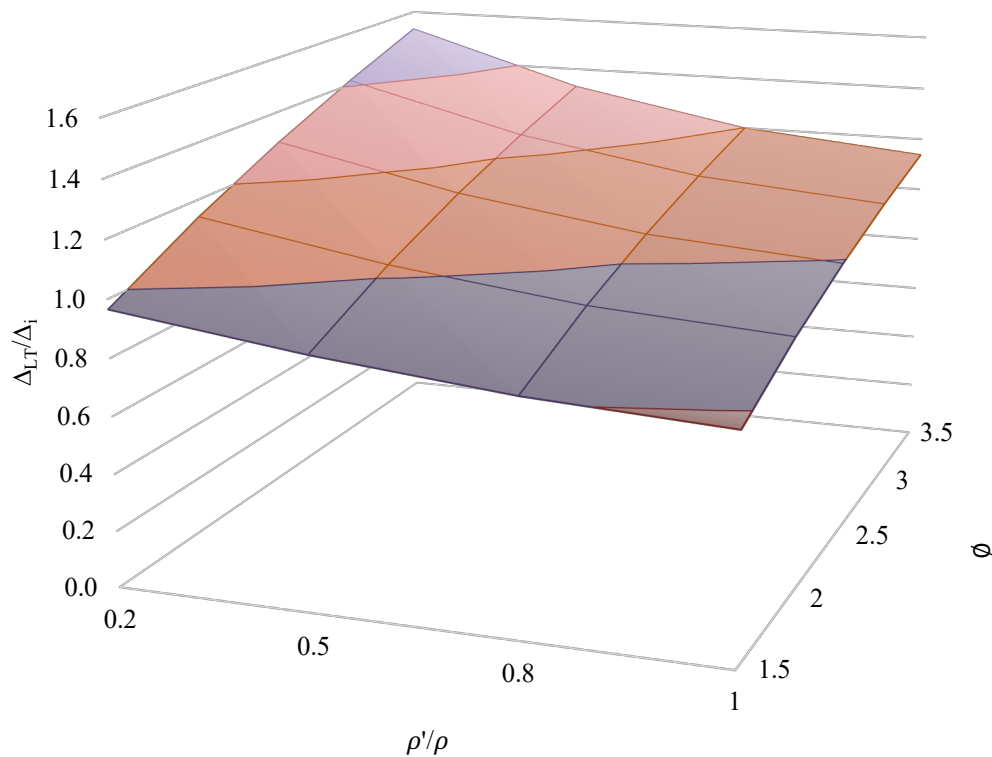
Figure 4-13: Variation of Long-Term Deflection of Double Reinforced Members with Creep Coefficient and ρ′/ρ

Equation 4-3 shows the form of a multiple regression analysis equation, where A, B, and C are the coefficients of regression.

$$\frac{\Delta_{LT}}{\Delta_i} = A(\emptyset) + B\left(\frac{\rho'}{\rho}\right) + C + Error \tag{4-3}$$

Table 4-2 shows the coefficients obtained by regression for beams with different reinforcement ratios. The coefficient "A" corresponding to the contribution of the creep coefficient to the long-term deflection is independent of ρ. However, coefficients "B" and "C" vary with ρ. Therefore, ρ must be included in the regression analysis.

Table 4-2: Coefficients of Regression for Different Reinforcement Ratios

ρ	A	B	C
0.018	0.22	-0.41	0.82
0.014	0.22	-0.36	0.78
0.01	0.22	-0.30	0.72
0.008	0.22	-0.26	0.69
0.006	0.22	-0.21	0.66

Figure 4-14 shows that "B" and "C" vary linearly with ρ, and therefore could be replaced by linear equations such as

$$B = B'(1+D\rho) \tag{4-4}$$

$$C = C'(1+E\rho) \tag{4-5}$$
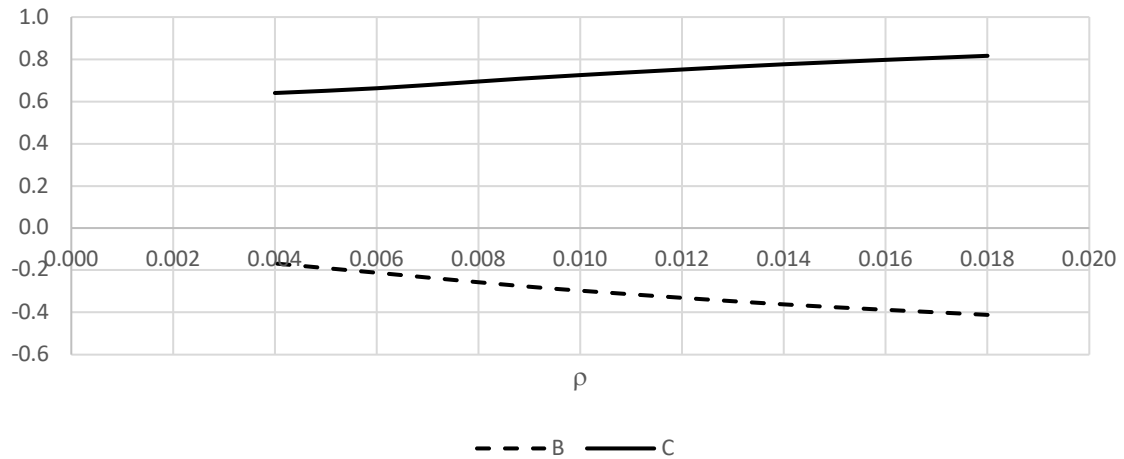
Figure 4-14: Variation of Regression Coefficients with Reinforcement Ratio

Combining Equations 4-4 and 4-5 with Equation 4-3 yields the following form for a linear regression equation

$$\frac{\Delta_{LT}}{\Delta_i}=A(\emptyset)+B'\left(\frac{\rho'}{\rho}\right)+B'D\,(\rho') + C'E(\rho) +E \pm \text{Error} \qquad (4\text{-}6)$$

A multiple regression analysis yields the following simplified equation for computing the long-term deflection of doubly reinforced members based on the short-term deflection:

$$\frac{\Delta_{LT}}{\Delta_i}=0.23(\emptyset)\text{-}0.2\left(\frac{\rho'}{\rho}\right)\text{-}21.8\,(\rho') + 13.4\,(\rho) +0.7 \qquad (4\text{-}7)$$

All parameters are statistically significant, and the standard error of regression is 0.045. This implies that the error of Equation 4-7 is roughly $\pm\,10\%$

Assuming a creep coefficient of 2.5 corresponding to a relative humidity of 50% and age at loading of 7 days, and $\rho'/\rho = 0.3$ for beams (as determined in Section 4.1.3), Equation 4-4 can be simplified to yield:

$$\Delta_{LT}=[1.22\text{-}21.8\,(\rho') + 13.4\,(\rho)]\Delta_i \qquad (4\text{-}8)$$

4.3.3   Alternative Multiplier for Deflection of Singly Reinforced Members

Figure 4-14 shows the variation of Δ_{LT}/Δ_i with ρ and $\emptyset$ for single reinforced members. A multiple regression analysis (considering $\emptyset$ and ρ as the independent variables) is sufficient to obtain a simplified equation for computing long-term deflections based on short-term deflections.
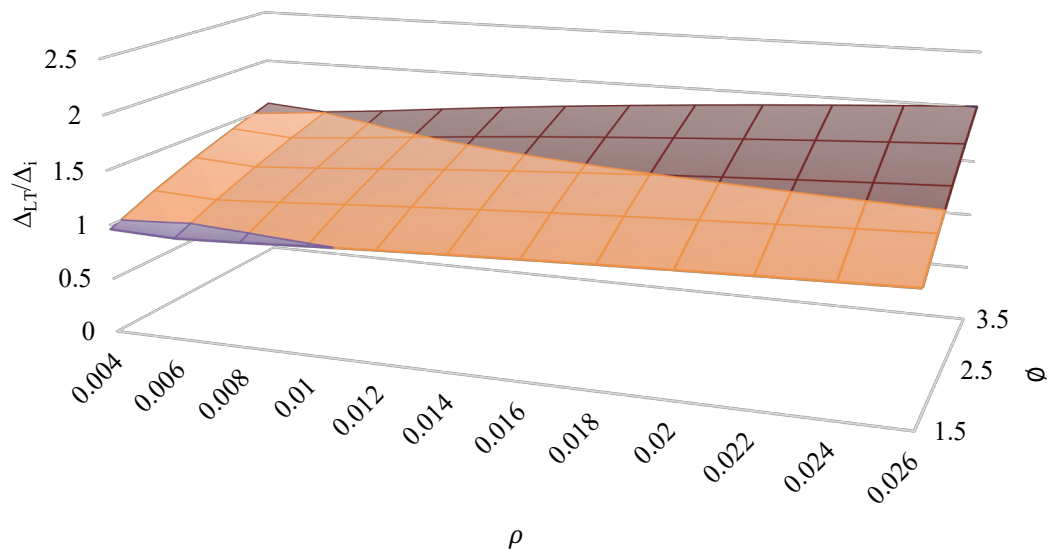
Figure 4-15: Variation of Long-Term Deflection of Single Reinforced Members with Creep Coefficient and ρ'/ρ

The simplified equation for computing long-term deflections of single reinforced members based on short-term deflection is:

$$\frac{\Delta_{LT}}{\Delta_i}=0.35(\emptyset)+23.4\,(\rho)+0.4 \qquad\qquad (4\text{-}9)$$

The standard error of regression is 0.038.

Equation 4-6 can be simplified by assuming a creep coefficient of 2.5 to yield:

$$\Delta_{LT}=[1.28+23.4\,(\rho)]\Delta_i \qquad\qquad (4\text{-}10)$$

Figure 4-16 shows variation in the long-term deflection of singly reinforced members computed using Equation 4-7 for doubly reinforced members with $\rho' = 0$, and Equation 4-8 for singly reinforced members (both based on a creep coefficient of 2.5). Equation 4-7 underestimates the long-term deflection by up to 14% and becomes increasingly unconservative as ρ increases. The discrepancy is likely due to the effect of restrained shrinkage, which is most significant in singly reinforced members and increases with ρ. This also reinforces the necessity of deriving unique equations for singly and doubly reinforced members.
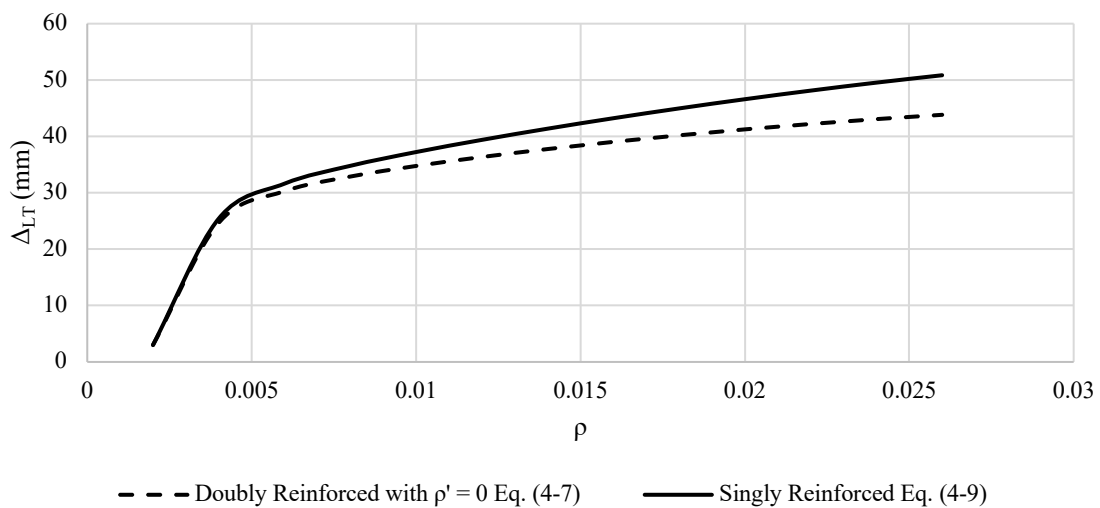
Figure 4-16: Comparison Between Δ_{LT} Computed Using Equations 4-7 and 4-8

4.3.4   Comparison Between A23.3 and Alternative Methods

Figure 4-17 (a) through (e) shows a comparison between long-term deflections computed using the Mechanics-Based Method, Δ_{LT}, the Unified Multiplier Method, Δ_{LT} (A23.3), and the Simplified Alternative Method (Equations 4-7 and 4-9), Δ_{LT} (Simplified). The Simplified Alternative Method is clearly in good agreement with the Mechanics-Based Method and can therefore be used to obtain a good approximation of the long-term deflections.

(a) ρ' = 0

(b) ρ' = 0.2ρ

(c) ρ' = 0.5ρ

(d) ρ' = 0.8ρ

(e) ρ' = ρ
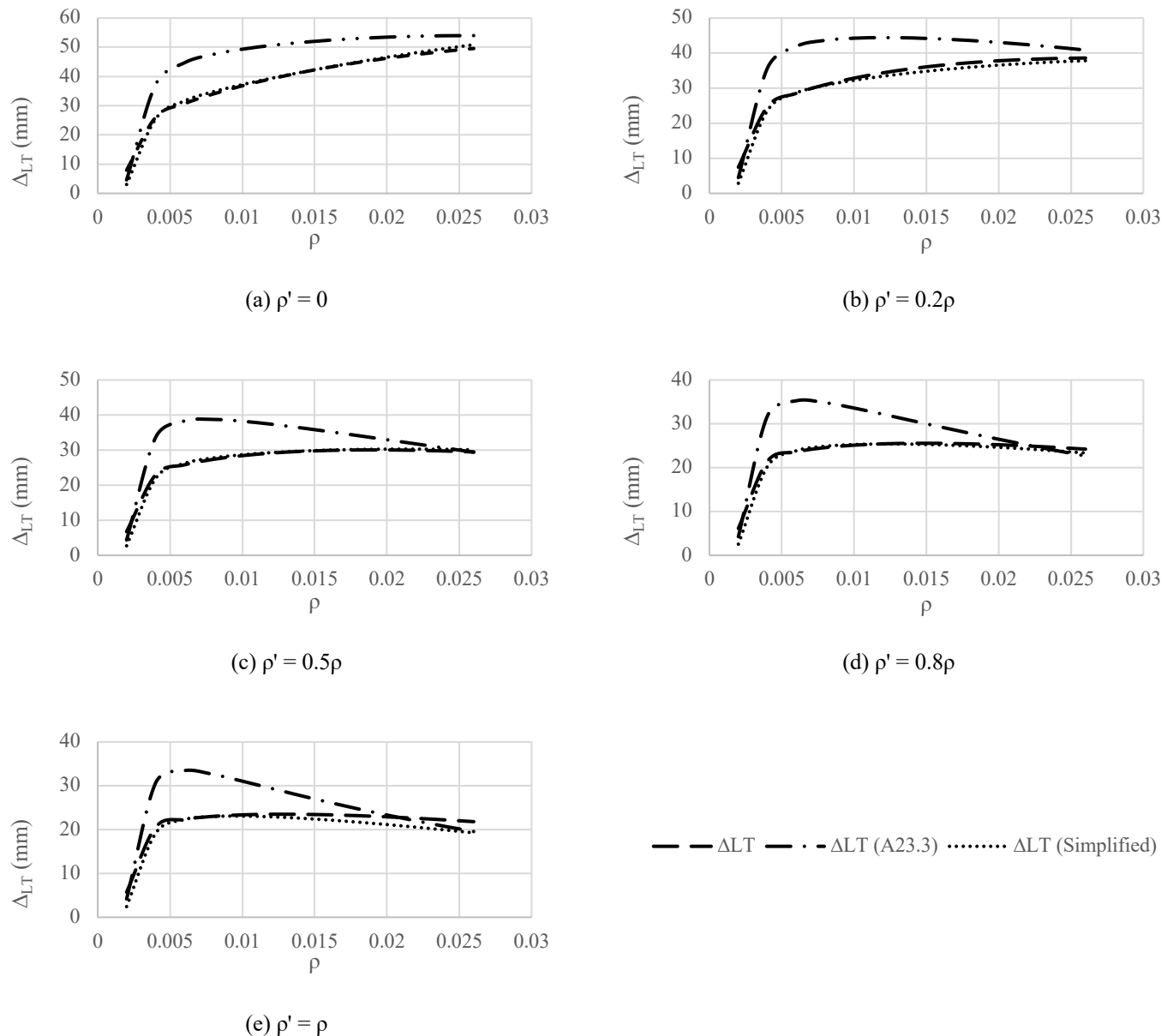
Figure 4-17: Comparison between Mechanics-Based, A23.3, and Alternative Methods for Computing Long-Term Deflections

The Alternative Simplified Methods presented in this section were derived based on: concrete compressive strength, f'_c = 30MPa; reinforcement steel yield strength, f_y = 400MPa; span-to-depth ratio, ℓ/h = 14; aspect ratio, b/h = 0.67; and, effective depth to overall depth, d/h = 0.9. Factors such as b/h, d/h, and f'_c (through the modulus of rupture, f_r) have a similar impact on the effective moment of inertia and hence the short-term and

long-term deflections of cracked concrete members, and therefore do not significantly influence the long-term to short-term deflection ratio. Moreover, Tang and Lubell (2008) showed that the flexural rigidity is essentially insensitive to $f_y \geq 400$MPa because E_s remains constant for steel with higher yield strengths. Therefore, the Alternative Simplified Method is applicable to most practical cases.

The universality of the Alternative Simplified Method was verified using a parametric study based on long-term deflections computed using the Mechanics-Based Method and those computed using the Alternative Simplified Method, and by quantifying test/predicted ratios for experimental programs by Washa and Fluck's (1952) and Gilbert and Nejadi's (2004). Table 4-3 shows a comparison between dimensional and material properties used in the derivation of the Alternative Simplified Method, and those belonging to Washa & Fluck's (1952) and Gilbert and Nejadi's (2004) test specimens. It also shows the mean test/predicted ratios computed for Washa and Fluck's and Gilbert and Nejadi's specimens based on the Alternative Simplified Method. The Alternative Simplified Methods yielded accurate mean test/predicted ratios of 0.97 for Washa and Fluck's (1952) specimens and 1.05 for Gilbert and Nejadi's (2004) specimens, despite their dimensional and material properties being different than those used to develop the Alternative Simplified Method. Gilbert and Nejadi's specimens with an applied moment to cracking moment ratio (M_s/M_{cr}) less than 1.8 were excluded from this analysis for reasons that will be discussed in the next section.

Table 4-3: Test/Predicted Ratios Based on the Alternative Simplified Method

	f'c (MPa)	fy (MPa)	ℓ/h	b/h	d/h	Mean Test/Predicted	COV (%)
Alternative Method	30	400	14	0.67	0.9	-	-
Washa & Fluck (1952)	18 - 23	320 - 380	30 - 70	0.75 - 4	0.8 - 0.85	0.97	13.8
Gilbert & Nejadi (2004)	18	500	10 - 20	0.75 - 2.5	0.8 - 0.9	1.05	4.2

4.4 Considerations for Lightly Loaded Members

The effect of tension stiffening, as quantified using the effective moment of inertia, is most significant when the service moment, M_s is close in magnitude to the design cracking moment, M_{cr}, where M_{cr} is based on the reduced or full modulus of rupture depending on the drying period before loading as discussed in Chapter 3. Figure 4-18 shows that the variation of Δ_{LT}/Δ_i with increasing ρ'/ρ for various reinforcement ratios. The Δ_{LT}/Δ_i ratio is generally shown to decrease with ρ'/ρ for all reinforcement ratios and increase with ρ for $\rho'/\rho < 0.5$. However, the curve representing $\rho = 0.004$ (corresponding to $M_s/M_{cr} = 1.35$, as shown in Figure 4-2) appears to be an outlier. The Δ_{LT}/Δ_i ratio for $\rho = 0.004$ is greater than Δ_{LT}/Δ_i for $\rho = 0.006$ ($M_s/M_{cr} = 2.0$) when $\rho'/\rho < 0.4$ and greater than Δ_{LT}/Δ_i for all other reinforcement ratios when $\rho'/\rho < 0.4$. The ratio of $I_e/I_{cr} = 1.20$ for $\rho = 0.004$ and 1.05 when $\rho = 0.006$, which indicates that the effect of tension stiffening is greater for $\rho = 0.004$ than for $\rho = 0.006$.
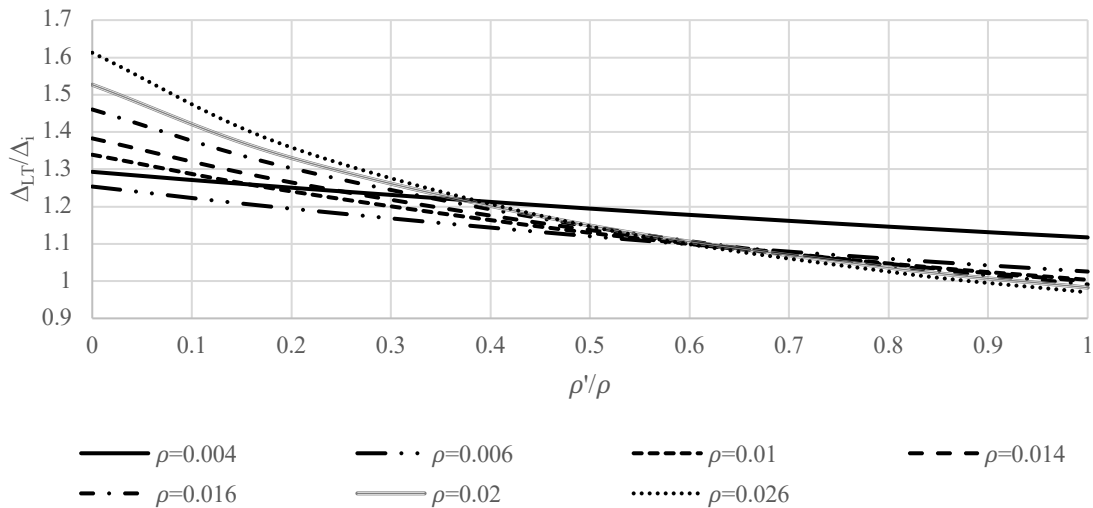
Figure 4-18: Variation of Long-Term Deflection with ρ'/ρ

Members with low M_s/M_{cr} experience low compressive strain in the concrete and hence reduced short-term deflections due to the applied load. They also experience reduced long-term deflections since the long-term deflection is strongly correlated to the applied load. However, the reduction in short-term deflection is more severe than the reduction in long-term deflection, which will yield large Δ_{LT}/Δ_i ratios for lightly loaded members. This was

observed in Gilbert and Nejadi's (2004) test specimens where members with low M_s/M_{cr} ratios were found to experience significantly larger Δ_{LT}/Δ_i ratios than those with high M_s/M_{cr} ratios.

Figure 4-19 shows the variation of Δ_{LT}/Δ_i with M_s/M_{cr} for Gilbert and Nejadi's (2004) and Washa and Fluck's (1952) test specimens. Experimental values for Δ_{LT}/Δ_i were reported in both studies, while experimental M_s/M_{cr} values were reported by Gilbert and Nejadi (2004) only. A reduced modulus of rupture was used to compute M_s/M_{cr} for Washa and Fluck's (1952) specimens since they were exposed to drying for 14 days prior to loading and therefore experienced significant restrained shrinkage. Chapter 3 showed that this approach yields accurate short-term deflections for Washa and Fluck's (1952) specimens and is therefore appropriate. Members with $M_s/M_{cr} > 1.75$ experience Δ_{LT}/Δ_i ratios clustered in the range of 1.0-2.0. On the other hand, members with $M_s/M_{cr} < 1.75$ exhibit a widely dispersed Δ_{LT}/Δ_i ratios, ranging from 2.5 to 4.4. The A23.3 Multiplier (which was found in Section 4.3.2 to be conservative for lightly reinforced members and therefore is expected to be conservative for Gilbert and Nejadi's (2004) test specimens) implies that Δ_{LT}/Δ_i has a maximum value of 2.0, and so is unconservative in this case.

▲ Gilbert & Nejadi (2004)   ● Washa & Fluck (1952)
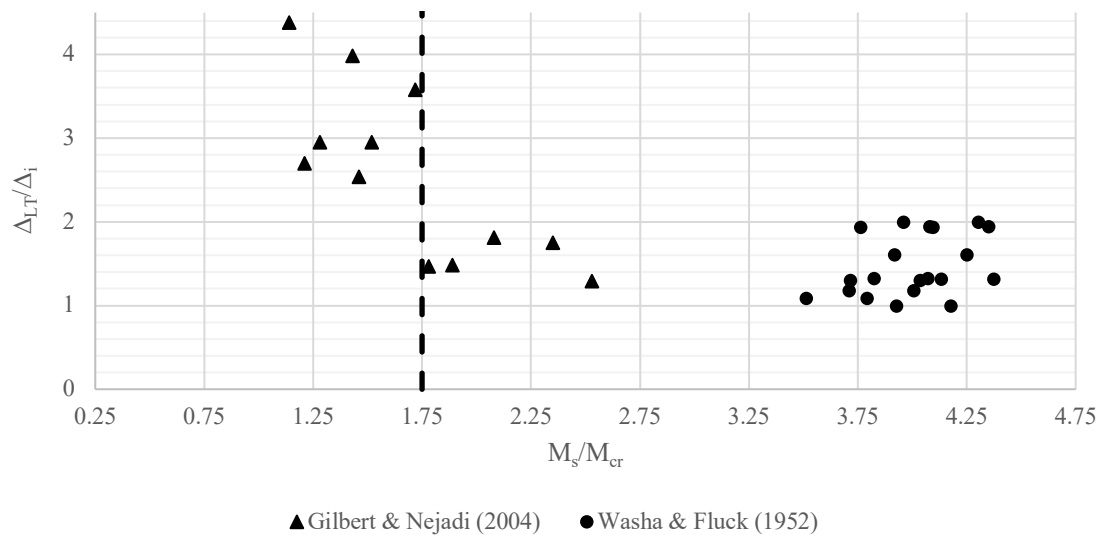
Figure 4-19: Variation of Δ_{LT}/Δ_i with M_s/M_{cr}

Quantifying the impact of tension stiffening on the short-term deflection, and consequently Δ_{LT}/Δ_i, is beyond the scope of this study. However, based on parametric studies and

experimental data analyses, Δ_{LT}/Δ_i seems inconsistent for M_s/M_{cr} ratios less than 1.75, and excessive reliance on the Alternative Simplified Method based on the long-term to short-term deflection ratio is not preferred. Using the Mechanics-Based Method as reported in Chapter 3 yields accurate long-term deflections regardless of the M_s/M_{cr} and is therefore more appropriate in these cases. The Δ_{LT}/Δ_i ratio was found using a parametric study, such as the one shown in Figure 4-13, to be stable and consistent for $M_s/M_{cr} \geq 2$, corresponding to $\rho \geq 0.006$, and the simplified analysis to determine the long-term deflection based on the short-term deflection is appropriate.

4.5   Conclusions

This chapter presented a critique of the A23.3 Multiplier Method for computing the long-term deflection based on the short-term deflection. It also presented a comparison between the A23.3 Multiplier and the Mechanics-Based Method presented in Chapter 3 for computing long-term deflections. An Alternative Simplified Method for computing long-term deflections based on short-term deflections was proposed for singly and doubly reinforced members. The conclusions of this chapter are as follows:

1. The A23.3 Multiplier is very similar to Branson's (1977) Empirical Method derived using three different experimental studies. The studies had unique load durations, ages at loading, cross-section geometry, and ambient environmental conditions. These factors have a significant impact on the long-term deflection and deriving an empirical equation based on the combination of these data sets may be inappropriate.

2. The long-term deflection computed using the A23.3 Multiplier decreases with an increase in the reinforcement ratio, ρ, and the maximum concrete compressive strain, hence the ratio of service to cracking moment M_s/M_{cr}. In fact, it should increase with increasing ρ because the long-term deflection is strongly dependent on the magnitude of the applied load. It also approaches a constant value in members with tension to compression reinforcement ratio greater than approximately 0.4 since compression reinforcement is effective in reducing long-term deflections.

3. The A23.3 Multiplier was found to consistently overestimate the long-term deflection of lightly reinforced members where M_{cr} is computed based on a reduced modulus of rupture. For example, for $\rho = 0.006$ and a compression reinforcement ratio, $\rho'/\rho = 0.5$, the Mechanics-Based Method predicts a long-term deflection that is only 67% of that computed using the A23.3 Multiplier.

4. The creep deflection contributes 75-100% of the long-term deflection, while shrinkage contributes only 0-25%. These results are based on a shrinkage strain, $\varepsilon_{sh,u}$, of 800$\mu\varepsilon$, and a creep coefficient, $\emptyset$, of 2.5, corresponding to a relative humidity of 50% and age at loading of 7 days. These conditions are typical interior members in a building, as well as exterior members in the least humid cities in Canada. Shrinkage contributes to no more than 10% of the long-term deflections in environments where the annual mean relative humidity is 70% (e.g., exterior members in south-western Ontario).

5. Simplified methods for computing long-term deflections based on short-term deflections must account for the creep coefficient, ρ'/ρ for doubly reinforced members, and ρ for single-reinforced members.

6. Equations for computing the long-term deflection, Δ_{LT}, based on the short-term deflection, Δ_i, can be derived using multiple regression analysis. The long-term deflection for singly reinforced members is

$$\frac{\Delta_{LT}}{\Delta_i} = 0.35(\emptyset) + 23.4\,(\rho) + 0.4 \tag{4-9}$$

with a standard error of 0.038. The long-term deflection of doubly reinforced members is given as

$$\frac{\Delta_{LT}}{\Delta_i} = 0.23(\emptyset) - 0.2\left(\frac{\rho'}{\rho}\right) - 21.8\,(\rho') + 13.4\,(\rho) + 0.7 \tag{4-7}$$

with a standard error of 0.045.

7. Members with low service moment to cracking moment ratios, M_s/M_{cr}, are likely to experience reduced short-term deflections due to applied loads, while the long-term deflections due to creep and shrinkage will be similar to those for more heavily loaded members. This will result in large and inconsistent Δ_{LT}/Δ_i ratios. The inconsistency is most pronounced for M_s/M_{cr} ratios less than 1.75 or $\rho < 0.006$ and use of Equations 4-7 and 4-9 to compute long to short-term deflection ratio is not preferred. The long-term deflection of these members can be accurately and conservatively predicted using the Mechanics-Based Method described in Chapter 3.

Chapter 5

5   Summary, Conclusions, and Future Work

5.1   Summary

The time-dependent deflection of reinforced concrete flexural members due to creep and shrinkage can cause severe serviceability problems (especially if deflection-sensitive elements are present) if not adequately accounted for. Creep is a load-dependent, intrinsic material property that causes time-dependent strain increments in the concrete, hence additional curvature and deflection. It also results in a reduction in the effective Young's Modulus of the concrete, which causes a lowering of the neutral axis and therefore a reduction in the maximum compression stress. Creep of concrete is quantified using the creep coefficient, which is the ratio of strain increments due to creep to the immediate strain due to the applied load. Shrinkage is a drying property and is characterized using only the ultimate shrinkage strain. ACI 209 (2008) recognizes four models for computing creep coefficients and ultimate shrinkage strains. Several studies attempt to quantify the accuracy of these models based on experimental data from the RILEM and NU Databanks. Designers and researchers often assume a creep coefficient of 2.5 in long-term deflection calculations (e.g. Scanlon and Bischoff, 2008; Gilbert, 1999; Dilger, 1982). Branson (1977) proposes a creep coefficient of 2.2 and a shrinkage strain of $700\mu\varepsilon$ for members loaded at 7 days and exposed to a relative humidity of 50% (typical of members in the interior of a building, or exterior members in the least humid Canadian cities such as Calgary and Edmonton).

Various methods for computing incremental deflections due to creep and shrinkage are reported in the literature. The Cement Association of Canada's (CAC) Concrete Design Handbook (CAC, 2016) presents a Mechanics-Based method based on empirical methods proposed by Branson (1977). Creep deflection is computed by applying a multiplier, that is a function of the creep coefficient, to the short-term deflection. This method accounts for the increase in strain and due to creep but does not accurately account for the lowering of the neutral axis. The shrinkage deformation of a flexural member is primarily due to restraint from the reinforcing steel, which causes residual stresses in the top and bottom fibers and hence additional strains, curvature, and deflection. Shrinkage deflection is

computed by applying an empirical multiplier, that is a function of the ratio of tension and compression reinforcement, to the ultimate shrinkage strain to obtain shrinkage curvatures and hence deflections. Branson (1977) recommended creep coefficients and ultimate shrinkage strain values, based on the relative humidity and age at loading, to facilitate creep and shrinkage deflection computations. Other empirical methods include the method proposed by Gilbert and Kilpatrick (2017), which presents an improvement to the method in the AS3600-2009 (AS, 2009) code provisions.

Analytical methods for computing long-term deflections due to creep and shrinkage can be derived using fundamental principles of mechanics. Creep deflections are computed by first calculating the location of the long-term neutral axis using mechanics-based equations readily available in the Concrete Design Handbook (CAC, 2016), but replacing the modular ratio with a time-dependent modular ratio. Subsequently, the magnitude of the maximum compressive stress in the concrete is computed based on the long-term neutral axis depth and the cracked moment of inertia. Finally, creep strains and curvatures are computed to obtain creep deflections. Shrinkage deflections are computed by calculating the force in the reinforcing steel due to restrained shrinkage, and subsequently computing residual stresses and strains in the top and bottom fibers. The shrinkage curvature and deflection are then computed based on these residual strains.

The A23.3 design standard (CSA, 2014) presents a simplified method for computing the long-term deflection by applying a multiplier, that is a function of the sustained load duration and the compression reinforcement ratio, to the short-term deflection. This method was empirically derived by Branson (1977) based on the results of three experimental studies (Washa and Fluck, 1952; Hollington, 1970; Yu and Winter, 1960), each with a unique load duration, ages at loading, cross-section geometry, and ambient environmental conditions.

Chapter 2 presented an overview of the four widely used models for predicting creep coefficients and ultimate shrinkage strains, namely ACI 209 (ACI 209, 2008); B3 (Bazant and Baweja, 1995, 2000); GL2000 (Gardner and Lockman, 2000); and, CEB-FIP MC90-99 (Comite Europeen du Beton, 1999). All prediction models have been calibrated using experimental data from the RILEM and NU Databanks and are at least partly empirical. It also presents an overview of five studies (Gardner, 2004; Al-Manaseer and Lam, 2005;

Bazant and Panula, 2000; Bazant and Li, 2008; and, Al-Manaseer and Prado, 2015) that assess the accuracy of the models by quantifying and statistically evaluating test/predicted ratios based on data from the RILEM and NU Databanks

Chapter 3 presented an investigation of the accuracy of Branson's (1977) Method as described in the Concrete Design Handbook (CAC, 2016), the Mechanics-Based Mechanics-Based Method, and Gilbert and Kilpatrick's (2017) Method in predicting the long-term deflection of 30 simply supported test specimens by Washa and Fluck (1952) and Gilbert and Nejadi (2004). The accuracy of the methods was assessed by quantifying test/predicted ratios and the consistency by quantifying their coefficient of variation. The tested specimens by Washa and Fluck (1952) had a reinforcement ratio of 1.6-1.7% and a sustained load duration of 900 days. They also featured a range of compression to tension reinforcement ratios to demonstrate the efficiency of compression reinforcement in reducing the long-term deflection. These specimens were used in the derivation of Branson's (1977) and Gilbert and Kilpatrick's (2017) empirical methods. The tested specimens by Gilbert and Nejadi (2004) were singly reinforced with reinforcement ratios between 0.5 and 0.8% and had a sustained load duration of 400 days. These specimens were used in the derivation of Gilbert and Kilpatrick's (2017) Method.

Chapter 4 presented a critique of the existing A23.3 Multiplier Method and proposed an Alternative Simplified Method for computing long-term deflections based on short-term deflections. Unique equations were derived for singly and doubly reinforced members using multiple regression analyses. It also presented a comparison between the Mechanics-Based Method, the A23.3 Multiplier Method, and the Alternative Simplified Method. Special considerations for lightly-loaded members were also discussed.

5.2   Conclusions

The conclusions of this study are as follows:

1. Creep and shrinkage predictions obtained using the four widely used prediction models for a given set of parameters can differ by up to 30%.

2. Each of the studies that by others to evaluate the accuracy of prediction models uses a unique data subset from the RILEM and NU Databanks and/or unique statistical

indicators and therefore yield contradicting outcomes, despite their theoretical and mathematical soundness. This makes it difficult to quantify the prediction error.

3. A mean ranking of the models where each of the aforementioned studies was considered of equal importance showed that B3 (Bazant and Baweja, 1995, 2000) is the most effective model in predicting the ultimate shrinkage strain, and GL2000 (Gardner and Lockman, 2000) is the most effective in predicting creep. The CEB-FIP (Comite Europeen du Beton, 1999) method, which forms the basis of the method presented in the Canadian Highway Bridge Design Code (CSA, 2014) was found to be the least accurate for predicting the creep coefficients and ultimate shrinkage strains.

4. A23.3 code provisions (CSA, 2014) recommend computing short-term deflections using an effective moment of inertia based on reduced modulus of rupture to account for the effect of restrained shrinkage. This may overestimate the short-term deflection of members not exposed to drying prior to loading since the effects of restrained shrinkage are likely slight.

5. The Concrete Design Handbook provisions (CAC, 2016) for computing ultimate shrinkage strains and creep coefficients are simplifications of the values tabulated by Branson (1977) and are unconservative for members exposed to a relative humidity less than 70% and age at loading less than 28 days. This may ultimately result in the underestimation of long-term deflections, such as in the case of Washa and Fluck's (1952) test specimens where the mean test/predicted ratio is 1.34. Incremental deflections due to creep and shrinkage can be more accurately predicted using the method described in the Concrete Design Handbook using creep coefficients and shrinkage strains tabulated by Branson (1977).

6. The Mehcnaics-based Mechanics-Based Method yields accurate and slightly conservative mean test/predicted ratios of 0.94 and 0.92 for Wash and Fluck's (1952) and Gilbert and Nejadi's (2004) test specimens, respectively. The associated coefficients of variation are 10.3% for Washa and Fluck's (1952) specimens and 5.0% for Gilbert and Nejadi's (2004) specimens.

7. The Mechanics-Based Method shows that the creep deflection contributes 75-100% of the total long-term deflection while shrinkage contributes only 0-25%. These values are based on a creep coefficient of 2.5 and an ultimate shrinkage strain of 800με, corresponding to a relative humidity of 50% and age at loading of 7 days. The contribution of shrinkage decreases as the relative humidity increases.

8. The A23.3 Multiplier Method produces an illogical trend where the long-term deflection decreases with an increase in the reinforcement ratio, ρ, hence the ratio of service to cracking moment M_s/M_{cr} and the maximum concrete compressive strain. It also overestimates the long-term deflection of lightly reinforced members where M_{cr} is computed based on the specified reduced modulus of rupture.

9. Alternative Simplified Methods for computing the long-term deflection, Δ_{LT}, of singly and doubly reinforced members based on the short-term deflection, Δ_i, can be derived from the Mechanics-Based Method using multiple regression analysis. The long-term deflection multiplier for singly reinforced members is

$$\frac{\Delta_{LT}}{\Delta_i} = 0.35(\emptyset) + 23.4\,(\rho) + 0.4$$

with a standard error of 0.038. The long-term deflection multiplier for doubly reinforced members is

$$\frac{\Delta_{LT}}{\Delta_i} = 0.23(\emptyset) - 0.2\left(\frac{\rho'}{\rho}\right) - 21.8\,(\rho') + 13.4\,(\rho) + 0.7$$

with a standard error of 0.045.

10. Members with low M_s/M_{cr} ratios (e.g., less than 1.75 or $\rho < 0.006$) are likely to experience reduced short-term deflections due to applied loads. This will result in large and inconsistent Δ_{LT}/Δ_i ratios and the use of the Alternative Simplified Method to compute long- to short-term deflection ratio is not preferred. The long-term deflection of these members can be accurately and conservatively predicted using the Mechanics-Based Method.

5.3   Recommendations for Future Work

Recommendations for future work are as follows:

1. There is a surprising dearth of experimental studies on the long-term deflection of steel reinforced concrete beams under sustained loads. The majority of existing studies are at least three decades old and do not consider concretes loaded at young ages or lightly-reinforced members. The use of now common high-strength steel (e.g.,650MPa yield strength) implies that a smaller reinforcement ratio is required to satisfy ultimate limit states and current construction practice often requires members to be loaded at three days. Moreover, existing experimental studies often fail to report information on environmental ambient conditions, which are crucial in the time-dependent analysis of concrete structures. Therefore, state-of-the-art experimental studies that account for the requirements of current construction practice and that report all the necessary information needed to conduct a comprehensive time-dependent analysis are necessary. These studies must also examine the impact of restrained shrinkage and lightly-loaded members on the short-term and long-term deflections.

2. The effect of tension stiffening is of particular significance in members with reduced M_s/M_{cr} ratios. Parametric studies show that members with M_s/M_{cr} ratios less than 1.75 (corresponding to $\rho < 0.006$, typical of two-way slabs) have an effective to cracked moment of inertia ratio greater than 1.05 and therefore experience reduced short-term deflections. This phenomenon was observed in Gilbert and Nejadi's (2004) test specimens with M_s/M_{cr} less than 1.72. Hollington (1970) also observed reduced cracking in test specimens where M_s was sufficiently close to M_{cr} compared to their companion specimens with larger M_s/M_{cr} Therefore, a study that quantifies the impact of tension stiffening on the short and long-term deflection of lightly loaded members is necessary.

3. Continue efforts to develop models that can accurately predict creep coefficients and shrinkage strains to further enhance the accuracy long-term deflection predictions, particularly for concretes subjected to early loadings.

References

ACI Committee 209. (2008). *209.2R-08 Guide for Modeling and Calculating Shrinkage and Creep in Hardened Concrete.* Farmington Hills: American Concrete Institute.

ACI Committee 318. (2014). *318-14 Building Code Requirements for Structural Concrete and Commentary.* Farmington Hills: American Concrete Institute.

ACI Committee 435. (1978). Proposed Revisions by Committee 435 to ACI Building Code and Commentary Provisions on Deflections. *ACI Journal, 75*(6), 229-238.

Al-Manaseer, A., & Lam, J.-P. (2005). Statistical Evaluation of Shrinkage and Creep Models. *ACI Materials Journal, 102*(3), 170-176.

American Society for Testing and Materials. (2016). *Standard Test Method for Compressive Strength of Hydraulic Cement Mortars (Using 2-in. or [50-mm] Cube Specimens.* West Conshohocken: ASTM International.

Bazant, Z. P. (1972). Prediction of Concrete Creep Effects Using Age-Adjusted Effective Modulus Method. *ACI Journal, 69*(4), 212-219.

Bazant, Z. P., & Kim, J.-K. (1991). Improved Prediction Model for Time-dependent Deformations of Concrete: Part 1-Shrinkage. *Materials and Structures, 24*, 327-345.

Bazant, Z. P., & Panula, L. (1978). Practical Prediction of Time-dependent Deformations of Concrete Part I-IV. *Materials and Structures, 11*(5-6).

Bischoff, P. H. (2007). Rational Model for Calculating Deflection of Reinforced Concrete Beams and Slabs. *Canadian Journal of Civil Engineering, 34*(8), 992-1002.

Branson, D. E. (1977). *Deformation of Concrete Structures.* United States of America: McGraw-Hill.

British Standards Institute. (2016). *Methods of Testing Cement. Determination of Strength.* BSI.

Brooks, J. J. (2005, January 1). 30-year Creep and Shrinkage of Concrete. *Magazine of Concrete Research, 30*(9), pp. 545-556.

Brooks, J. J. (2015). *Concrete and Masonry Movements.* Oxford: Buttworth Heinmann.

Brooks, J. J., & Neville, A. (1977). A Comparison of Creep, Elasticity and Strength of Concrete in Tension and in Compression. *Magazine of Concrete Research, 29*(100), 131-141.

Cement Association of Canada. (2016). *Concrete Design Handbook – 4th Edition.* Ottawa: Cement Association of Canada.

Comité Euro-International du Béton. (1970). *CEB-FIP Recommendations for the Design and Construction of Concrete Structures.* Paris-London: CEB Bulletin d'Information.

Comité Euro-International du Béton. (1978). *CEB-FIP Model Code for Concrete Structures.* Paris-London: CEB Bulletin d'Information, No. 124.

Comité Europeen du Béton. (1993). *"CEB-FIP Model Code 1990.* Lausanne: CEB Bulletin d'Information.

Comité Europeen du Béton. (1999). *Structural Concrete—Textbook on Behaviour, Design and Performance.* Federation Internationale du Beton.

Dilger, W. (1982). Creep Analysis of Prestressed Concrete Structures Using Creep-Transformed Section Properties. *PCI Journal, 27*(1), 98-119.

Dilger, W., & Neville, A. (1971). Method of Creep Analysis of Structural Members. *ACI Special Publication: Designing for Effects of Creep, Shrinkage, and Temprature in Structures, SP-27*, 349-379.

Gardner, N. J., & Lockman, M. J. (2001). Design Provisions for Drying Shrinkage and Creep of Normal-Strength Concrete. *ACI Materials Journal, 98*(2), 159-167.

Gilbert, R. I. (1988). *Time Effects in Concrete Structures.* Amsterdam: Elsevier Science Publishers.

Gilbert, R. I. (1999). Deflection Calculation for Reinforced Concrete Structures—Why We Sometimes Get It Wrong. *ACI Structural Journal, 96*(6), 1027-1032.

Gilbert, R. I. (2001). Deflection Calculation and Control - Australian Code Amendments and Improvements. *ACI Special Publication: Code Provisions for Deflection Control in Concrete Structures, SP-203*, 45-78.

Gilbert, R. I. (2008). Calculation of Long-Term Deflection. *CIA Seminar.* Brisbane.

Gilbert, R. I. (2012). Creep and Shrinkage Induced Deflections in RC Beams and Slabs. *ACI Special Publication: Andy Scanlon Symposium on Serviceability and Safety of Concrete Structures: From Research to Practice, SP-284*, 1-16.

Gilbert, R. I., & Nejadi, S. (2004). *An experimental study of flexural cracking in reinforced concrete members under sustained loads.* University of New South Wales, Sydney.

Gilbert, R. I., & Ranzi, G. (2011). *Time-Dependent Behaviour of Concrete Structures.* Oxon, United Kingdom: Spon Press.

Hollington, M. R. (1970). *A Series of Long-Term Tests To Investigate The Deflexion of a Representative Precast Concrete Floor Component.* London: Cement and Concrete Association.

International Federation for Structural Concrete (fib). (2012). *FIB Model Code 2010.* Lausanne.

Kilpatrick, A. E., & Gilbert , R. I. (2018). Simplified Calculation of the Long-Term Deflection of Reinforced Concrete Flexural Members. *Australian Journal of Structural Engineering, 19*(1), 34-43.

Large, G. (1957). *Basic Reinforced Concrete Design: Elastic and Creep.* New York: Ronald Press.

MacGregor, J. G., & Bartlett, F. M. (2000). *Reinforced Concrete, Mechanics and Design, 1st Canadian Edition.* Scarborough: Prentice-Hall.

Mancuso, C., & Bartlett, F. M. (2016). ACI 318-14 Criteria for Computing Instantaneous Deflections. *ACI Structural Journal, 114*(5), 1299-1310.

Mija, H., Roman, W., & Bazant, Z. (2015). Comprehensive Database for Concrete Creep and Shrinkage: Analysis and Recommendations for Testing and Recording. *ACI Materials Journal, 112*(4), 547-558.

Miller, A. (1958). Warping of Reinforced Concrete Due to Shrinkage. *Journal of the American Concrete Institute, 29*(11), 939-950.

Neville, A., Dilger, W., & Brooks, J. (1983). *Creep of Plain and Structural Concrete.* London: Construction Press.

Orta, L. (2009). *Restrained Shrinkage in Bridge Decks with Concrete Overlays.* London, Ontario, Canada: The School of Graduate and Postdoctoral Studies The University of Western Ontario.

Pauw, A., & Meyers, B. L. (1964). Effect of Creep and Shrinkage on the Behavior of Reinforced Concrete Members. *ACI Special Publication: Symposium on Creep of Concrete, 9*, 129-158.

Scanlon, A., & Bischoff, P. H. (2008). Shrinkage Restraint and Loading History Effects on Deflection of Flexural Members. *ACI Structural Journal, 105*(4), 498-506.

Shaikh, A. F., & Branson, D. E. (1970). Non-Tensioned Steel in Prestressed Concrete Beams. *Journal of the Prestressed Concrete Institute, 15*(1), 14-36.

Tang, J., & Lubell, A. (2008). Influence of Longetudinal Reinforcement on One-Way Slab Deflection. *Canadian Journal for Civil Engineering, 35*, 1076-1087.

Washa, G. W., & Fluck, P. G. (1952). Effect of Compressive Reinforcement on the Plastic Flow of Reinforced Concrete Beams. *Journal of the American Concrete Institute, 49*(10), 89-108.

Zhou, W., & Kokai, T. (2010). Deflection Calculation and Control for Reinforced
    Concrete Flexural Members. *Canadian Journal of Civil Engineering, 37*, 131-
    134.

Appendix A: Ranking of Models by Al-Manaseer and Prado (2015)

Tables A-1 and A-2 show the ranking of the models by Al-Manaseer and Prado (2015), after each phase of the screening process, using the various statistical indicators and the two available databanks. These Tables are essentially reproductions of similar tables in Al-Manaseer and Prado (2015).

Table A-1: Comparison of Shrinkage Strains (Al-Manaseer and Prado, 2015)

	ACI 209		B3		GL2000		MC90-99	
	RILEM	NU	RILEM	NU	RILEM	NU	RILEM	NU
V_{CEB} (%)								
Phase 1	47	50	43	48	49	53	49	54
Rank	2	2	1	1	3	3	3	4
Phase 2	47	50	41	47	48	52	45	50
Rank	3	2	1	1	4	3	2	2
Phase 3	45	45	39	39	46	46	44	44
Rank	3	3	1	1	4	4	2	2
V_m(%)								
Phase 1	71	71	79	78	88	87	76	76
Rank	1	1	3	3	4	4	2	2
Phase 2	71	71	77	78	87	87	74	74
Rank	1	1	3	3	4	4	2	2
Phase 3	71	71	77	78	87	87	74	74
Rank	1	1	3	3	4	4	2	2
F_{CEB} (%)								
Phase 1	102	100	421	411	319	312	1015	994
Rank	1	1	3	3	2	2	4	4
Phase 2	73	72	81	81	86	86	102	101
	1	1	2	2	3	3	4	4
Phase 3	72	71	81	81	85	85	103	103
Rank	1	1	2	2	3	3	4	4
M_{CEB}								
Phase 1	1.05	1.07	1.31	1.27	1.27	1.22	2.05	2.01
Rank	1	1	3	3	2	2	4	4
Phase 2	1.03	1.05	1.03	1.00	1.05	1.02	1.21	1.18
Rank	1	3	1	1	2	2	3	4
Phase 3	1.04	1.07	1.04	1.04	1.07	1.06	1.23	1.23
Rank	1	3	1	1	2	2	3	4

Table A-2: Comparison of Creep Strains (Al-Manaseer and Prado, 2015)

	ACI 209		B3		GL2000		MC90-99	
	RILEM	NU	RILEM	NU	RILEM	NU	RILEM	NU
	V_{CEB} (%)							
Phase 1	45	47	43	42	44	44	48	61
Rank	3	3	1	1	2	2	4	4
Phase 2	45	47	43	42	44	44	48	57
Rank	3	3	1	1	2	2	4	4
Phase 3	39	40	39	36	40	37	44	42
Rank	1	3	1	1	2	2	3	4
	V_m(%)							
Phase 1	41	39	46	31	45	36	38	39
Rank	2	3	4	1	3	2	1	3
Phase 2	41	39	46	31	45	36	38	35
Rank	2	4	4	1	3	3	1	2
Phase 3	40	37	45	30	44	35	37	31
Rank	2	4	4	1	3	3	1	2
	F_{CEB} (%)							
Phase 1	33	36	44	34	34	39	33	1677
Rank	1	1	3	3	2	2	4	4
Phase 2	33	35	44	34	43	36	33	49
	1	2	3	1	2	3	1	4
Phase 3	32	34	44	34	43	36	33	48
Rank	1	1	4	1	3	2	2	3
	M_{CEB}							
Phase 1	0.98	0.90	1.13	0.97	1.10	0.99	0.89	3.30
Rank	1	3	4	2	2	1	3	4
Phase 2	0.98	0.90	1.13	0.97	1.10	0.99	0.89	0.99
Rank	1	3	4	2	2	1	3	1
Phase 3	0.98	0.91	1.14	0.97	1.10	0.99	0.89	0.91
Rank	1	3	4	2	2	1	3	3

Appendix B: Test and Predicted Short- and Long-Term Deflections for Individual Test Specimens

Tables B1 and B3 show the test and predicted short and long-term deflections using the Mechanics-Based Method and Gilbert and Kilpatrick's (2017) Method. The long-term deflection computations were based on the experimental creep coefficient, $\emptyset(t,t_o)$, and shrinkage strain, $\varepsilon_{sh,u}$, values shown.

Table B2 shows the test and predicted short and long-term deflections using the CAC Concrete Design Handbook (CAC, 2016) Method. The long-term deflection computations were based on methods for computing the creep coefficients, C_t, and ultimate shrinkage strains $\varepsilon_{sh,u}$, described in the Concrete Design Handbook.

Table B4 shows the geometric and material properties for Washa and Fluck's (1952) and Gilbert and Nejadi's (2004) test specimens.

Table B-1: Test and Predicted Deflections Based on the Mechanics-Based Method

Spec.	Test				Predicted: Mechanics-Based Method						Test/ Pred.
	Δ_i (mm)	Δ_{LT} (mm)	Δ_{Total} (mm)	$\varepsilon_{sh,u}$ $(\times 10^{-6})$	$\emptyset(t,t_o)$	Δ_i (mm)	Δ_{cr} (mm)	Δ_{sh} (mm)	Δ_{LT} (mm)	Δ_{Total} (mm)	
Washa & Fluck (1952)											
B3	26.4	60.0	86.4	720	4.45	26.7	54.0	16.7	70.7	97.4	0.89
B6	26.4	60.0	86.4	720	4.45	25.8	51.5	16.1	67.6	93.4	0.93
C3	47.8	92.9	140.7	720	4.40	43.6	91.4	30.3	121.7	165.3	0.87
C6	47.8	92.9	140.7	720	4.40	42.8	88.0	29.7	117.8	160.5	0.89
E3	63.0	121.9	184.9	720	4.35	49.3	95.3	32.7	128.0	177.3	1.04
E6	63.0	121.9	184.9	720	4.35	51.6	102.2	34.2	136.4	188.0	0.99
B2	24.9	40.1	65.0	720	4.45	25.4	52.0	4.5	56.5	81.9	0.95
B5	24.9	40.1	65.0	720	4.45	24.8	48.8	4.5	53.3	78.0	0.97
C2	43.4	57.2	100.6	720	4.40	41.9	91.9	9.5	101.4	143.3	0.87
C5	43.4	57.2	100.6	720	4.40	40.9	86.3	9.5	95.9	136.8	0.89
E2	55.9	72.9	128.8	720	4.35	47.2	92.3	9.3	101.6	148.8	1.02
E5	55.9	72.9	128.8	720	4.35	48.9	100.8	9.3	110.0	158.9	0.99
B1	23.4	27.6	51.0	720	4.45	24.5	49.0	0.0	49.0	73.5	0.89
B4	23.4	27.6	51.0	720	4.45	23.9	46.2	0.0	46.2	70.1	0.91
C1	40.1	39.9	80.0	720	4.40	40.6	87.8	0.0	88.8	129.4	0.83
C4	40.1	39.9	80.0	720	4.40	40.0	84.8	0.0	85.8	125.8	0.84
D1	11.9	15.8	27.7	720	4.30	14.3	18.4	0.0	18.4	32.7	0.85
D4	11.9	15.8	27.7	720	4.30	14.0	18.2	0.0	18.2	32.2	0.86
E1	59.4	64.6	124.0	720	4.35	45.3	64.1	0.0	64.1	109.4	1.12
E4	59.4	64.6	124.0	720	4.35	46.8	65.0	0.0	65.0	108.8	1.09
Mean											**0.94**
COV (%)											**10.30**
Gilbert & Nejadi (2004)											
B1a	4.9	7.2	12.1	825	1.71	6.2	5.7	1.2	6.9	13.0	0.93
B1b	2.0	5.4	7.4	825	1.71	3.7	3.7	1.2	4.9	8.5	0.87
B2a	5.0	7.4	12.4	825	1.71	6.2	5.7	1.4	7.1	13.3	0.93
B2b	2.0	5.9	7.9	825	1.71	3.8	3.7	1.4	5.1	8.9	0.88
B3a	5.8	7.5	13.3	825	1.71	6.4	5.9	1.9	7.8	14.2	0.94
B3b	2.0	5.9	7.9	825	1.71	3.7	3.6	1.9	5.5	9.2	0.86
S1a	7.1	18.0	25.1	825	1.71	13.7	13.1	1.8	14.9	28.7	0.88
S1b	3.7	16.2	19.9	825	1.71	9.0	9.4	1.8	11.2	20.1	0.99
S2a	10.6	19.2	29.8	825	1.71	16.3	15.0	2.6	17.6	33.9	0.88
S2b	4.4	17.5	21.9	825	1.71	10.3	10.0	2.6	12.6	22.9	0.96
S3a	11.8	20.7	32.5	825	1.71	15.3	14.4	3.2	17.6	33.0	0.99
S3b	5.0	17.9	22.9	825	1.71	10.8	10.4	3.2	13.6	24.5	0.94
Mean											**0.92**
COV (%)											**4.98**

Table B-2: Test and Predicted Deflections Based on Concrete Design Handbook Method

Spec.	Test			Predicted: CAC Concrete Design Handbook							Test/ Pred.
	Δ_i (mm)	Δ_{LT} (mm)	Δ_{Total} (mm)	$\varepsilon_{sh,u}$ ($\times10^{-6}$)	C_t	$\Delta_i+\Delta_{cr}$ (mm)	Δ_{cr} (mm)	Δ_{sh} (mm)	Δ_{LT} (mm)	Δ_{Total} (mm)	
				Washa & Fluck (1952)							
B3	26.4	60.0	86.4	349	1.40	58.3	31.6	6.5	38.1	64.8	1.33
B6	26.4	60.0	86.4	349	1.40	56.3	30.6	6.5	37.1	62.8	1.37
C3	47.8	92.9	140.7	349	1.40	95.4	51.7	11.3	63.0	106.6	1.32
C6	47.8	92.9	140.7	349	1.40	93.5	50.7	11.3	62.0	104.8	1.34
E3	63.0	121.9	184.9	349	1.40	107.8	58.5	13.0	71.5	120.8	1.53
E6	63.0	121.9	184.9	349	1.40	112.7	61.1	13.0	74.2	125.7	1.47
B2	24.9	40.1	65.0	349	1.40	47.0	21.6	4.0	25.6	51.0	1.27
B5	24.9	40.1	65.0	349	1.40	45.8	21.0	4.0	25.0	49.7	1.31
C2	43.4	57.2	100.6	349	1.40	77.7	35.7	6.9	42.6	84.6	1.19
C5	43.4	57.2	100.6	349	1.40	75.7	34.8	6.9	41.7	82.6	1.22
E2	55.9	72.9	128.8	349	1.40	88.1	40.9	9.3	50.2	97.4	1.32
E5	55.9	72.9	128.8	349	1.40	91.3	42.4	9.3	51.7	100.6	1.28
B1	23.4	27.6	51.0	349	1.40	40.6	16.2	0.0	16.2	40.6	1.26
B4	23.4	27.6	51.0	349	1.40	39.6	15.8	0.0	15.8	39.6	1.29
C1	40.1	39.9	80.0	349	1.40	67.6	27.0	0.0	27.0	67.6	1.18
C4	40.1	39.9	80.0	349	1.40	66.6	26.6	0.0	26.6	66.6	1.20
D1	11.9	15.8	27.7	349	1.40	23.9	9.5	0.0	9.5	23.9	1.16
D4	11.9	15.8	27.7	349	1.40	23.4	9.4	0.0	9.4	23.4	1.18
E1	59.4	64.6	124.0	349	1.40	76.3	31.0	0.0	31.0	76.3	1.62
E4	59.4	64.6	124.0	349	1.40	78.8	32.0	0.0	32.0	78.8	1.57
				Mean							**1.32**
				COV (%)							**10.13**
				Gilbert & Nejadi (2004)							
B1a	4.9	7.2	12.1	287	1.15	12.2	6.0	0.7	6.7	12.9	0.94
B1b	2.0	5.4	7.4	287	1.15	7.3	3.6	0.7	4.3	8.0	0.93
B2a	5.0	7.4	12.4	287	1.15	12.3	6.1	0.7	6.8	13.0	0.95
B2b	2.0	5.9	7.9	287	1.15	7.6	3.7	0.7	4.5	8.3	0.95
B3a	5.8	7.5	13.3	287	1.15	12.5	6.2	0.9	7.1	13.4	0.99
B3b	2.0	5.9	7.9	287	1.15	7.4	3.7	0.9	4.5	8.3	0.96
S1a	7.1	18.0	25.1	287	1.15	27.1	13.4	1.4	14.8	28.5	0.88
S1b	3.7	16.2	19.9	287	1.15	17.7	8.7	1.4	10.1	19.1	1.04
S2a	10.6	19.2	29.8	287	1.15	32.2	15.9	1.5	17.4	33.7	0.88
S2b	4.4	17.5	21.9	287	1.15	20.4	10.1	1.5	11.6	21.9	1.00
S3a	11.8	20.7	32.5	287	1.15	30.3	15.0	1.8	16.8	32.1	1.01
S3b	5.0	17.9	22.9	287	1.15	21.4	10.6	1.8	12.4	23.2	0.99
				Mean							**0.96**
				COV (%)							**5.14**

Table B-3: Test and Predicted Deflections Based on Gilbert and Kilpatrick (2017)

Spec.	Test			Predicted: Gilbert & Kilpatrick (2017)							Test/Pred.
	Δ_i (mm)	Δ_{LT} (mm)	Δ_{Total} (mm)	$\varepsilon_{sh,u}$ ($\times 10^{-6}$)	$\varnothing(t,t_o)$	Δ_i (mm)	Δ_{cr} (mm)	Δ_{sh} (mm)	Δ_{LT} (mm)	Δ_{Total} (mm)	
				Washa & Fluck (1952)							
B3	26.4	60.0	86.4	720	4.45	26.7	31.1	26.6	57.7	84.4	1.02
B6	26.4	60.0	86.4	720	4.45	25.8	30.1	26.6	56.7	82.5	1.05
C3	47.8	92.9	140.7	720	4.40	43.6	50.1	44.1	94.1	137.8	1.02
C6	47.8	92.9	140.7	720	4.40	42.8	49.1	43.8	92.9	135.7	1.04
E3	63.0	121.9	184.9	720	4.35	49.3	54.1	51.9	106.0	155.3	1.19
E6	63.0	121.9	184.9	720	4.35	51.6	56.6	52.0	108.6	160.1	1.15
B2	24.9	40.1	65.0	720	4.45	25.4	15.6	23.5	39.1	64.6	1.01
B5	24.9	40.1	65.0	720	4.45	24.8	15.2	22.9	38.1	62.8	1.03
C2	43.4	57.2	100.6	720	4.40	41.9	25.4	39.2	64.6	106.6	0.94
C5	43.4	57.2	100.6	720	4.40	40.9	24.8	38.2	63.0	103.9	0.97
E2	55.9	72.9	128.8	720	4.35	47.2	28.1	45.1	73.2	120.4	1.07
E5	55.9	72.9	128.8	720	4.35	48.9	29.1	46.9	76.0	124.9	1.03
B1	23.4	27.6	51.0	720	4.45	24.5	9.3	16.4	25.7	50.1	1.02
B4	23.4	27.6	51.0	720	4.45	23.9	9.0	15.9	24.9	48.8	1.05
C1	40.1	39.9	80.0	720	4.40	40.6	15.2	27.3	42.5	83.1	0.96
C4	40.1	39.9	80.0	720	4.40	40.0	15.0	26.8	41.8	81.8	0.98
D1	11.9	15.8	27.7	720	4.30	14.3	5.3	7.1	12.4	26.7	1.04
D4	11.9	15.8	27.7	720	4.30	14.0	5.1	7.2	12.3	26.3	1.05
E1	59.4	64.6	124.0	720	4.35	45.3	17.0	31.2	48.2	93.5	1.33
E4	59.4	64.6	124.0	720	4.35	46.8	17.5	32.0	50.1	96.9	1.28
				Mean							**1.05**
				COV (%)							**10.19**
				Gilbert & Nejadi (2004)							
B1a	4.9	7.2	12.1	825	1.71	6.2	1.6	5.1	6.6	12.8	0.94
B1b	2.0	5.4	7.4	825	1.71	3.7	0.9	4.9	5.8	9.5	0.78
B2a	5.0	7.4	12.4	825	1.71	6.2	1.6	4.9	6.5	12.8	0.97
B2b	2.0	5.9	7.9	825	1.71	3.8	1.0	4.8	5.8	9.6	0.82
B3a	5.8	7.5	13.3	825	1.71	6.4	2.0	5.2	7.2	13.6	0.98
B3b	2.0	5.9	7.9	825	1.71	3.7	1.2	5.1	6.3	10.0	0.79
S1a	7.1	18.0	25.1	825	1.71	13.7	3.2	11.8	15.0	28.7	0.87
S1b	3.7	16.2	19.9	825	1.71	9.0	2.1	11.2	13.3	22.2	0.90
S2a	10.6	19.2	29.8	825	1.71	16.3	4.7	12.5	17.2	33.5	0.89
S2b	4.4	17.5	21.9	825	1.71	10.3	2.9	12.2	15.2	25.5	0.86
S3a	11.8	20.7	32.5	825	1.71	15.3	5.1	12.8	17.9	33.2	0.98
S3b	5.0	17.9	22.9	825	1.71	10.8	3.6	12.7	16.3	27.1	0.84
				Mean							**0.89**
				COV (%)							**8.13**

Table B-4: Details of Washa and Fluck's (1952) and Gilbert and Nejadi's (2004) Test Specimens

Spec.	b (mm)	h (mm)	d (mm)	d' (mm)	ℓ_n (mm)	A_s (mm²)	A_s' (mm²)	$f_c'(t_o)$ (MPa)	$E_c(t_o)$ (MPa)	$\emptyset(t,t_o)$	$\varepsilon_{sh,u}$ (×10⁻⁶)	t_c (days)	t_o (days)	t (days)	M_a (kNm)
							Washa & Fluck (1952)								
B3	152	203	165	0	6096	400	0	18.8	17995	4.45	720	5	14	912	7.25
B6	152	203	165	0	6096	400	0	22.8	19512	4.45	720	5	14	912	7.25
C3	305	127	108	0	6350	516	0	18.8	17995	4.40	720	5	14	912	6.03
C6	305	127	108	0	6350	516	0	21.8	18891	4.40	720	5	14	912	6.03
E3	305	76	64	0	5334	284	0	22.8	19512	4.35	720	5	14	912	1.96
E6	305	76	64	0	5334	284	0	18.4	17444	4.35	720	5	14	912	1.96
B2	152	203	165	34	6096	400	200	18.8	17995	4.45	720	5	14	912	7.25
B5	152	203	165	34	6096	400	200	22.8	19512	4.45	720	5	14	912	7.25
C2	305	127	108	24	6350	516	258	18.8	17995	4.40	720	5	14	912	6.03
C5	305	127	108	24	6350	516	258	21.8	19512	4.40	720	5	14	912	6.03
E2	305	76	64	11	5334	284	142	22.8	19512	4.35	720	5	14	912	1.96
E5	305	76	64	11	5334	284	142	18.4	17444	4.35	720	5	14	912	1.96
B1	152	203	165	34	6096	400	400	18.8	17995	4.45	720	5	14	912	7.25
B4	152	203	165	34	6096	400	400	22.8	19512	4.45	720	5	14	912	7.25
C1	305	127	108	24	6350	516	516	18.8	17995	4.40	720	5	14	912	6.03
C4	305	127	108	24	6350	516	516	21.8	18891	4.40	720	5	14	912	6.03
E1	305	76	64	11	5334	284	284	22.8	19512	4.35	720	5	14	912	1.96
E4	305	76	64	11	5334	284	284	18.4	17444	4.35	720	5	14	912	1.96

Gilbert & Nejadi (2004)														
B1a	250	348	300	0	3500	398	0	18.3	22820	1.70	825	14	14	380	24.90
B1b	250	348	300	0	3500	398	0	18.3	22820	1.70	825	14	14	380	17.00
B2a	250	333	300	0	3500	400	0	18.3	22820	1.70	825	14	14	380	24.80
B2b	250	333	300	0	3500	398	0	18.3	22820	1.70	825	14	14	380	16.80
B3a	250	333	300	0	3500	623	0	18.3	22820	1.70	825	14	14	380	34.60
B3b	250	333	300	0	3500	600	0	18.3	22820	1.70	825	14	14	380	20.80
S1a	400	161	130	0	3500	224	0	18.3	22820	1.70	825	14	14	380	6.81
S1b	400	161	130	0	3500	224	0	18.3	22820	1.70	825	14	14	380	5.28
S2a	400	161	130	0	3500	338	0	18.3	22820	1.70	825	14	14	380	9.87
S2b	400	161	130	0	3500	338	0	18.3	22820	1.70	825	14	14	380	6.81
S3a	400	161	130	0	3500	452	0	18.3	22820	1.70	825	14	14	380	11.40
S3b	400	161	130	0	3500	452	0	18.3	22820	1.70	825	14	14	380	8.34

Appendix C: Example Calculation Using Mechanics-Based Method

This appendix shows a detailed calculation of the short- and long-term deflections computed using the Mechanics-Based Method for Washa and Fluck's (1952) Specimen B5. The member was loaded at 14 days and the load was sustained for 915 days (i.e., $t_o = 14$ and $t = 915$).

Material Properties

$f'_{c,14} = 22.8$ MPa	$E_{c,14} = 19510$ MPa
$\emptyset(t,t_o) = 4.45$	$\varepsilon_{sh,t} = 720$ µε
$f_y = 320$ MPa	$E_s = 200$ GPa
$f_r = 2.9$ MPa (calculated)	$n = 10.2$ (calculated)

Geometric Properties

$b = 152.4$ mm	$h = 203.2$ mm
$d = 165.2$ mm	$d' = 33.8$ mm
$A_s = 400$ mm^2	$\rho = 0.016$
$A'_s = 200$ mm^2	$\rho' = 0.008$
$\ell_n = 6096$ mm	$M_a = M_s = 7.25$ kNm
$I_g = 106 \times 10^6$ mm^4 (calculated)	$E_c I_g = 2068.3$ kNm^2 (calculated)
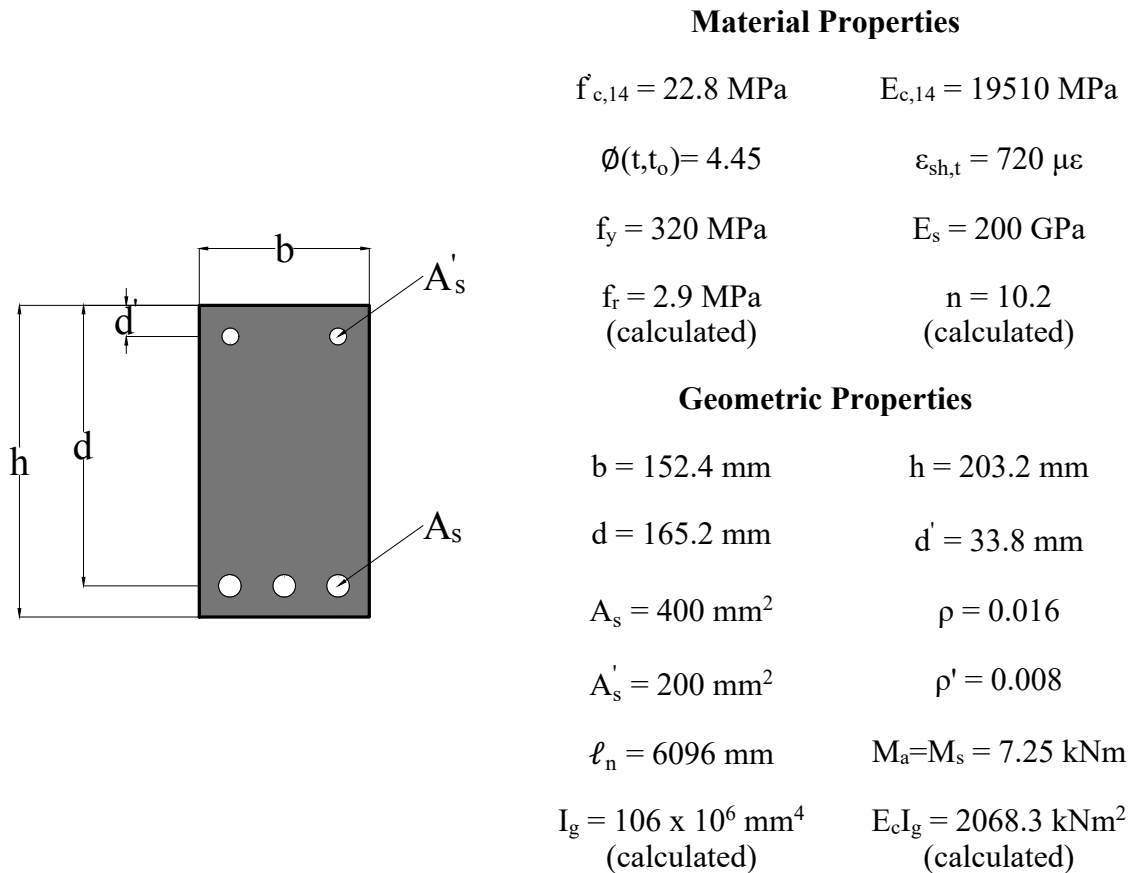
Figure C-1: Geometric and Material Properties of Specimen B5 (Washa and Fluck, 1952)

1. <u>Short-term deflection</u>

   (a) Compute the depth of the neutral axis, kd:

      From the CAC Concrete Design Handbook:

$$kd= \frac{\sqrt{2dB\left(1+\frac{rd'}{d}\right)+(1+r)^2-(1+r)}}{B}$$ (3-33)

where

$$r=\frac{(n-1)A'_s}{A_s}$$ (3-34)

and

$$B = \frac{b}{nA_s}$$ (3-35)

Substituting the values shown in Figure C-1 into Equations (3-33) to (3-35) yields:

kd = 69.9 mm

(b) Compute the cracked moment of inertia, I_{cr}:

$$I_{cr}= \frac{1}{3}b(kd)^3+nA_s(d-kd)^2+(n-1)A'_s(kd-d')^2$$ (3-36)

$I_{cr} = 56.8 \times 10^6 \text{ mm}^4$

The flexural rigidity of the cracked section is therefore:

$E_cI_c = 2068 \text{ kNm}^2$

(c) Compute the effective moment of inertia, I_e, using the Branson Equation (Equation 3-2) based on $0.5M_{cr}$ or the Bischoff Equation (Equation 3-3) based on $0.67M_{cr}$ where M_{cr} is the cracking moment based on the full modulus of rupture, f_r. Using the Branson Equation based on $0.5M_{cr}$ (to maintain consistency with A23.3-14 provisions):

$$I_e=I_{cr}+\left(I_g-I_{cr}\right)\left(\frac{0.5M_{cr}}{M_a}\right)^3$$

$\underline{I_e = 58.1 \times 10^6 \text{ mm}^4}$

$E_cI_e = 1134 \text{ kNm}^2 < E_cI_g \therefore \text{ok}$

(d) Compute the short-term deflection using Equation (3-1) as

$$\Delta_i=\frac{5(7.25\times10^6)(6100^2)}{48(19512)(58.1 \times 10^6)} = \textbf{24.8mm}$$

2. Creep Deflection

(e) Compute the depth of the time-dependent neutral axis, $\overline{kd}$, and corresponding time-dependent cracked moment of inertia, $\overline{I_{cr}}$, using Equations (3-33) to (3-36) based on the age-adjusted modular ratio:

$$\overline{n}=E_s/\overline{E_c} = n[1+ \chi(t,t_o)\emptyset(t,t_o)]$$

Assuming $\chi(t,t_o) = 0.8$ for reasons outlined in Section 3.3.1 and $\emptyset(t,t_o)= 4.45$ from Figure C-1 yields:

$\underline{\overline{n} = 46.5}$

$\underline{\overline{E_c} = 4278.9 \text{ MPa}}$

$\underline{\overline{kd} = 96.5 \text{ mm}}$ (i.e., $\overline{kd} = 4.6kd$)

$\underline{\overline{I_{cr}} = 169.8 \times 10^6 \text{ mm}^4}$

The corresponding time-dependent flexural rigidity is

$\underline{\overline{E_c}\overline{I_{cr}} = 726.6 \text{ kNm}^2} < E_cI_g \therefore \text{ok}$

This is roughly one-third of the instantaneous rigidity computed in Step (b).

(f) Compute the stress in the concrete after creep has taken place, $\overline{\sigma(t,t_o)}$, using Equation (3-6):

$$\overline{\sigma(t,t_o)} = \frac{M_s \overline{kd}}{\overline{I}_{cr}}$$

$\overline{\sigma(t,t_o)} = 4.2$ MPa

(g) Compute the creep strain, $\overline{\varepsilon_{cr}(t,t_o)}$, using Equation (3-7):

$$\overline{\varepsilon_{cr}(t,t_o)} = \emptyset(t,t_o) \frac{\overline{\sigma(t_o)}}{E_c(t_o)}$$

$\overline{\varepsilon_{cr}(t,t_o)} = 9.43 \times 10^{-4}$ mm/mm

(h) Compute the average curvature due to creep, $\overline{\psi_{cr}(t,t_o)}$, using Equation (3-8):

$$\overline{\psi_{cr}(t,t_o)} = \frac{\overline{\varepsilon_{cr}(t,t_o)}}{\overline{kd}}$$

$\overline{\psi_{cr}(t,t_o)} = 9.77 \times 10^{-6}$ mm^{-1}

(i) Compute the creep deflection, Δ_{cr}, using Equation (3-9) as:

$$\Delta_{cr} = \frac{5(9.77 \times 10^{-6})(6096)^2}{48} = \mathbf{38.2mm}$$

3. Shrinkage Deflection

(j) Compute the force in the concrete at the level of the top reinforcement, $F_{c,t}$ and the bottom reinforcement, $F'_{c,t}$:

$$F_{c,t} = \frac{-E_s A_s \varepsilon_{sh,t}}{1 + \overline{n}\rho \left(\frac{d}{h}\right)\left(1 + 12\left(\frac{d}{h} - 0.5\right)^2\right)}$$

$F_{c,t} = 24.9$ kN (tension)

$$F'_{c,t} = \frac{-E_s A'_s \varepsilon_{sh,t}}{1 + \bar{n}\rho' \left(\frac{d}{h}\right)\left(1 + 12\left(0.5 - \frac{d'}{h}\right)^2\right)}$$

$\underline{F'_{c,t} = 16.9 \text{ kN (tension)}}$

(k) Compute the residual stress at the top fiber, $\sigma_{sh,t,T}$, and the bottom fiber, $\sigma_{sh,t,B}$:

$$\sigma_{sh,t,T} = \frac{F_{c,t}}{A_g} + \frac{F_{c,t}(d-0.5h)(-0.5h)}{I_g} + \frac{F'_{c,t}}{A_g} - \frac{F'_{c,t}(d'-0.5h)(0.5h)}{I_g}$$

$\underline{\sigma_{sh,t,T} = 0.93 \text{ MPa}}$

$$\sigma_{sh,t,B} = \frac{F_{c,t}}{A_g} - \frac{F_{c,t}(d-0.5h)(0.5h)}{I_g} + \frac{F'_{c,t}}{A_g} + \frac{F'_{c,t}(d'-0.5h)(0.5h)}{I_g}$$

$\underline{\sigma_{sh,t,B} = 1.77 \text{MPa}}$

(l) Compute the residual strain at top fiber $\varepsilon_{sh,t,T}$, and the bottom fiber $\varepsilon_{sh,t,B}$:

$$\varepsilon_{sh,t,T} = \frac{\sigma_{sh,t,T}}{\overline{E_c}}$$

$\underline{\varepsilon_{sh,t,T} = 217.6 \ \mu\varepsilon}$

$$\varepsilon_{sh,t,B} = \frac{\sigma_{sh,t,B}}{\overline{E_c}}$$

$\underline{\varepsilon_{sh,t,T} = 313.2 \ \mu\varepsilon}$

(m) Compute the shrinkage curvature, $\psi_{sh,t}$, and the radius of curvature, R:

$$\psi_{sh,t} = \frac{\varepsilon_{sh,t,B} - \varepsilon_{sh,t,T}}{h}$$

$\underline{\psi_{sh,t} = 0.96 \times 10^{-6} \text{ mm}^{-1}}$

$\underline{R = 1039000 \text{ mm}}$

(n) Compute the shrinkage deflection, $\Delta_{sh,t}$:

$$\Delta_{sh,t} = 1039000 - \sqrt{(1039000)^2 - \left(\frac{6096}{2}\right)^2} = \textbf{4.5 mm}$$

(o) Compute the total long-term deflection, Δ_{LT}:

$$\Delta_{LT} = \Delta_{cr} + \Delta_{sh,t} = 38.2 \text{ mm} + 4.5 \text{ mm} = \textbf{42.7 mm}$$

(p) Compute the total deflection at 915 days, Δ_T:

$$\Delta_T = \Delta_i + \Delta_{LT} = 24.8 \text{ mm} + 42.7 \text{ mm} = \textbf{67.5 mm}$$

Table C-1: Test and Predicted Long-Term Deflections for Beam B5 (Washa and Fluck, 1952)

	Test	Predicted	Test/Predicted
Δ_i (mm)	24.9	24.8	1.00
Δ_{LT} (mm)	40.1	42.7	0.94
Δ_T (mm)	65.0	67.5	0.96

Appendix D: Regression Analysis Input Data

Tables D-1 shows the long- to short-term deflection ratios (obtained from the Mechanics-Based Method described in Chapter 3), Δ_{LT}/Δ_i, of doubly reinforced members corresponding to various combinations of creep coefficients, $\emptyset$, compression reinforcement ratio, ρ', and tension reinforcement ratio, ρ. Table D-2 shows the variation of Δ_{LT}/Δ_i with $\emptyset$ and ρ for singly reinforced members. These data points were used in the regression analyses to derive the Alternative Simplified Equations for computing long-term deflections based on short-term deflections, presented in Chapter 4.

Table D-1: Doubly Reinforced Members

Δ_{LT}/Δ_i	$\emptyset$	ρ'/ρ	ρ	ρ'
1.11	1.50	0.20	0.018	0.0036
0.95	1.50	0.50	0.018	0.009
0.83	1.50	0.80	0.018	0.0144
0.77	1.50	1.00	0.018	0.018
1.29	2.00	0.20	0.018	0.0036
1.10	2.00	0.50	0.018	0.009
0.96	2.00	0.80	0.018	0.0144
0.89	2.00	1.00	0.018	0.018
1.45	2.50	0.20	0.018	0.0036
1.21	2.50	0.50	0.018	0.009
1.06	2.50	0.80	0.018	0.0144
0.99	2.50	1.00	0.018	0.018
1.58	3.00	0.20	0.018	0.0036
1.31	3.00	0.50	0.018	0.009
1.14	3.00	0.80	0.018	0.0144
1.06	3.00	1.00	0.018	0.018
1.71	3.50	0.20	0.018	0.0036
1.40	3.50	0.50	0.018	0.009
1.21	3.50	0.80	0.018	0.0144
1.12	3.50	1.00	0.018	0.018
1.07	1.50	0.20	0.014	0.0028
0.94	1.50	0.50	0.014	0.007
0.83	1.50	0.80	0.014	0.0112
0.78	1.50	1.00	0.014	0.014
1.25	2.00	0.20	0.014	0.0028

1.09	2.00	0.50	0.014	0.007
0.96	2.00	0.80	0.014	0.0112
0.90	2.00	1.00	0.014	0.014
1.41	2.50	0.20	0.014	0.0028
1.21	2.50	0.50	0.014	0.007
1.07	2.50	0.80	0.014	0.0112
1.00	2.50	1.00	0.014	0.014
1.54	3.00	0.20	0.014	0.0028
1.31	3.00	0.50	0.014	0.007
1.15	3.00	0.80	0.014	0.0112
1.07	3.00	1.00	0.014	0.014
1.66	3.50	0.20	0.014	0.0028
1.39	3.50	0.50	0.014	0.007
1.22	3.50	0.80	0.014	0.0112
1.14	3.50	1.00	0.014	0.014
1.03	1.50	0.20	0.01	0.002
0.92	1.50	0.50	0.01	0.005
0.83	1.50	0.80	0.01	0.008
0.78	1.50	1.00	0.01	0.01
1.20	2.00	0.20	0.01	0.002
1.07	2.00	0.50	0.01	0.005
0.96	2.00	0.80	0.01	0.008
0.90	2.00	1.00	0.01	0.01
1.35	2.50	0.20	0.01	0.002
1.19	2.50	0.50	0.01	0.005
1.07	2.50	0.80	0.01	0.008
1.00	2.50	1.00	0.01	0.01
1.48	3.00	0.20	0.01	0.002
1.29	3.00	0.50	0.01	0.005
1.16	3.00	0.80	0.01	0.008
1.08	3.00	1.00	0.01	0.01
1.60	3.50	0.20	0.01	0.002
1.38	3.50	0.50	0.01	0.005
1.23	3.50	0.80	0.01	0.008
1.15	3.50	1.00	0.01	0.01
1.00	1.50	0.20	0.008	0.0016
0.91	1.50	0.50	0.008	0.004
0.83	1.50	0.80	0.008	0.0064
0.78	1.50	1.00	0.008	0.008

1.17	2.00	0.20	0.008	0.0016
1.05	2.00	0.50	0.008	0.004
0.96	2.00	0.80	0.008	0.0064
0.91	2.00	1.00	0.008	0.008
1.31	2.50	0.20	0.008	0.0016
1.18	2.50	0.50	0.008	0.004
1.07	2.50	0.80	0.008	0.0064
1.01	2.50	1.00	0.008	0.008
1.44	3.00	0.20	0.008	0.0016
1.28	3.00	0.50	0.008	0.004
1.16	3.00	0.80	0.008	0.0064
1.09	3.00	1.00	0.008	0.008
1.55	3.50	0.20	0.008	0.0016
1.37	3.50	0.50	0.008	0.004
1.23	3.50	0.80	0.008	0.0064
1.16	3.50	1.00	0.008	0.008
0.97	1.50	0.20	0.006	0.0012
0.90	1.50	0.50	0.006	0.003
0.83	1.50	0.80	0.006	0.0048
0.79	1.50	1.00	0.006	0.006
1.14	2.00	0.20	0.006	0.0012
1.05	2.00	0.50	0.006	0.003
0.97	2.00	0.80	0.006	0.0048
0.92	2.00	1.00	0.006	0.006
1.28	2.50	0.20	0.006	0.0012
1.17	2.50	0.50	0.006	0.003
1.08	2.50	0.80	0.006	0.0048
1.03	2.50	1.00	0.006	0.006
1.41	3.00	0.20	0.006	0.0012
1.28	3.00	0.50	0.006	0.003
1.17	3.00	0.80	0.006	0.0048
1.11	3.00	1.00	0.006	0.006
1.52	3.50	0.20	0.006	0.0012
1.37	3.50	0.50	0.006	0.003
1.25	3.50	0.80	0.006	0.0048
1.18	3.50	1.00	0.006	0.006
1.00	1.50	0.20	0.004	0.0008
0.94	1.50	0.50	0.004	0.002
0.88	1.50	0.80	0.004	0.0032

0.85	1.50	1.00	0.004	0.004
1.18	2.00	0.20	0.004	0.0008
1.10	2.00	0.50	0.004	0.002
1.04	2.00	0.80	0.004	0.0032
1.00	2.00	1.00	0.004	0.004
1.33	2.50	0.20	0.004	0.0008
1.24	2.50	0.50	0.004	0.002
1.16	2.50	0.80	0.004	0.0032
1.12	2.50	1.00	0.004	0.004
1.47	3.00	0.20	0.004	0.0008
1.36	3.00	0.50	0.004	0.002
1.27	3.00	0.80	0.004	0.0032
1.22	3.00	1.00	0.004	0.004
1.58	3.50	0.20	0.004	0.0008
1.46	3.50	0.50	0.004	0.002
1.36	3.50	0.80	0.004	0.0032
1.30	3.50	1.00	0.004	0.004

Table D-2: Singly Reinforced Members

Δ_{LT}/Δ_i	$\emptyset$	ρ
1.25	1.50	0.018
1.48	2.00	0.018
1.69	2.50	0.018
1.88	3.00	0.018
2.06	3.50	0.018
1.19	1.50	0.014
1.41	2.00	0.014
1.60	2.50	0.014
1.78	3.00	0.014
1.94	3.50	0.014
1.11	1.50	0.01
1.32	2.00	0.01
1.49	2.50	0.01
1.65	3.00	0.01
1.80	3.50	0.01
1.07	1.50	0.008
1.26	2.00	0.008

1.43	2.50	0.008
1.58	3.00	0.008
1.72	3.50	0.008
1.03	1.50	0.006
1.21	2.00	0.006
1.37	2.50	0.006
1.52	3.00	0.006
1.64	3.50	0.006
1.04	1.50	0.004
1.23	2.00	0.004
1.40	2.50	0.004
1.55	3.00	0.004
1.68	3.50	0.004

Curriculum Vitae

Name: Ziad Elaghoury

Post-secondary   University of Windsor
Education and   Windsor, Ontario, Canada
Degrees: 2013-2017 B.A.Sc.

                             Western University
                             London, Ontario, Canada
                             2018-2019 M.E.Sc

Related Work   Teaching Assistant
Experience   Western University
                             2018-2019

Publications:
Elaghoury, Z., and Bartlett, F.M. (2019). Long-term Deflections of RC Beams.
Proceeding of the 2019 CSCE Annual Conference, Laval, Quebec, Canada, pp. 10.